POSITRON LIFETIME MODULATION BY ELECTRIC FIELD INDUCED POSITRONIUM FORMATION ON A GOLD SURFACE

THESIS

Daniel J. Higgins, Captain, USAF

AFIT/NUCL/ENP/12-M03

DEPARTMENT OF THE AIR FORCE
AIR UNIVERSITY

AIR FORCE INSTITUTE OF TECHNOLOGY

Wright-Patterson Air Force Base, Ohio

AFIT/NUCL/ENP/12-M03

POSITRON LIFETIME MODULATION BY ELECTRIC FIELD INDUCED POSITRONIUM FORMATION ON A GOLD SURFACE

THESIS

Presented to the Faculty

Department of Engineering Physics

Graduate School of Engineering and Management

Air Force Institute of Technology

Air University

Air Education and Training Command

In Partial Fulfillment of the Requirements for the

Degree of Master of Science in Nuclear Engineering

Daniel J. Higgins, BS

Captain, USAF

March 2012

AFIT/NUCL/ENP/12-M03

POSITRON LIFETIME MODULATION BY ELECTRIC FIELD INDUCED POSITRONIUM FORMATION ON A GOLD SURFACE

Daniel J. Higgins, BS
Captain, USAF

Approved:

Larry W. Burggraf, PhD (Chairman) — 12 Mar 2012 — Date

Lt Col Christopher S. Williams (Member) — 7 Mar 12 — Date

Maj Benjamin R. Kowash (Member) — 12 Mar 2012 — Date

Abstract

The purpose of this project is to study the lifetime and annihilation mode of positrons, the antimatter counterpart to electrons, and the formation rate of positronium on a gold surface modified by gold nanoparticles under the influence of radial electric fields measured using two independent systems.

The positron annihilation photon pair/triplet spectroscopy system uses a sodium iodide ring detector segmented into six detection regions providing rough position sensitivity to measure the ratio of two to three photon positron annihilation events. An increased rate of three photon annihilation events and a decreased rate of two photon annihilation events are observed when the source is exposed to an externally applied radial electric field. This change is found to be statistically significant suggesting an increased rate of positronium formation.

The second system conducts positron lifetime spectroscopy on the same source and measures the effect of radial electric fields on positron lifetime. It uses barium fluoride, a fast inorganic scintillator, to measure the lifetime of a positron directly by comparing the time of arrival of a gamma ray accompanying positron birth in Na-22 with photons resultant from positron annihilation. Prolongated positron lifetimes, found to be statistically significant, are observed in the source when exposed to electric fields.

The effects on positron annihilation and lifetime observed using each system are consistent with each other and suggest that the lifetime of positrons on a gold surface can be modulated by the application of strong radial electric fields.

Acknowledgments

I'd like to thank my advisor Dr Larry Burggraf and my committee members Lt Col Christopher Williams and Maj Benjamin Kowash for all that they've taught me during my time at AFIT. It is their instruction that has given me confidence and competence in this field.

I am grateful to Dr Michael Lindsay and Dr Mario Fajardo from the Air Force Research Laboratory at Eglin AFB for introducing me to their research which helped me kick start my own project.

I'd also like to thank my fellow students who have been invaluable colleagues throughout this project. Specifically, I'd like to thank Capt Steve Jiménez for his help on the vacuum system, 1st Lt Ariella Walker for taking the time to introduce me to the project, 2nd Lt Jack FitzGerald for his thoughtful opinions, and Capt Joel Gearhart for his well informed advice and insight. I'd also like to thank Ms Nikki Sheppard for supporting me during the most challenging moments.

Dan Higgins

Table of Contents

Page

List of Figures

Figure Page

Figure Page

List of Tables

List of Equations

Page

POSITRON LIFETIME MODULATION BY ELECTRIC FIELD INDUCED POSITRONIUM FORMATION ON A GOLD SURFACE

I. Introduction

Overview

The purpose of this project is to the study the lifetime and annihilation mode of positrons and their propensity to form positronium under the influence of various electric fields on the surface of a gold coated capillary tube. The particle of interest in this experiment is the positron; it is a fundamental particle similar to the electron except with positive charge, it is the antiparticle of the electron[4]. When a particle and its corresponding antiparticle collide with each other, they can mutually annihilate releasing energy in the form of photons[5]. By studying the photons given off in positron-electron annihilation, information can be learned about the nature and behavior of the positron that would not otherwise be possible due to its short lifetime. In this experiment annihilation photons are studied using inorganic scintillation crystals with varying geometries, response times, and luminescence characteristics. The mode of annihilation, either by emitting two photons or three, along with the lifetime of the positron is studied.

When a positron and electron annihilate the mass of the two particles is converted into energy. The energy of annihilation is 1022 keV originating from the rest mass energy of both particles each contributing an equal share. The primary mode of annihilation for an electron positron pair is to emit two photons in opposite directions

each carrying away 511 keV of energy. It is also possible for an annihilation event to produce three photons which are emitted in a range of energy below 511 keV and travel at a variety of angles depending on the partition of energy[17]. These two modes of annihilation, two photon or three photon events, are known to occur at a ratio of 372 to 1 in copper metal[23]. Variations to this ratio occur depending on the surrounding electron environment and material density. This ratio is studied in the positron annihilation radiation spectroscopy portion of this experiment using both position and energy discrimination using a thalium doped sodium iodide (NaI) crystal, a common inorganic scintillation detection material. This detector is built in a ring configuration segmented into six detection regions. This partition of the NaI ring detector provides a rough position sensitivity that allows for an improved discrimination between two photon annihilation events and three photon annihilation events. This differs from traditional methods of measuring this ratio which do not utilize position sensitivity and are solely reliant on energy discrimination. With position sensitivity included as part of the analysis a larger energy range is permissible to include Compton scatter events while maintaining confidence in the proper identification of two and three photon annihilation events.

Earlier work on this system was performed at AFIT by 2nd Lt Robert Slaughter and 2nd Lt Ariella Walker. Lt Slaughter prepared a positron source that created an environment favorable to positronium formation. Liquid sodium chloride (NaCl) was injected into a thin capillary tube with a silver inner lining. The tube is then heated and radioactive Na-22 is deposited along the interior wall. Also, gold nanoparticles are deposited through an evaporative method onto the exterior surface. External electric fields can be applied to the capillary tube to energize positrons and to polarize

positronium. Lt Slaughter studied positron lifetimes and the ratio of three and two photon positron annihilations in various dodecaborate ion concentrations. Lt Walker adopted the same capillary tube setup and studied positron annihilations under the influence of various applied electric fields. This previous work is taken further by conducting thorough spectroscopy on the capillary tube source to validate the observation of positronium formation. Also, new data handling techniques are developed to make large scale data analysis possible in a reasonable amount of time.

Positrons can also interact with electrons by entering into a quasi-stable bound state in which an atom is formed between the two particles called positronium[1]. Due to the different allowable spin states for electrons and positrons, positronium can take two different forms. In the parallel spin state ortho-positronium is formed while para-positronium is formed in the anti-parallel configuration. Along with energy and momentum, spin must also be conserved in an annihilation event. Because of this, an electron-positron pair will much more readily mutually annihilate if they have anti-parallel spin. This results in a much shorter typical lifetime in para-positronium than ortho-positronium. Ortho-positronium can have lifetimes as long as 142 ns, much longer relative to the typical lifetime of an unbound positron[2]. Para-positronium annihilation is difficult to distinguish from free positrons, however ortho-positronium can be identified by long lifetimes and by three photon annihilation events. Due to a need to conserve angular momentum during an annihilation event, the electron positron pair in isolated ortho-positronium can only annihilate with the emission of an odd number of quanta, typically three. The emission of one quanta is possible, however it is forbidden for free positronium since it requires interaction with a third body for conservation of

momentum[1]. A decrease in the ratio of two photon annihilation to three photon annihilations could indicate an increased rate of formation of positronium. However, it is possible for positronium to form without these signatures if the effect of ortho-positronium pick off annihilation is a significant contributor. Pick off annihilation occurs more readily in materials with a high electron density and is discussed in further detail in chapter II.

The manner in which positrons interact on a material surface and material interfaces is also studied by diffusing positrons through the walls of a thin gold coated capillary tube via an applied external electric field. The formation of positronium on the surface and its effect on positron lifetime is studied as well. The lifetime of a positron is in part determined by how quickly it diffuses down to thermal energy to allow for it to annihilate with an electron rather than scatter. At a range of energy known as the Ore gap the likelihood of positrons to interact with electrons by forming positronium reaches a maximum[2]. Below this energy range positrons have less than the binding energy to form positronium and above this energy range ionizations and elastic scattering are the dominant interaction. Positronium most readily forms in materials with an ionization potential below the binding energy to form positronium such as in gold. For this reason a gold coated capillary tube is used to create an environment favorable for the formation of positronium. Delivering positrons onto the surface of a material at an energy corresponding to the Ore gap and its effects on positron lifetime and annihilation mode is also studied in this project to find further evidence of the presence of positronium.

This method was first studied by 2nd Lt Robert Slaughter and continued by 2nd Lt Ariella Walker. Their work found that applying external electric fields can influence the

formation of positronium, however the results were dependant on a low number of counts due to inefficiencies in data handling codes and lacked thorough validation of observed effects by way of spectroscopy at various stages of the data handling. 2nd Slaughter's work found evidence of positronium formation at a high rate on the gold surface of the capillary tube. 2nd Lt Walker found this effect to be maximized when 75 V is applied across the capillary tube wall and 600 V is applied to polarize positronium formed on the surface.

Motivation

The primary interest in positrons in modern research is the study of positron annihilation spectroscopy which can be used as a probe to non-destructively investigate the interior structure of solid materials[22]. This is possible because positrons are unlikely to impart enough momentum to dislocate an atom in even a fragile crystal lattice yet are able to diffuse into the material with relative ease. Also of interest is the interaction of gas molecules with surface formed positronium which can be studied using the capillary tube system demonstrated in this project. The annihilation of the positrons is dependent on the density of the electronic environment into which it is diffused. Once annihilated the resultant photons are high enough energy that they can typically escape the material without much attenuation. This means that they can be easily identified and when paired with the detection of its coincident partner annihilation photon traveling in the opposite direction, the point of origin can be identified. This can provide information about how far the positron, or the radioactive isotope from which it was born, diffused into the material before annihilation occurred.

The radioisotope used in this experiment is Na-22 which decays into Ne-22 by emission of a positive beta β+ particle. This particle is a positron and its emission or birth is accompanied by the emission of a 1.274 MeV gamma ray after a 3.7 ps delay. The detection of this birth gamma ray followed by the detection of the annihilation radiation allows for the lifetime of a positron to be measured. This lifetime is dependent on the density of electrons to which it is exposed. Long lifetimes correspond to voids while short lifetimes correspond to pockets of dense material.

These characteristics of positrons make them useful for conducting tomography on the interior of sensitive materials such as semiconductors[34], munitions, ageing nuclear weapons, and even the human body such as in a positron emission tomography (PET) scan[26]. For precise measurements to be made, a thorough understanding of the nature of positron annihilation and positronium formation is needed.

Approach

This research, through the characterization of positron annihilation, seeks to find evidence of positronium formation. The first method used is to measure the ratio of quanta of light emitted in positron annihilation using a NaI ring detector[10,11]. The rough position sensitivity of this detector, provided by its segmentation into six detection regions, along with the reasonable energy resolution of NaI provides a means of discriminating two photon annihilation events from three photon annihilation events. An increase in the rate of three photon events as compared to two photon events is taken to coincide with an increased rate of positronium formation. The next complimentary method used in this project to detect the presence of positronium is to measure the

lifetime of positrons using BaF_2 scintillators paired with fast photomultiplier tubes in a digital positron annihilation lifetime spectroscopy (PALS) method. By taking the difference in timing of annihilation photons from birth gammas and including a correction for the birth gamma delay, the lifetime of a positron can be directly measured. Longer lifetimes are taken to coincide with an increased rate of positronium formation. Both methods are used on a source system comprised of a Na-22 doped capillary tube in a vacuum chamber with electrodes attached to allow for the application of a radial electric field through the capillary tube wall. This system is designed to create an environment optimal for the formation of positronium.

II. Theory

Positrons

The positron is a subatomic positively charged elementary particle. It is the antimatter counterpart of the electron and the two are identical in every way except that they are oppositely charged. The intrinsic angular momentum of positrons is in half integer values of the Plank constant divided by 2π denoted ħ meaning that they are fermions. Positrons, along with electrons, are first generation leptons and interact by gravity, electromagnetism and the weak force. They can interact with electrons either by scattering or by mutual annihilation since they are antimatter counterparts of each other. When annihilation occurs energy is released in the form of photons. The rest mass energy of the electron positron pair, and consequently the energy of annihilation, is found by

$$E = m_{e^+}c^2 + m_{e^-}c^2 + T_{cm} = h\nu_1 + h\nu_2 \quad (1)$$

where m_{e^+} is the mass of a positron, m_{e^-} is the mass of an electron, c is the speed of light in a vacuum, and T_{cm} is the kinetic energy of the center of mass of the electron-positron pair at the time of annihilation[5]. From the center of mass frame of reference $T_{cm} = 0$ and the energy of annihilation is 1022 keV. The energy is divided equally between the two annihilation photons $h\nu_1$ and $h\nu_2$ which are emitted in opposite directions each carrying 511 keV of energy.

The existence of the positron was first postulated by Paul Dirac in 1928 as part of a publication on the quantum mechanical nature of the electron[4]. The solutions derived in this paper were equally correct for either a positively or negatively charged electron,

although Dirac did not expressly attribute the nature of this duality to the existence of the positron. In 1932 Carl Anderson discovered the positron by observing the curvature of ion trails left by positrons under the influence of strong magnets which curved in the opposite direction of those left by electrons.

Both being fermions, the electron and the positron abide by the Pauli Exclusion Principle. The two particles cannot occupy the same space at the same time so the overlap of their wave functions results in the conversion of mass to energy in the form of mutual annihilation. The positron annihilation rate λ is the reciprocal of the positron lifetime τ and is given by the overlap of the positron density wavefunction Ψ_{e^+} with the electron density wavefunction Ψ_{e^-}.

$$\frac{1}{\tau} = \lambda = \langle \Psi_{e^-} | \hat{\lambda} | \Psi_{e^+} \rangle \tag{2}$$

This means that the lifetime of a positron varies with the electron density of the medium[2]. It is by this property that positrons may be useful in studying the internal structure of a wide variety of materials.

The radioisotope positron source used in this experiment is Na-22 which decays into Ne-22 with a half life $t_{½}$ of 2.6027 years by positive beta β+ decay. Positive beta decay occurs when a proton in the nucleus of an atom decays into a neutron by the weak force releasing a positron and an electron neutrino via an intermediate virtual W^+ boson. The mass of the positron is created by a change in the binding energy of the nucleus as $m = E/c^2$. The birth of a positron is accompanied by the emission of a 1.274 MeV gamma ray after a 3.7 ps delay. The detection of this birth gamma ray followed by the

detection of the annihilation radiation provides the necessary information for measuring positron lifetime.

Positrons do not always immediately annihilate with electrons. They can also interact by entering into a quasi-stable bound state forming an exotic atom called positronium. Positronium can take two different forms based on different allowable spin state combinations of the electron positron pair. The parallel spin state configuration results in the formation of ortho-positronium, while the antiparallel configuration forms para-positronium. An electron-positron pair will much more readily mutually annihilate if they have anti-parallel spin. This results in a much shorter typical lifetime in para-positronium than ortho-positronium. Ortho-positronium has a typical lifetime of approximately 142 ns which is much longer than the typical 125 ps for para-positronium. Ortho-positronium can annihilate in three ways, pick-off annihilation, spin flip, or by three photon emission. In spin flip, the spin of one of the two particles will suddenly undergo a change in orientation causing the positronium to annihilate intrinsically. Pick off annihilation requires the presence of a third body. The ortho-positronium interacts with an electron from a nearby atom which annihilates with the positron. This interaction leaves behind a positively charged ion and a free electron. Typically the free electron will quickly associate with the ion to return to neutral charge. Pick-off annihilation can significantly reduce the lifetime of ortho-positronium and can influence the ratio of two to three photon annihilation events. The rate that pick off annihilation occurs is dependent on the the electronic environment, particularly the density of electrons, in which the ortho-positronium is present.

The annihilation of ortho-positronium by three photon emission is governed by conservation of angular momentum. Positronium annihilation can result in n number of photons given by

$$(-1)^n = (-1)^{L+S} \tag{3}$$

where L is the angular momentum and S is the positronium spin state. Since the spins of the electron-positron pair are antiparallel in para-positronium, the atom forms the singlet state and $S = 0$. In ortho-positronium the triplet state is formed and $S = 1$. For ground state positronium at $L = 0$, ortho-positronium is only allowed to annihilate into an odd number of photons. The emission of one quantum is possible, however it is forbidden for free positronium since it requires interaction with a third body for conservation of momentum. Annihilation by two photons in para-positronium distributes the energy of annihilation equally between the two and annihilation by three photons can result in a range of annihilation photon energy from 0 to 511 keV. These three photons are emitted coplanar and at a wide range of angles from one another depending on the distribution of energy. Annihilation by four or more photons is also possible, however the lower order processes dominate.

The longer relative lifetime of ortho-positronium means that the detection of long lived positrons can be taken as a sign of an increased rate of positronium formation which forms in the ortho state or the para state at a rate of 3 to 1. Ortho-positronium can also be detected by measuring a change in the ratio of two to three photon annihilation events. Due to a need to conserve angular momentum during an annihilation event, the electron positron pair in ortho-positronium can only annihilate with the emission of an odd number of quanta.

When a positron enters a material it usually does so with a large amount of energy. It loses energy through emission of Bremsstrahlung radiation and collisions. When it collides at high energy it forms elongated pockets of electron-ion pairs known as spurs. As the positron energy decreases it forms blobs which are spherical pockets of electron-ion pairs. In the final blob in a positron trail the positron has lost most of its energy. Now at thermal energy and in the presence of many free electrons the formation of positronium becomes probable. Positronium can form either quasi-free, meaning it is born outside the blob or confined, born inside the blob. This is possible because the positron wave function is more diffuse than an electron-ion pair wave function meaning that the positron wave function extends beyond the edges of the blob. Positronium forms when the energy of the positron is at a range of energies known as the Ore gap, lower than the ionization potential of the atoms or molecules in its immediate vicinity, but higher than 6.8 eV, the minimum binding energy for ground state positronium. This occurs most readily in materials with an ionization potential less than 6.8 eV since the positron does not need to deliver any energy to form positronium.

The depth of penetration of a high energy positron into a material is dependent on the stopping power of the material. A high energy positron can lose energy and become thermalized in a material through either elastic collisions or the emission of Bremsstrahlung radiation. Once thermalized in this manner annihilation and positronium formation become the dominant mode of interaction. The stopping power of material is the rate of energy loss $\frac{dE}{dx}$ of the positron and is given by

$$-\left(\frac{dE}{dx}\right)_{total} = -\left(\frac{dE}{dx}\right)_{radiation} - \left(\frac{dE}{dx}\right)_{collision} \quad (4)$$

A difference in the stopping power on electrons and positrons known as the Barkas effect arises due to their difference in charge. At high energy the electron or positron interact with electric fields at a high enough rate that individual fields are blurred together forming and electric field macro effect. At these energies both particles interact in a material the same. At low energy the electron or the positron spends more time near any particular electric field and can interact with it individually. The Coulombic attraction between a positron and the many electrons present in a material cause the positron to become thermalized much more quickly.

The penetrating nature of positrons and the manner in which their annihilation can be detected make them useful for conducting non destructive interrogation of the interior of solid materials. A thorough understanding of the nature of positron annihilation and positronium formation is necessary for precise measurements to be made.

Other experiments have shown that the lifetime of positrons and the annihilation mode either by emission of two or three photons can be influenced by the application of external electric or magnetic fields. At the University of Guelph in Ontario, Canada an experiment conducted by Stevens and Lichtenberger showed a prolongation of positron lifetimes in polyethylene through the use of electric fields. The setup included two nickel foils that sandwiched Na-22. The nickel foil layer was surrounded by a layer of polyethylene which was in turn surrounded by a layer of brass. Various voltages were applied to the brass layer placing an electric field across the polyethylene. The results indicate that positrons can be influenced to form positronium at a higher rate with applied electric fields[24].

Table 1. Positron Lifetimes in Polyethylene with Applied Electric Fields[24]

E (kV/cm)	I_1 (%)	I_2 (%)	I_3 (%)	I_4 (%)	τ_1 (nsec)	τ_2 (nsec)	τ_3 (nsec)	τ_4 (nsec)
0	23.5	46.6	10.6	19.3	0.145	0.352	0.663	2.39
30	19.1	49.8	11.6	19.5	0.147	0.349	0.660	2.39
60	18.3	50.8	11.4	19.5	0.145	0.348	0.651	2.39
90	17.4	52.4	11.7	18.5	0.144	0.345	0.640	2.38
100	16.4	51.6	13.4	18.6	0.145	0.343	0.629	2.37
110	14.3	52.2	14.6	18.8	0.144	0.335	0.600	2.34
120	13.9	51.1	16.6	18.5	0.144	0.327	0.583	2.34

The first lifetime and intensity shown here are associated with para-positronium annihilation while the fourth is associated with ortho-positronium annihilation. The intermediate lifetimes are associated with positrons associated with polar sites and ortho-positronium pickoff annihilation in column I_3. Lifetimes are not observed to change dramatically with applied field, however, intensity changes show that as field strength increases para-positronium formation is diminished. This occurs as pickoff annihilation and positronic molecule formation is correspondingly enhanced. Ortho-positronium formation is diminished much less by the applied field than is para-positronium formation.

Inorganic Scintillators

As part of this experiment gamma ray spectroscopy was conducted using scintillation detectors. This method of radiation detection relies on the physical process of scintillation in which a flash of light is produced in a transparent material due to an ionizing event caused by radiation incident upon the scintillation crystal which acts as the detection medium. This flash of light is then incident upon a photocathode material in a photomultiplier tube (PMT) located within the same casing as the scintillation crystal

separated only by a thin transparent window. Due to the photoelectric effect this results in the emission of a free electron from the photocathode which causes measurable current and voltage changes in the associated detection electronics.

Scintillation detectors, commonly referred to as scintillators, are grouped into organic and inorganic scintillators based on the nature of the crystal used as the detection medium. In this experiment two types of inorganic scintillators were used, a thallium activated sodium iodide (NaI) detector and a barium fluoride (BaF_2) detector. The NaI detector is a type of alkali halide detector and is one of the most commonly used inorganic scintillators in the field of radiation detection having been around since the late 1940's. Its high light output, low cost of production, and long history have made NaI detectors the traditional standard. After decades of advancements in scintillation detector technology many other materials have been introduced as viable alternatives. More recently BaF_2 has become a desirable alternative due to its fast timing characteristics.

The emission of scintillation photons in inorganic scintillators is due to the de-excitation of electrons across a band gap from the conduction band, in which they are essentially free electrons within the crystalline structure, to the valence band, in which they are bound to a particular molecule. The electrons are initially at the ground state in the valence band. Radiation in the form of high energy photons or charged particles incident on the crystal can interact with these electrons exciting them to the conduction band. This normally requires approximately three times the band gap energy to produce one electron-hole pair which is on the order of 20 eV and is material dependant. The "hole" is simply a location in the crystal in which a positive ion needs only one electron to fill an electron shell. This hole can travel throughout the crystal from one molecule to

the next under the influence of an external electric field. The photocathode materials used in the PMT to detect scintillation photons are normally optimized to detect light in either the visible or ultraviolet (UV) region of the electromagnetic spectrum. In a pure crystal the scintillation photons emitted would typically not fall in this region and would be lost to the detection electronics. To solve this problem an impurity known as an activator is intentionally adulterated into the scintillation crystal. This material provides new allowed energy states within the band gap into which de-exciting electrons can fall. These new allowed energy states, known as activator excited states, give rise to an increased range of scintillation photon energies that are emitted. An activator material can be chosen to create an energy state that results in a scintillation photon that is easily detected in the PMT. Since this photon will be of less energy than the band gap energy of the scintillation crystal, the bulk of the material in the detection medium will be transparent to the scintillation photon allowing greater luminescence to be incident on the photocathode.

A common drawback of inorganic scintillators is that they typically have a long decay time which can cause signal pileup in high pulse rate detection applications. This is largely due to phosphorescence in which an electron settles into a long lived energy state of the activator material in which de-excitation to the ground state is either forbidden or improbable. Additional energy is needed, usually from thermal energy, to elevate to a level from which de-excitation to the ground state is possible. This causes a delay in the emission of some photons picked up by the PMT and is known as afterglow. Electron capture at activator sites and some electron energy transitions to the ground

created by it do not result in the emission of a visible photon and act as loss mechanisms in the scintillator.

A motivation for using inorganic scintillators is that the light yield tends to be more linearly proportional to the deposited radiation energy than in organic scintillators. NaI detectors have an absolute scintillation efficiency of 12% and yield very close to 1 photon per electron hole pair formed. The high number of nucleons per atom and high crystal density of typical inorganic scintillators tend to make them more ideal for gamma ray spectroscopy than organics. NaI detectors offer typical resolutions of 7% at 662 keV with a decay time of 230 nanoseconds. BaF_2 meanwhile is the fastest known scintillator with a sub-nanosecond decay time of approximately 600 ps for a 220 nm wavelength component of its emission spectrum. BaF_2 has a two phase response with a slow component decaying at 630 ns with a wavelength centered on 310 nm[35]. The yield of scintillation photons for a given amount of energy deposited within the crystal is much lower for BaF_2 than for NaI meaning that BaF_2 exhibits much poorer energy resolution. NaI emits approximately 38,000 photons per MeV of energy deposited by radiation while BaF_2 produces only 10,900 photons, 85% of which originates from the slow component. The fast component in BaF_2 makes this material useful in fast timing applications such as time of flight measurements, positron emission tomography, and most importantly for this experiment positron lifetime studies.

III. Experimental Setup

Pair/Triplet Annihilation Photon Spectroscopy

Hardware

A cylindrical ring detector made up of six thallium doped sodium iodide (NaI) inorganic scintillation detectors shaped and assembled together to form one large cylindrical ring shaped system is the detection system used for the positron pair/triplet annihilation photon spectroscopy system (or 2γ3γ system). This ring detector is 18 cm in length, has an outer diameter of 20 cm and an inner diameter of 13 cm.

Figure 1. Sodium Iodide Ring Detector

A radioactive source can be centered inside the detector and radiation can be detected in several directions around the source. Each of the six sections of the ring detector is itself a NaI scintillator and is attached at one end of the ring detector to a photomultiplier tube (PMT) for collection and amplification of scintillation photons.

These sections are labeled A through F rotating clockwise when facing the front of the ring detector.

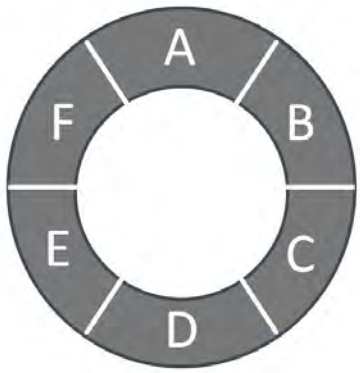

Figure 2. NaI Ring Detector Partition

This labeling becomes important during data analysis and provides coarse position sensitivity to radiation detection. To function properly the PMTs need to have a high applied bias voltage. This is delivered by Ortec model 556 high voltage (HV) supplies. Three HV supplies were available for this system; each with two output ports, sufficient for all six PMTs. Every device in this experiment requiring electricity was plugged into a Tripp-Lite power protection AC voltage regulator and line noise filter. This device ensured that the shape and amplitude of the signal waveforms in this experiment are not influenced by the tiny voltage fluctuation present in the electricity from a wall outlet.

The signals from the PMTs were carried to a battery of nearby preamplifiers Ortec model 113. The purpose of the preamplifiers was to introduce a long decay time to a pulse allowing full collection of charge from the PMT for a given scintillation event occurring inside the scintillation material. The preamplifiers were located as close as possible to the PMTs to minimize the effect of noise that might result from capacitive loading in the interconnecting cables.

The output signal from the preamplifiers each led to an input port on one of two XIA Digital Gamma Finder model 4C (DGF4C) data digitization devices. In this document these devices will be referred to as XIA cards. The function of the XIA cards was to digitize the preamplifier analog signal regulated by parameters set on a computer using Igor Pro 6.0, a controlling software program. The XIA cards were docked in a Wiener CC32 Camac crate controller which provided power to the cards and interconnected them to a nearby desktop computer running the Igor Pro software. The computer in this experiment was a Hewlett Packard HP dx5150. Each XIA card had four inputs labeled channels 0 through 3. PMTs A and D were connected channels 1 and 2 on the primary XIA card and PMTs B, C, E, and F were connected to channel 0, 1, 2, and 3 respectively on a secondary XIA card.

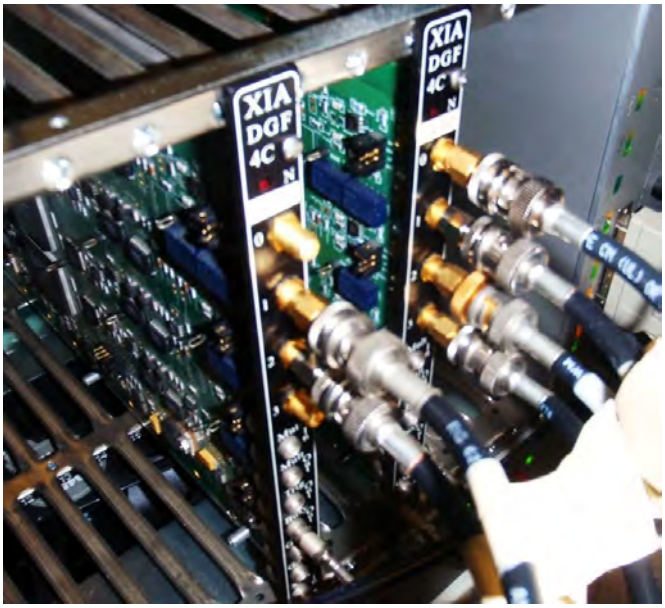

Figure 3. XIA Card Connections

The two XIA cards were connected together using a mixed logic fan-in/fan-out device by Phillips Scientific model 757. This logic gate device read the busy out signal from each port of the XIA cards and transmited back into the sync in ports on all XIA card channels. This was done to sync the XIA cards together in a manner such that all channels would take a reading anytime one channel was triggered by a radiation event.

In a preliminary experimental setup, used during system calibration, the signals from the PMTs were fed one at a time into a preamplifier Ortec model 142, then a linear amplifier Ortec model 572, which led to a timing single channel analyzer (SCA) Ortec model 551, followed by a timer counter Ortec model 996. The signal was characterized at each step in this setup using a digital phosphor oscilloscope Tektronix model TDS5104B.

Calibration

To optimize the bias applied to the PMTs from the HV supplies a preliminary experimental setup was used.

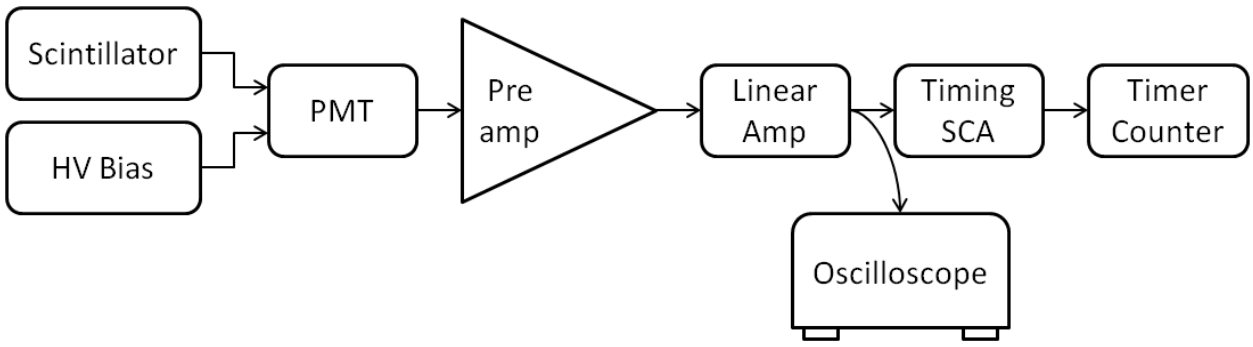

Figure 4. Preliminary 2γ3γ Setup Schematic

The oscilloscope was used to provide a visual of the signal at various stages so that parameters could be adjusted on each device so that the pulse could be optimized for the following device. The HV bias was varied from 500 to 1200 V with 100 V intervals and counts were collected from each channel one at a time on the timer counter for 60 second increments. This was done to find a voltage that results in a linear relationship between the number of counts and the voltage applied. Once a voltage range of interest was identified, counts were again measured over that range but in 5 or 10 V increments until an ideal voltage was determined. An ideal voltage was found in this manner for each of the six channels. Each PMT was paired with one other PMT with a similar ideal voltage. These PMT pairs were each connected to common HV supply since only three HV bias supplies were available. The lower of the two ideal biases was chosen as the setting used on the HV bias during the primary experimental setup on the 2γ3γ system.

Table 2. 2γ3γ System Bias Configuration

Channel	PMT	Ideal Bias [V]	HV Unit	Bias Setting [V]
A	1	860	1	835
B	2	835	1	835
C	3	910	3	890
D	4	960	2	930
E	5	930	2	930
F	6	890	3	890

Once this calibration was complete the system could be setup in the 2γ3γ system primary setup using the XIA cards.

The digital data acquisition parameters of the XIA cards were optimized in Igor Pro. The trigger voltage, voltage resolution, gain, and offset voltage were calibrated

using an oscilloscope feature within Igor Pro. A trigger of 40 mV was chosen to reduce the influence of noise. Voltage resolution was optimized by reducing the vertical axis of the window while still ensuring that the peak voltage remained completely visible. An equal gain for each channel of 0.164 was set so that the voltages for each channel were roughly proportional to one another. The offset voltage can be fine tuned for each channel by manually incrementing the offset a tiny amount at a time until the baseline of each channel lines up.

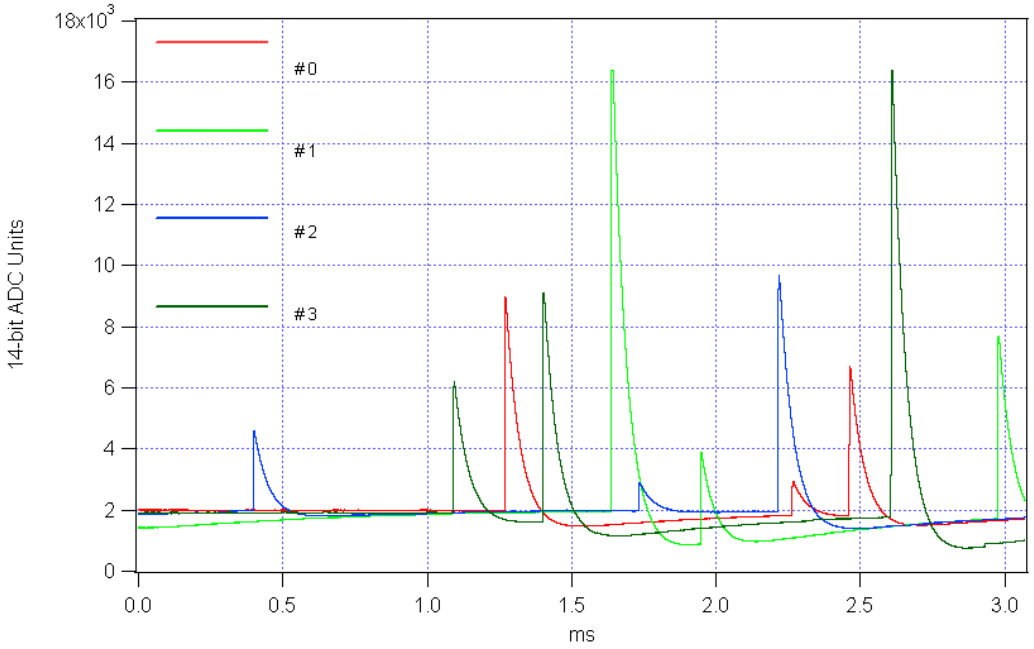

Figure 5. Igor Pro oscilloscope view of Na-22 source

Signal pulses from each channel were characterized by analyzing waveforms in Igor Pro to optimize the resolution in the eventual gamma spectra. This was done for each channel individually to account for small differences in the scintillation crystals and

PMTs for each channel. The decay time was characterized by fitting an exponential decay function.

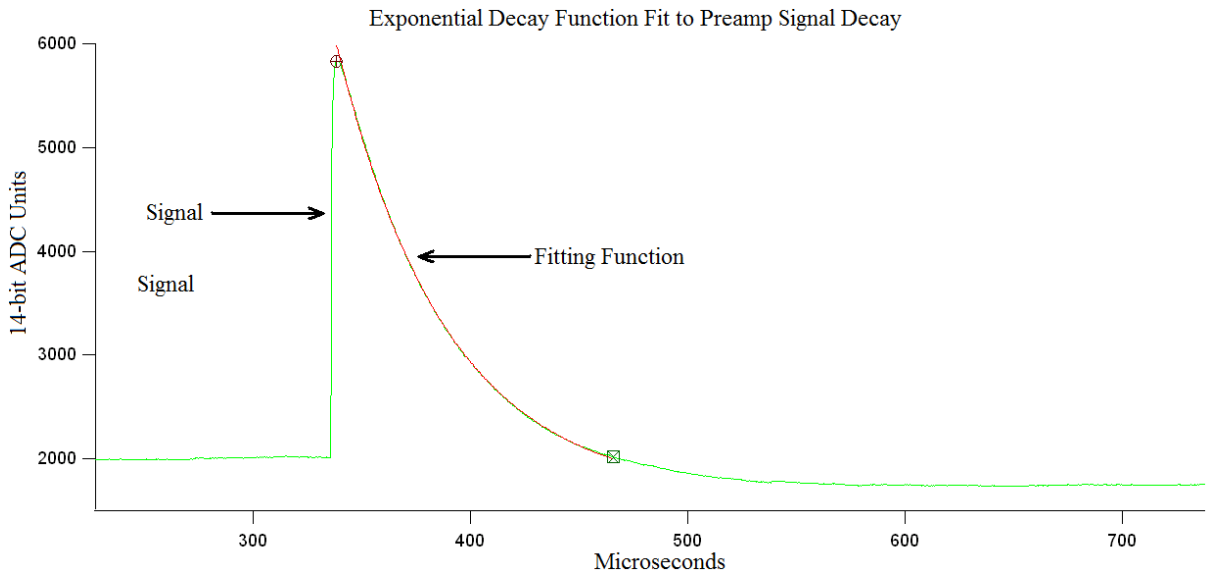

Figure 6. Preamp decay function fitting in Igor Pro. This was performed to optimize the resolution for the gamma spectra generated by the NaI ring detector.

The decays calculated for each PMT were all slightly different due to subtle differences in the time it takes to populate luminescent states in each of the scintillation materials which is not instantaneous. This affects the decay time because it influences the timing of slower scintillation photons from phosphorescence or delayed fluorescence. It is assumed in this experiment that the population of optical levels in the scintillation crystals can be characterized by a Gaussian distribution $f(t)$ so that the overall scintillation response signal is described by

$$\frac{I}{I_0} = f(t)e^{-\frac{t}{\tau}} \tag{5}$$

where τ is time constant describing the decay of the pulse. This characterization of the pulses within Igor Pro calibrated the system for optimal resolution.

Table 3. 2γ3γ System Pulse Characterization

Channel	Offset [V]	Time Constant Tau [μs]	Uncertainty [± μs]
A	1.0000	49.3987	0.2846
B	1.0110	49.1849	0.1816
C	0.9800	47.4480	0.1607
D	1.0100	48.2198	0.1560
E	1.0100	47.6233	0.3517
F	0.9850	47.905	0.1877

The next step to calibrate the 2γ3γ system was to derive an energy calibration equation for each channel. This was done in this experiment by collecting data from four different radionuclides with a known and easily identifiable dominant decay mode radiation energy.

Table 4. Isotopes for 2γ3γ Energy Calibration

Radioisotope	Radiation Energy [keV]
Co-57	122.1
Na-22	511 and 1274
Cs-137	662
Co-60	1173 and 1333

The isotope of greatest interest in this experiment was Na-22 since the system is meant to detect the annihilation of the positrons emitted by this isotope. All other isotopes were chosen to help calibrate the 2γ3γ system in energy as accurately as possible at the energies of interest for Na-22, particularly the 511 keV energy of annihilation.

Gamma spectra were generated on each channel from data collected for 1 hour from each isotope one at a time. Key features were identified in the spectra such as full energy peaks and Compton continua.

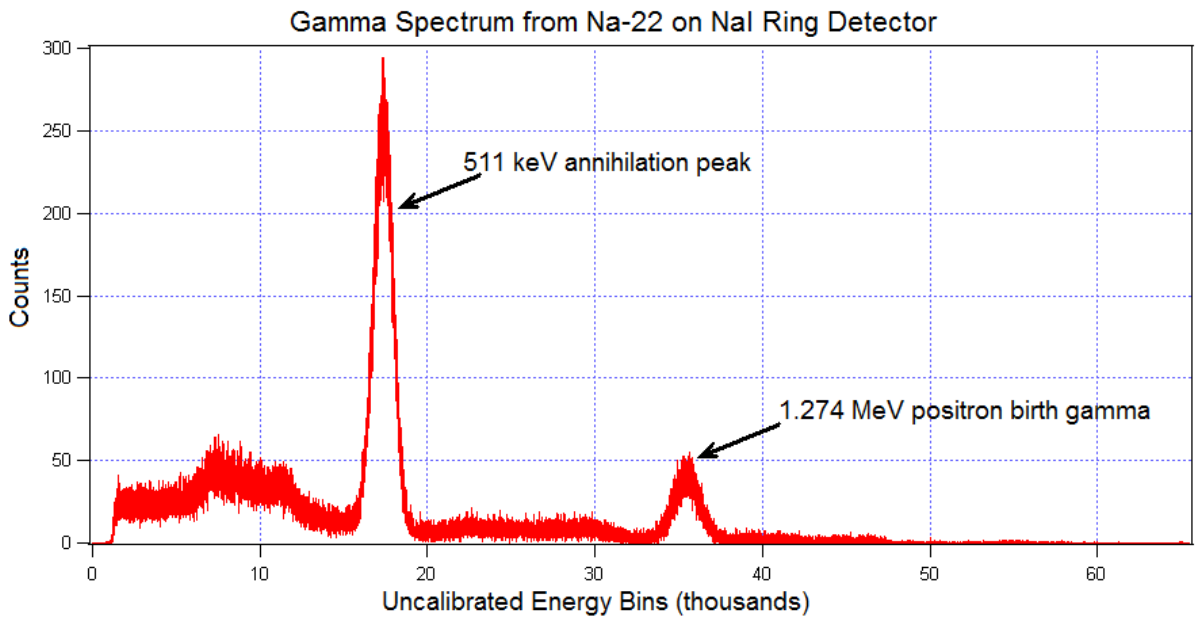

Figure 7. Gamma spectrum of Na-22 generated in Igor Pro from the NaI ring detector

Once key features were identified the energy of that event was compared to the bin in which they appeared and energy calibration equations were calculated. To determine the exact bin to which a feature corresponds, the feature was fit to a Gaussian distribution the peak of which was the central bin of the feature.

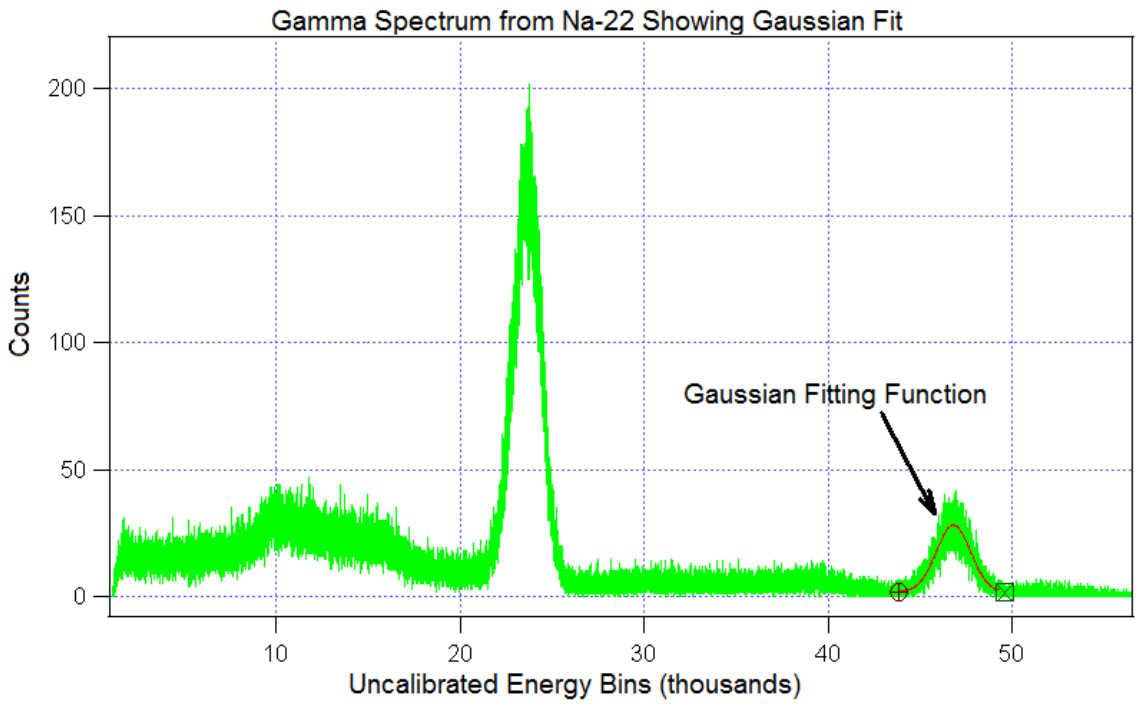

Figure 8. Gaussian fitting gamma spectrum features was performed to identify central bin and to determine the detectors resolution at that energy.

Fitting a feature to a Gaussian curve also helps to determine the resolution of the detector at that energy. The resolution R was determined by comparing the energy E of a feature to the full width of the Gaussian distribution fit to that feature at half of the peak height typically referred to as the full width half max (FWHM).

$$R = \frac{FWHM}{E} \tag{6}$$

This was performed for each of the peaks of interest for each isotope on all six channels with the exception of Co-60. The 1173 keV and 1333 keV peaks from Co-60 could be identified, however, they had too much overlap to be definitively discriminated for Gaussian fitting. This was due to the mediocre energy resolution of the NaI scintillator.

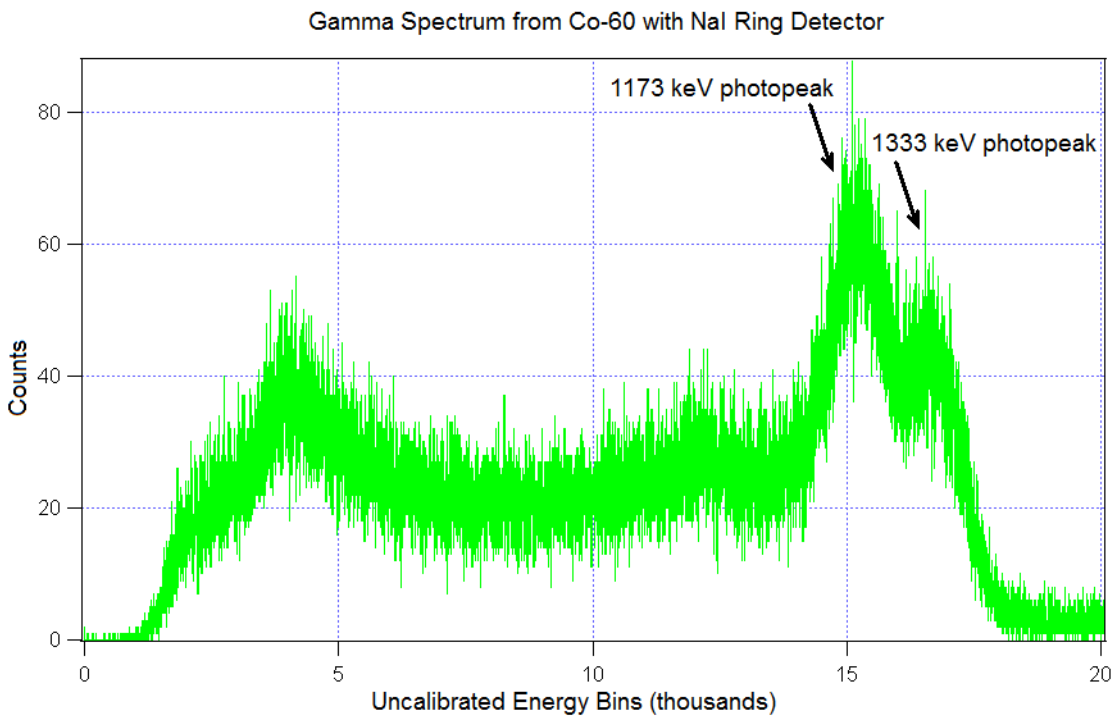

Figure 9. The gamma spectrum from Co-60 reveals two energy peak which could not be resolved from one another. Therefore Co-60 was not used in the energy calibration of the 2γ3γ system.

A plot was created for each channel comparing bins to energy. An energy calibration was generated by fitting a second order polynomial equation to the data points. The accuracy of this model was determined by calculating a correlation coefficient (R^2 value) between the fit equation and the data points.

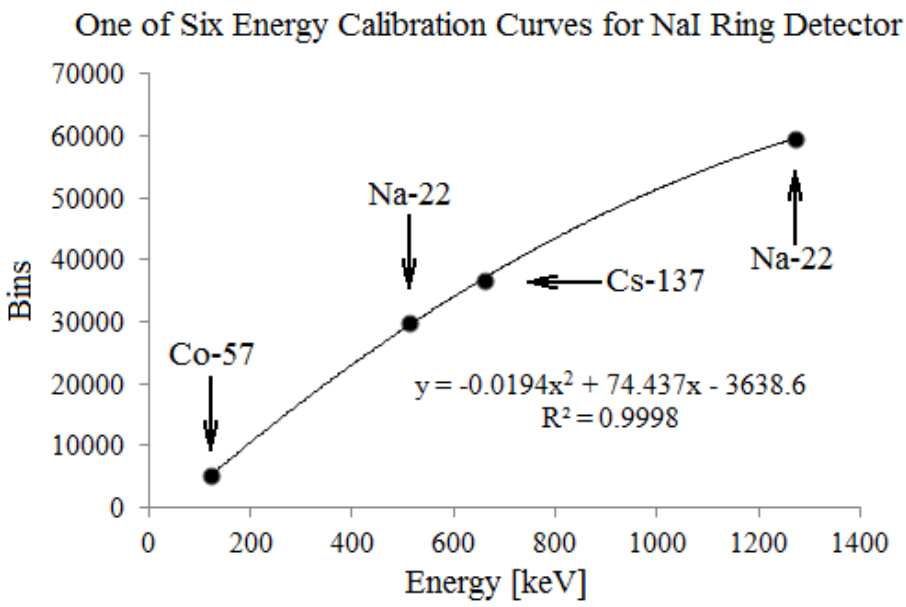

Figure 10. NaI ring detector energy calibration curve

The closer R^2 is to 1 the better the model fits the data points. The minimum R^2 value on the six energy calibration curves was 0.9947 which was an acceptable degree of accuracy. Each of the energy calibration curve equations and their respective R^2 values can be found in appendix A. The energy calibration curves were used during post processing.

The resolution of the NaI ring detector was plotted at various energies and was modeled using a decaying exponential to obtain an energy dependent resolution equation for each channel.

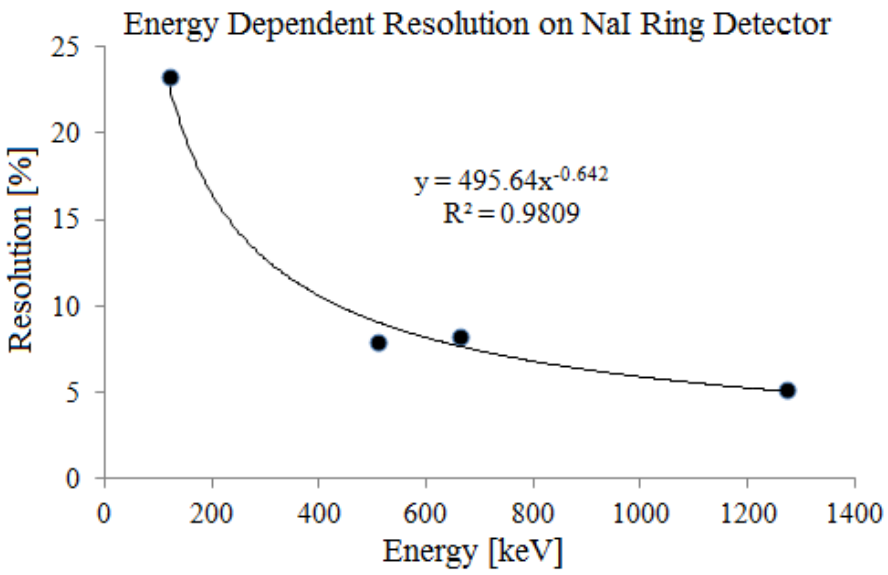

Figure 11. NaI ring detector energy dependent resolution curve.

The equations generated for each channel can be found in appendix B. These provide an estimate of the detector resolution at a large range of energies. Another benefit of the resolution plots is that it provides a visual for how rapidly the resolution becomes poor at low energy.

The NaI ring detector and the preamplifiers were placed inside of a small compartment surrounded by lead bricks, referred to in this document as a lead cave, to reduce noise by shielding them from background radiation and cosmic rays. With the calibrations described in this section the 2γ3γ system was ready for data collection.

Positron Lifetime Spectroscopy

Hardware

The experimental setup used to detect positron lifetimes includes two BaF_2 inorganic scintillation detectors, one to detect positron birth and the other to detect

positron annihilation. BaF_2 is chosen because it is the fastest known scintillator and timing is important since the lifetime of a positron is very fast. The tradeoff for the desirable timing characteristics is that BaF_2 has poor energy resolution and poor efficiency at high energy. Resolving various gamma spectrum features in energy from a BaF_2 detector is the greatest challenge in working with this material. One of the two BaF_2 detectors used in this experiment is larger than the other to compensate for the poor efficiency at high energy. With more material for a high energy photon to interact with the more likely that photon will deposit all of its energy in the larger scintillation crystal.

Each scintillation crystal is mated to an 8 stage Hamamatsu R2083 PMT designed for fast response. The purpose of this device is to detect and amplify the scintillation photons from the BaF_2 crystal. The gain generated by the PMT is dependent on the supply voltage provided by a HV bias supply Ortec model 556.

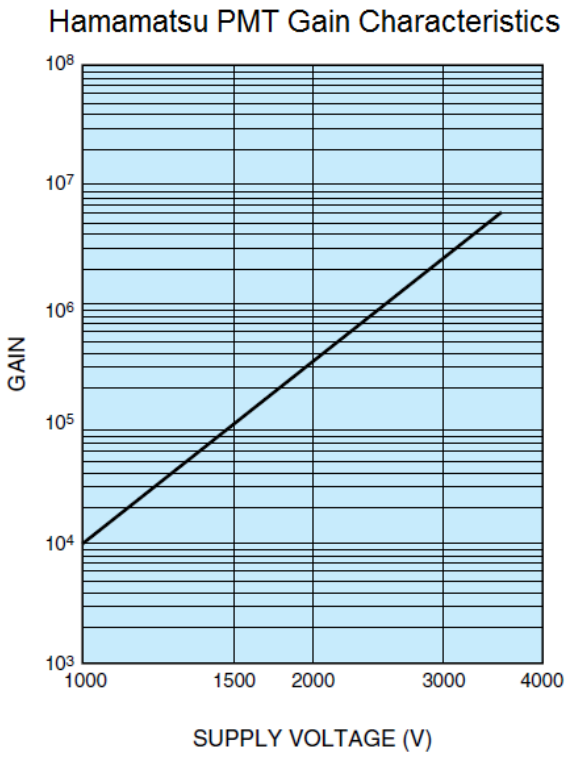

Figure 12. Supply voltage dependency of gain on hamamatsu PMT[36]

Due to the nature of the setup used in this experiment very sensitive voltage measurements must be made. For this reason it is desirable to have a predictable gain in each PMT. Both are connected to the same HV supply at 2500 V to achieve a 10^6 gain.

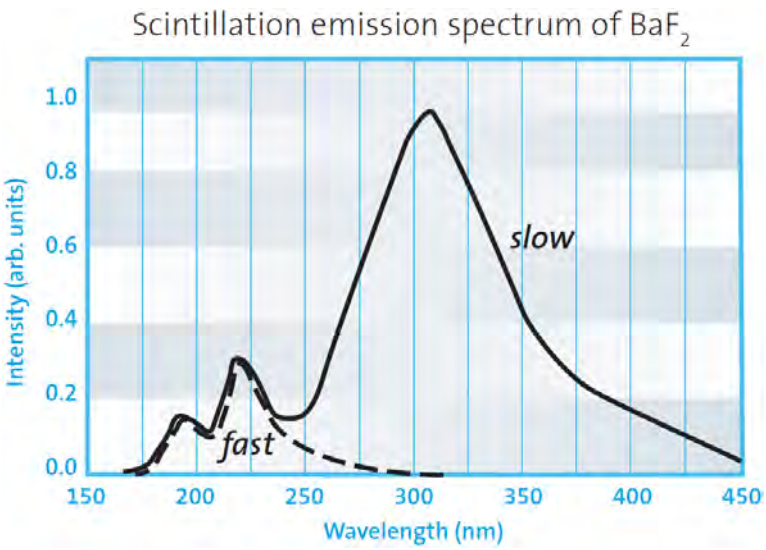

Figure 13. BaF_2 two phase emission spectrum[35]

BaF_2 is a unique scintillator in that it has multiple scintillation emission bands, some associated with a fast scintillation, the other slow. The decay time of the fast component, emitted in the UV bands at 220 and 195 nm, can be as quick as 600 ps while the slow component decays after 630 ns. The fast component is more desirable for timing applications, however at room temperatures the slow component dominates the light yield emitting 9500 photons per MeV of energy deposited in the detection region as compared to the fast component at a modest 1400 photons per MeV. The slow component scintillation photons peak at 310 nm and make up all of the light yield at any longer wavelengths.

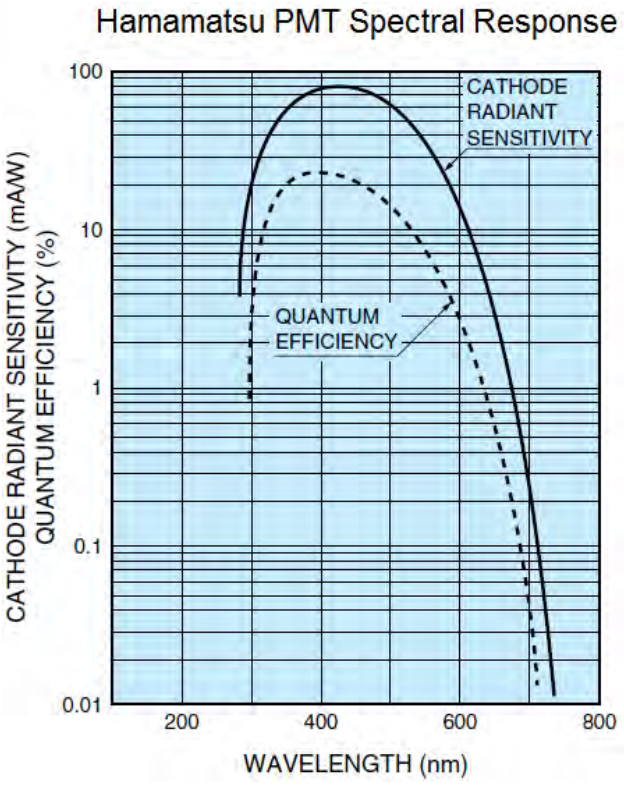

Figure 14. Radiant sensitivity of photocathode[36]

The PMTs in use in this experiment have a wavelength dependent sensitivity and quantum efficiency that fall off quickly at wavelengths not far below 300 nm. The slow component can be eliminated by raising the temperature of the BaF_2 crystal to approximately 200º C, however the means to do this were not available in this project.

All devices in this experiment requiring electricity are plugged into a Tripp-Lite power protection AC voltage regulator and line noise filter. This device ensures that the shape and amplitude of the signal waveforms in this experiment are not influenced by the tiny voltage fluctuation present in the electricity from a wall outlet. The voltage regulator and the HV supply are positioned on a different surface that the other devices in this

experiment to prevent the electric fields generated by these devices from interacting with the signal.

Figure 15. Positron lifetime spectroscopy setup

The PMT anodes are each connected to a 40 cm long RG-59B/U coaxial cables which have a characteristic impedance of 50 Ω. These cables carry the signal to a digital phosphor oscilloscope Tektronix model TDS5104B and have the same length to ensure that the signal from each PMT arrive at the oscilloscope with the same timing. At a late stage in this experiment the oscilloscope was traded out for a Tektronix model DPO7104, a newer model oscilloscope with improved sampling rate. The sampling rate of an oscilloscope, when set to maximum, must be divided equally between all channels in use and is the determining factor for the timing resolution of the oscilloscope. The original

oscilloscope could provide 400 ps per point when two channels were in use. Since the lifetime of a positron is on the order of nanoseconds, this was not sufficient. The replacement scope could provide 100 ps per point on two channels.

On the oscilloscope a setting is selected which applies a 50 Ω terminator to each channel to match the cable impedance and reduce the effect of ringing. Data collected by the oscilloscope is transmitted by a category 5 T568 Ethernet cable to a nearby Hewlett Packard HP dx5150 desktop computer which controls the oscilloscope and collects the data, details of which are presented in the data collection section later in this chapter.

Technique

Positron birth in Na-22 corresponds with a delayed 1.274 MeV gamma ray. Two photon annihilation events emit photons at 511 keV and three photon events emit photons in a range of energies below 511 keV. The positron lifetime measurement experiment portion of this project primarily focuses on the two photon annihilation mode. The positron lifetime spectroscopy system is designed to collect waveforms that represent the birth of a positron and subsequent annihilation of positrons and determine the difference in timing of these two events. These events occur rapidly, they are close to but not exactly coincident in time. Waveforms are collected in pairs, each covering the same 100 ns time period to capture the near coincident events of positron birth and annihilation.

Positron annihilation photons are emitted simultaneously and in opposite directions in the two photon annihilation mode. There is some risk that if both annihilation photons are detected, one by each detector, that coincident event might be misread as a positron lifetime. In this case the system would read the two signals simultaneously and a positron lifetime would be incorrectly recorded as lasting within the

timing resolution of the oscilloscope which is 200 ps for the older oscilloscope and 50 ps for the newer device. To prevent these false coincidences the two BaF_2 detectors are positioned perpendicular to one another with the detection region facing the same point. Also, the source is positioned far enough away that only one of any two photons released in opposite directions from each other and originating at the source will be incident on the detection face of the BaF_2 detectors. This way both detectors can measure the same source while mitigating the risk that two annihilation photons will be incorrectly measured as a lifetime event. If the electron positron pair is carrying momentum in the direction of the detectors upon annihilation the annihilation photons would travel in opposite directions in the particle reference frame, but not necessarily in the laboratory reference frame. This change in the angle of emission is unlikely to affect this experiment since the angle change maximizes at approximately 100 mrad for two photon annihilation[1].

There is a risk that a positron birth gamma could Compton scatter from one detector depositing some of its energy in both crystals generating two false annihilation signals. To prevent any photons interacting with one BaF_2 detector from Compton scattering and interacting with the other detector, a thin lead shield is positioned between the detectors while still allowing photons to travel undisturbed from the Na-22 source to one of the two BaF_2 detectors. During data analysis measurements were taken with and without the lead shielding. No difference could be identified on the spectra generated from the two setups.

The BaF_2 detectors in use in this experiment have a circular detection face and have a 5.1 cm diameter. By placing the source far enough away from the crystals to

prevent false coincidences the inefficiency of BaF_2 at high energy is exacerbated by a geometric inefficiency. The source emits radiation isotropically and to be incident on the detector face it must be emitted in an angle subtended by the detector. This solid angle is found by

$$\Omega = 2\pi\left(1 - \frac{d}{\sqrt{d^2 + a^2}}\right) \tag{7}$$

where d is the distance between the detector and the source and a is the radius of the detector face. In this experiment it is not enough for just one photon to be incident upon the detector. For a lifetime measurement to be made both the birth photon and one of the two annihilation photons must be incident. The probability of this occurring for any one positron is found by dividing by the total solid angle for both events.

$$P = \left(\frac{\Omega}{4\pi}\right)\left(\frac{2\Omega}{4\pi}\right) \tag{8}$$

In this experiment it can be expected that this will occur for 1.38% of all positrons born out of the Na-22 source. This is the first of many efficiency challenges in this system.

An alternate setup was used in this project during a experiment to obtain an energy calibration. In this alternate setup the BaF_2 scintillation crystal, PMTs, HV supplies, and voltage regulator were all connected in the same manner as in the primary experimental setup. The PMT anodes were connected to a preamplifier Ortec model 113 followed by a linear amplifier Ortec model 572. The signal is then passed to a multichannel analyzer (MCA) which sends the signal to a laptop computer running the GammaVision software. This setup was used to generate a gamma spectrum in GammaVision so that the BaF_2 detector response could be characterized from a variety of sources.

Data Collection

During data collection two sources were measured for positron lifetimes, both containing Na-22. The first was a small disk planchette source (source T107) which was measured to obtain a baseline and had an activity of 86.93 nCi on 25 October 2011. The other source was a long thin Na-22 filled capillary tube which sat inside of a vacuum tube which was prepared by 2nd Lt Ariella Walker. During data collection of the capillary tube the detectors were positioned perpendicular to each other on either side of the vacuum chamber. Data collection is controlled by a computer code developed in MatLab running on the desktop computer. The code can be found in its entirety in appendix F. This code allows the user to control the oscilloscope by changing parameters in the code. The pulses seen on the oscilloscope screen are a display of the data points that the oscilloscope has digitized from the analog signal read in from each channel in use. The data collection code was adapted from a previous version designed to detect coincident events. This original code read the waveform data points from the oscilloscope display, saved them and then sent them to the computer for storage and further analysis. This code was developed for a laboratory exercise in Nuclear Engineering 612. It has been adapted for faster data acquisition by collecting the digital data points in sets and sending them to the computer rather than to the screen. By using the oscilloscope's IP address the code prints commands directly to the oscilloscope processor allowing the user to change settings and parameters without turning knobs or pushing buttons which aids in optimizing the system. Connecting the two devices in this manner is set up by installing a driver for the oscilloscope on the desktop computer and communication is established using the TekVisa talker-listener program obtained online from Tektronix.

Once the code has established communication with the oscilloscope the system is first reset to factory defaults so that all settings are known from the start. Data configuration parameters are then established. One reading of a waveform from one channel across the full timeframe chosen at the voltage resolution chosen is referred to as a frame. The number of data points making up a frame is the record which is set to match the timing resolution of the oscilloscope. In this experiment frames are collected in sets of 1000 and contain 1000 data points each. Sets are sent to the computer one at a time as 1000 x 1000 matrices with each column representing one waveform. The sets are saved as .mat files, a format optimal for MatLab. The duration of any one data run is primarily dependent on the number of sets chosen by the user.

Parameters relating to the resolution of each waveform in voltage and timing are set in the code prior to beginning data acquisition by altering the vertical and horizontal scaling of the frame. Values for the voltage offset as well as the trigger voltage and timing offset are also communicated to the oscilloscope. Even the termination of 50 Ω for each channel is set in the code. Data acquisition is performed two sets at a time, one for each channel simultaneously, until either the desired number of sets has been collected or the acquisition is interrupted by the user. The duration of any one collection run depends on the activity of the source, the trigger voltage chosen and the number of sets desired. This can be a lengthy process so the code frequently displays messages stating the actions it is currently performing so that the user can determine if the code is working properly without interrupting a data collection run.

Source Assembly

Capillary Tube

The primary radiation of interest in this experiment comes from the birth and annihilation of positrons. The positron source is Na-22 which is injected as sodium chloride into a long thin capillary tube which itself is contained within a vacuum chamber tube. The vacuum chamber is narrow enough to fit into the interior of the NaI ring detector for measurements on the 2γ3γ system. During lifetime measurements the two BaF_2 detectors are positioned perpendicular to each other on either side of the vacuum chamber walls.

Figure 16. Capillary tube source system in vacuum chamber with while conducting lifetime measurements with BaF2 detectors. At the right end of the tube the hookups for the applied electric fields can be seen.

A thin capillary tube was chosen since it is effective at containing the Na-22 source while also moderating positrons as they travel through the capillary walls to the

exterior surface, a method adopted from 2nd Lt Robert Slaughter. Electrodes are connected to the inside and outside walls of the capillary tube which are in turn each connected to a bias voltage supply. This allows that a potential difference can be applied across the capillary tube wall. This potential difference creates a radial electric field through the capillary tube wall and can be used to push positrons through the material. Varying the strength of this electric field modifies at what energy the positrons arrive at the exterior surface. The field strength is optimized when the positrons arrive at the surface at an energy corresponding to the Ore gap which is conducive to forming positronium.

The capillary tube is multilayered and has an interior radius of 350 μm. The interior wall is lined with a 2.9 μm layer of silver followed by a silica layer that is 75 ± 20 μm thick. This silica makes up the majority of the body of the capillary tube and has a thin 25 μm coating of polyimide. A gold layer was applied on the exterior and was approximated to be 100 nm thick. The Na-22 source is injected into the interior of the tube and the positrons that are created as a result of β+ decay travel through the capillary tube wall.

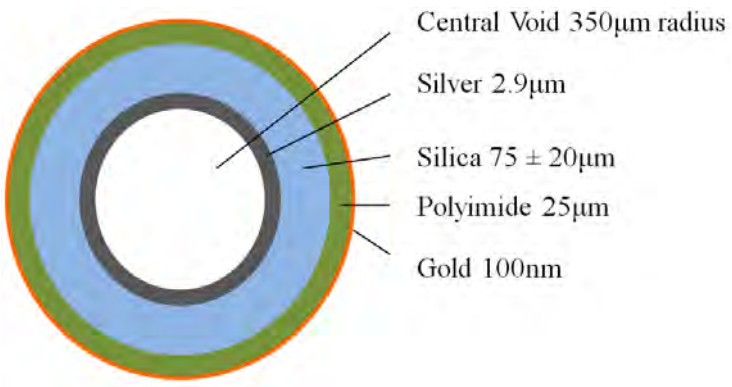

Figure 17. Cutaway diagram of capillary tube

The Na-22 is deposited along the interior wall by using a 22 gauge syringe to inject ^{22}NaCl inside. The tube was then heated on a hot plate to evaporate the liquid during which some of the radioactive material escaped. This is a method first used by 2nd Lt Slaughter and later adapted by 2nd Lt Walker to a method that involved heating both ends of the tube to prevent the escape of radioactive material during evaporation. 2nd Lt Slaughter applied a thin smooth layer of gold to exterior surface of the capillary tube. He then used a Torr Electron Beam Evaporation System (E-beam) to deposit gold nanoparticles on the exterior surface of the tube connected by nanoparticle linkers using a method developed by Professor Ioana Pavel and her students at Wright State University in Ohio. It was demonstrated by 2nd Lt Slaughter that electrical contacts could be made to the interior and exterior walls of the capillary tube to create an electric potential difference across the tube wall. A 22 gauge electrical wire and an electric feed through were used to make the connection to the interior wall. The connection to the exterior wall was made by wrapping a 22 gauge wire to the gold layer with a thin electrical wire and soldering the 22 gauge wire to another voltage feed through.

The exterior layer is intended to be the sight of positronium formation. Here gold nanoparticles were deposited through an evaporative method by 2nd Lt Robert Slaughter. A new injection of the radioactive Na-22 was prepared the following year by 2nd Lt Ariella Walker. The actual surface of the capillary tube is not smooth, there are many irregularities from being bumped and worked with causing wear and tear. Also the surface was not perfectly smooth when it was brand new due to the method used to deposit the gold particles.

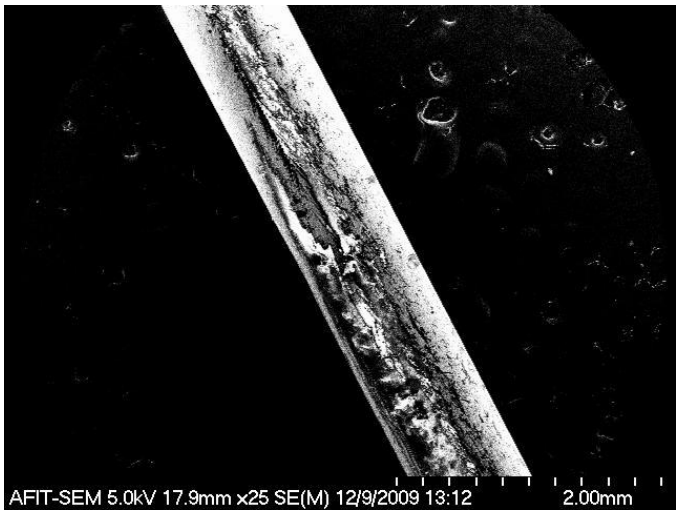

Figure 18. 25x Zoomed image of capillary tube showing exterior irregularities[10]

The electric field generated to push the positrons along is applied by two electrodes attached the capillary tube, one to the interior wall and the other to the exterior wall. The gold layer provides a medium for the positrons to form positronium however another important purpose of both the silver and gold layers is to carry the voltage applied at the electrodes. The electrodes are attached to connectors that can be accessed at one end on the exterior of the vacuum chamber tube. An interface with these

connectors was made using using metal pins shielded by a rubber and plastic gasket that screwed on to the exterior of the vacuum chamber. These pins were in turn wired to attachments compatible with HV bias supplies.

Figure 19. Electric field connectors for capillary tube source system

With this connection one HV bias supply can be connected to the interior wall of the capillary tube and another attached the exterior wall. The gold layer is connected to an Ortec bias supply model 660 which is set to 0V to establish the ground. A potential difference across the capillary tube wall is established by varying the voltage applied to the silver layer via the interior wall connector. An Ortec HV supply model 556 provides this voltage and was varied in this experiment from 0V to 2500V at various increments. The exterior of the vacuum chamber wall was connected to the ground as well. Measurements are taken on the capillary tube using both the $2\gamma3\gamma$ system and the positron lifetime system at various electric field strengths.

Previous work by 2nd Lt Ariella Walker using this system applied a small electric field across the capillary tube wall and a large electric field between the capillary tube and the vacuum chamber wall to polarize any positronium that might form on the surface. The alternative method of applying the field across the capillary tube wall was used to

prevent the positrons from leaving the surface once they pushed through the capillary tube wall.

The capillary tube is suspended at the center of the vacuum chamber tube to prevent positrons from annihilating with electrons in the interior chamber wall. At one end the capillary tube is held in the center by the connecting electrodes that supply the voltage difference. At the other end the capillary tube is suspended by fishing line strung across a polyethylene ring. Two pairs of fishing line were strung perpendicular to each other, the strings in each pair spaced by approximately 1.5 mm forming a tiny square shaped hole at the center of the ring. The end of the capillary tube rests in this square suspended by the fishing line.

The purpose of containing the capillary tube within a vacuum chamber is to minimize the number of air molecules that can interact with the exterior wall of the capillary tube since this might influence the lifetime of the positrons and positronium. The vacuum chamber is constructed of a stainless steel 10 inch long 2.75 inch diameter Kurt J. Lesker ConFlat cylindrical tube. At one end of this tube is an attachment which provides the housing for the electrodes attached to the capillary tube. At the opposite end are two T shaped Conflat joints. A Gamma Vacuum 10S TiTan ion pump sits on top of the first T joint and a Varian ionization gauge is meant to sit on top of the second joint connected by a KF-25 to Conflat 2.75 adapter nipple. During this experiment the nipple was not available due to delays in shipping so this section was sealed during data collection using a 2.75 inch stainless steel Conflat cap. After the second T joint is a right angle valve with a twist knob that can be used to seal off this section of the vacuum chamber. On the other side of this valve is a connector for a type 0531 TC vacuum gauge

which measured the pressure of the vacuum chamber. This gauge type is accurate down to 10^{-3} Torr and is displayed on an attached Varian multigauge. There is a port on the last section of the vacuum chamber for connecting a metal hose which connects to an Alcatel roughing pump model Drytel 1025.

The metal hose is attached using a quick release wing nut clamp and all other sections are mated using a copper metal ring seal. The copper ring is flat initially and placed at the center of two connecting pieces. When the bolts are tightened on the connecting joints thin circular edges on the Conflat pieces push into and deform the copper ring. This molds the ring to form a perfect seal in the connection despite slight imperfections that might exist in the metal at the connection location.

The roughing pump can achieve a vacuum of approximately 10^{-4} Torr, however the gauge is only accurate down to 10^{-3} torr. For pressures lower than this the ionization gauge must be used which is accurate down to 10^{-8} torr or further. Because the connecting nipple for the ionization gauge was not available during data collection it could not be determined if a vacuum lower than 10^{-3} torr was ever achieved. The ion pump is not designed to be started until a vacuum of at least 10^{-4} torr is established. Since this could not be determined, the ion pump was not started to prevent damaging the device. Data measurements taken in this experiment under vacuum are recorded as being conducted at less than 10^{-3} torr due to the limitations of the equipment available.

This source assembly includes the Na-22 filled capillary tube, the vacuum chamber and the HV supplies and connector assembly used to apply a potential difference across the capillary tube wall. This assembly was the primary source of interest for measurements taken using the $2\gamma3\gamma$ system and the positron lifetime system.

IV. Analysis and Results

Pair/Triplet Annihilation Photon Spectroscopy

Interpreting the Raw Data

The analysis of the data collected on the positron annihilation photon pair/triplet spectroscopy system (or 2γ3γ system) begins with a text file in the .dat format output by the Igor Pro program used to collect the data from the XIA digitization cards in the experimental setup. These files are produced as one document for each data collection run and contain the data collected from both XIA cards connected to all six sections of the sodium iodide (NaI) ring detector. The document begins with some header information which describes the module used, run number, start time, and data column labels. This header information applies to the first XIA card referred to in the data file as module 1. It is followed by all the data collected by module 1 which is connected to sections A and D of the NaI ring detector. For a detailed schematic of the NaI ring detector please reference the experimental setup section of this document in chapter III. After this raw data, which goes on for several thousand lines, there is a second set of header information, similar to the previous header, which this time applies to the second XIA card referred to as module 2. The only important part of the header information is the start time and the only important thing about the start time is that it must be the same in module 1 as it is in module 2. This lets the user know that the two XIA cards started in sync with one another and that any events read as simultaneous in the event record actually did occur simultaneously within a user defined tolerance. After the second header is the raw data collected by module 2 which is connected to sections B, C, E, and

F of the NaI ring detector and goes on for several thousand more lines to the end of the document.

Once it is verified that the start times match, the header information is no longer needed. The raw data are presented in four columns, the first of which is the event number. The two XIA cards are connected to each other in a manner such that when one section of the NaI detector picks up a radiation event that triggers the XIA channel to which it is connected all four channels of both XIA cards will take a measurement for a total of eight measurements for each event number. In the first XIA card two of the four available channels are not connected to the detector and always measure zero. Since the entire data from module 1 for the entire run is stacked on top of the data from module 2, the event numbers in the top and bottom sections of the raw data (associated with modules 1 and 2) correspond with each other. Event numbers increment by one for each measurement and number one through several thousand or several million depending on the duration of the measurement run. The second column of the raw data is the channel number on the XIA card of which there are four per XIA card numbering zero through three. Each event number appears in four rows each corresponding to a channel number indicated in column two all of which is repeated in the second half of the data corresponding with module 2. Column three indicates the uncalibrated energy measured by that channel for that event. Column four contains a time stamp for that event number. The time stamp is used to ensure that the measurements collected by each channel for a given event were all collected simultaneously. This time stamp is an automatically generated identifier created for each event by the XIA cards and does not correspond to any real time as observed by the experimenter.

To analyze this raw data the energies from column three must be calibrated which must be done for each channel individually since they each correspond to a different NaI crystal and photomultiplier tube (PMT). The energy calibration was calculated during the experimental setup phase of experimentation which generated a set of energy calibration equations. For more detailed information on energy calibration of the 2γ3γ system please refer to the experimental setup section of this document in chapter III. These calibration equations are applied during post processing. Once the energies have been calibrated then all the measured energies from all events and from both modules can be graphed out in a histogram to create a gamma spectrum.

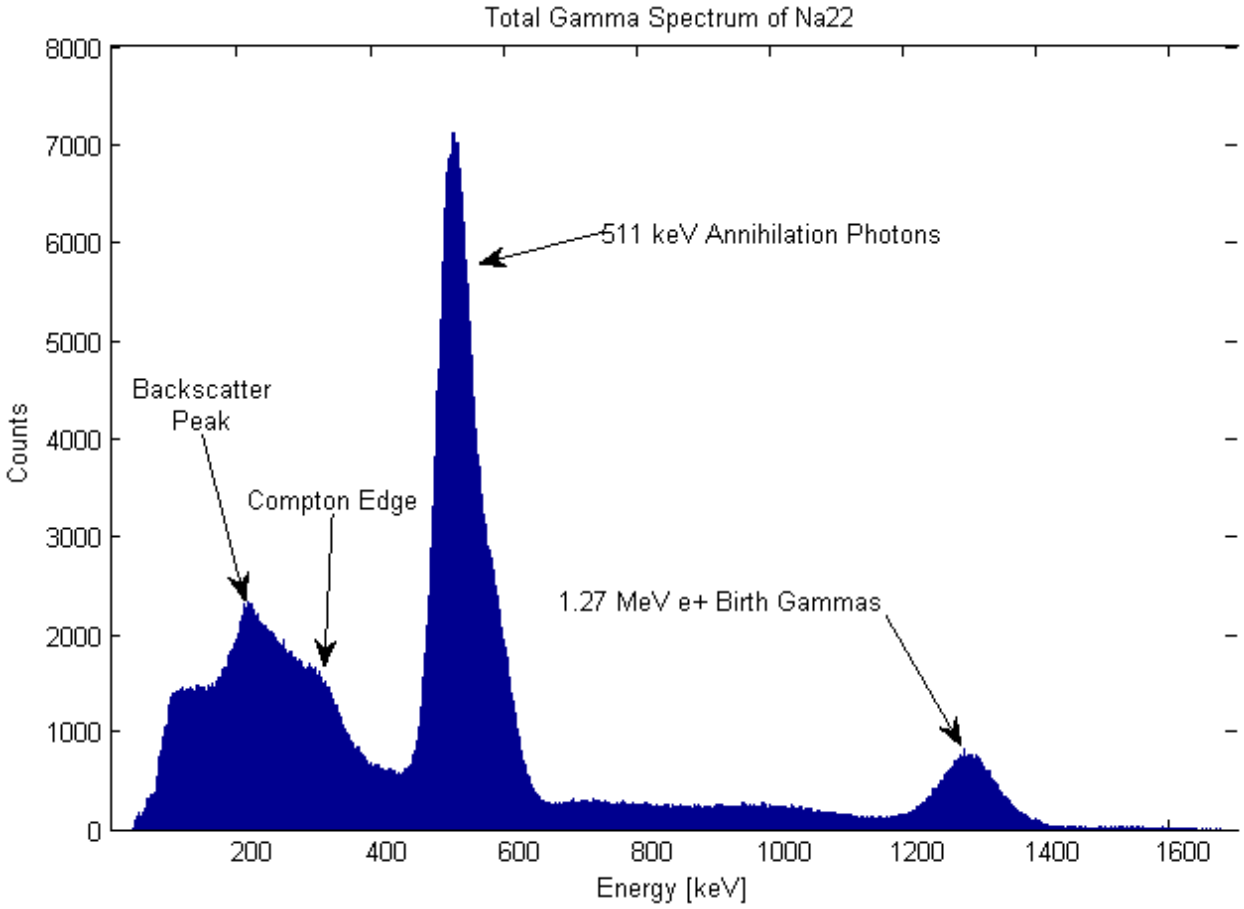

Figure 20. Gamma spectrum of Na-22 from all sections of NaI ring detector

With this spectrum key features can be identified such as the Compton spectrum, positron birth gammas at 1.274 MeV and the positron annihilation photons at 511 keV. Also identified in this spectrum is a peak sitting on top of the Compton edge at approximately 200 keV. At first it was theorized that this peak might correspond to three photon positron annihilation events since they should range in energy from zero to 511 keV peaking somewhere between 200 to 400 keV. Since the expected ratio of two and three photon annihilation events was found to be approximately 370 to 1 by Ore and Powell (1949) and later 372 to 1 as found by Bertolaccini, Bussolati, and Zappathe

(1965) events in the 511 keV photopeak should occur at approximately this same ratio to the events in the 200 keV peak after removing an estimation of the Compton spectrum. This ratio turned out to be approximately 16 to 1 which is significantly different from the 370 to 1 expected which suggests that a different effect is occurring to cause this feature. The experiment is conducted inside of a lead cave; surrounded by all that dense material the possibility of detecting backscatter photons is significant. A photon can backscatter by transferring some of its energy to an electron in the incident material, afterward the photon is deflected at some angle and sometimes it will be deflected by 180 degrees sending it in the opposite direction that it arrived at creating a backscatter. The Compton equation is

$$h\nu' = \frac{h\nu}{1 + \frac{h\nu}{m_0 c^2}(1 - cos\theta)} \tag{9}$$

where $h\nu$ is the energy of the incident photon, $h\nu'$ is the energy of the photon after scattering, $m_0 c^2$ is the rest mass energy of the recoil electron (assumed to initially be at rest), and θ is the scatter angle. In the case of this experiment the dominant photon energy is 511 keV and applying the Compton equation to this energy yields a spectrum of energies depending on the angle of scatter.

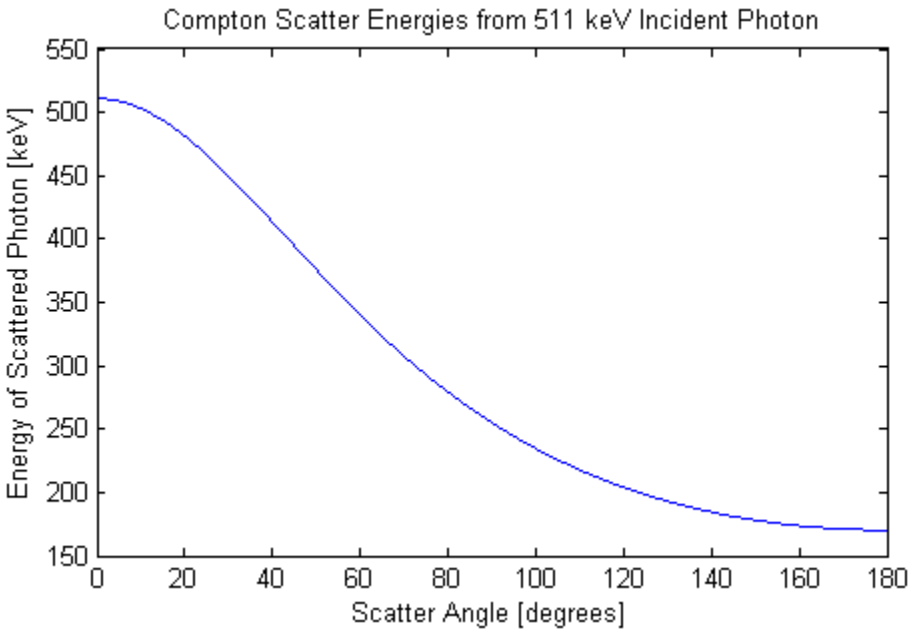

Figure 21. Compton scatter energy by angle of scatter for 511 keV photon

From this plot it can be seen that at true backscattered annihilation photon at 180 degrees would have energy of 170 keV, however it is also far more probable for the photon to scatter at an angle less than 180 degrees according to the Klein-Nishina formula

$$\frac{d\sigma_c}{d\Omega} = r_0^2 \left[\frac{1}{1+\alpha(1-\cos\theta)}\right]^3 \left[\frac{1+\cos\theta}{2}\right] \times \left[1 + \frac{\alpha^2(1-\cos\theta)^2}{(1+\cos^2\theta)[1+\alpha(1-\cos\theta)]}\right] \quad (10)$$

where r_0 is the classical electron radius and α is the photon energy in units of the electron rest energy. The photons do not need to truly backscatter to be detected by the NaI ring detector due to the large size of the ring detector and the close proximity to the lead cave wall. Because of this we would expect any backscatter peak to occur above 170 keV and below the energy associated with a 90 degree scatter which is 255 keV. The majority of the counts in the peak seen sitting on top of the Compton spectrum in the total gamma

spectrum from Na-22 is likely due to backscattered 511 keV annihilation photons and needs to be considered when counting three photon annihilation events since it sits in the same energy range.

In addition to using energy discrimination to identify annihilation events the NaI ring detector allows the implementation of a geometry discriminator. Once the raw data is calibrated in energy annihilation events can be identified by looking at all six channels for each event and determining if energy was detected within a certain range by more than one section of the ring detector. For two photon annihilation events there should be an appropriate amount of energy detected in two sections located opposite from each other in sections A and D, B and E, or sections F and C.

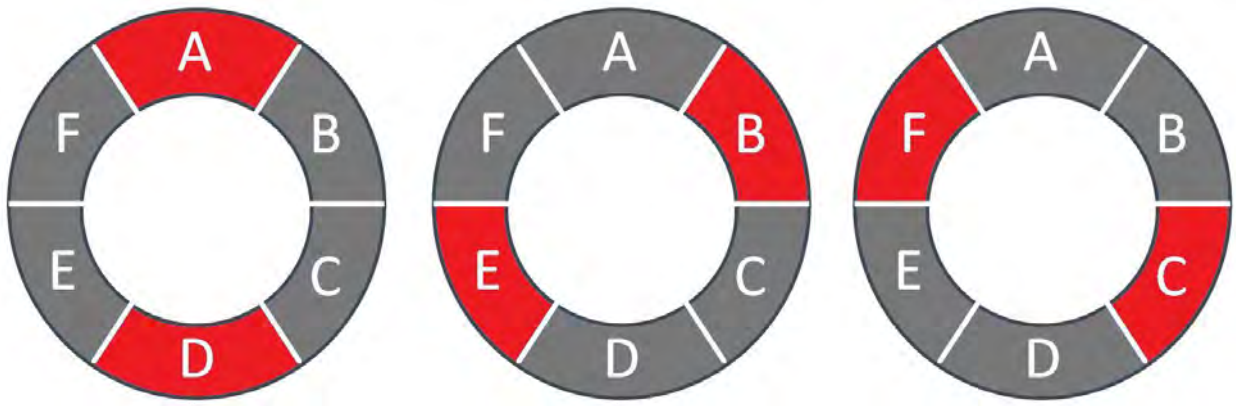

Figure 22. Detection configurations for two photon positron annihilation

For three photon annihilation events there should be an appropriate amount of energy detected in three sections located at 120 degrees from each other since this is the most probable configuration for three photon annihilation.

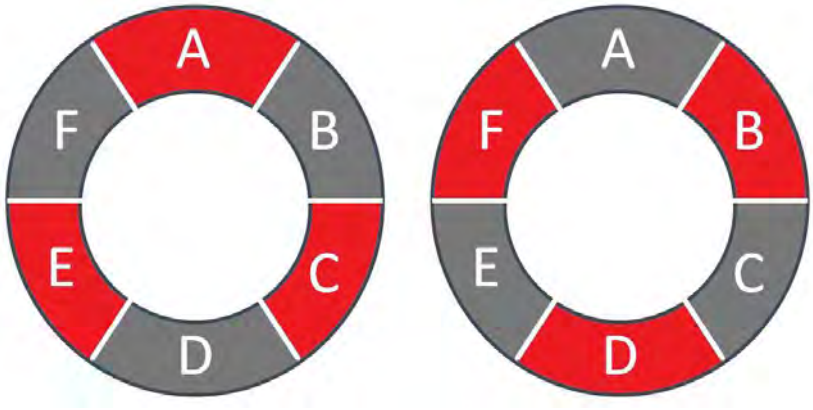

Figure 23. Detection configurations for three photon positron annihilation

If, for a given event, a signal is detected in more than one section of the ring detector at energies associated with either a two or three photon annihilation event and these energies are detected in sections needed to satisfy the appropriate geometry filter then the event is recorded as either a two photon or three photon annihilation event. Due to the mediocre resolution of the NaI detector there is overlap in energy between two and three photon annihilations. By including the geometry filter the uncertainty caused by this overlap is mitigated. Since three photon annihilations occur at lower energies they become mixed with the Compton spectrum of the two photon annihilations at 511 keV and the backscattered photons. Because of this ambiguity the geometry filter is essential for identifying true three photon annihilation events. The geometry filter can also be employed to discriminate backscatter photons from 511 keV annihilation photons that do not deposit all of their energy in the detector since a 511 keV photon must simultaneously be detected on the opposite side of the ring for it to count as a two photon annihilation event. With this in mind, the energies permitted to count a two photon annihilation event do not fall only within the full energy peak but rather extend all the way down into the

Compton spectrum. For two photon annihilations the energy discriminator requires that at least one of the two detected events must be within the full energy peak which helps to reduce the possibility of a false coincidence caused by background radiation. Similarly, the energy discriminator for three photon annihilation searches for events occurring at the most probable energies, however allows for one of the detected events to occur all the way down into the Compton spectrum while remaining above the trigger level.

Both the energy and geometry discriminators described in the previous paragraphs are applied to each event for the entire data run. The energy discriminator is described in more thorough detail in the data analysis code, step by step section later in this chapter. One final discriminator checks the time stamps for each event and ensures that all readings were taken simultaneously within a 50 ns tolerance for a given event. These three discriminators provide the basic framework for how an accurate counting of two and three photon annihilation events can be collected from the raw data.

Barriers to Accurate Data Analysis

The process described in the previous section would be all that is needed to count two and three photon annihilation events if the equipment used to collect data functioned perfectly and an unlimited amount of computer processing power was available. The first barrier to analyzing the data comes from the size of the data files created. Even a short run of just 30 seconds produces an output text file that is several megabytes and is thousands of lines long, far too long to efficiently analyze by hand. To achieve reliable results long data runs must be accomplished to improve the counting statistics of the final numbers. Data runs of 30 minutes or more produce file sizes in the gigabyte range and on the basic desktop computer that was used in this experiment merely attempting to

open these files results in crashing the computer. Even loading the data files into a computer code for analysis without actually opening the file exhausts the computer's memory resulting in an error. Because of this, data handling processes became the dominant barrier early on in developing a computer code for analysis.

Another barrier to data analysis came from the output data file format used by the data collection software, Igor Pro. The output file stacks the data from module 1 in its entirety on top of the data from module 2. This means that the information for a single event is partially located in one section of the data and partially in another section several thousand and sometimes millions of lines later. Furthermore, the header information included at the top of the data file is mostly useless and serves to confuse any analysis code developed. A further complicating factor of the header information is that it appears twice, not just at the top of the document but again for module 2 approximately (but not exactly) half way down the file. But the header information cannot be completely thrown out; there is one piece of important information in there. The start time for module 1, which is found in the first header, must match the start time for module 2, which is found in the second header, or else the data cannot be used. Checking these start times manually and then having a computer code throw out the rest of the header information is not an effectual method since simply opening the file can crash the computer.

Other barriers to analyzing the data come from the fact that the equipment used, particularly the XIA data digitization cards, did not always function exactly as advertised. The first problem was that the event numbers would not always correctly correspond between modules 1 and 2. When a data run initially starts the XIA cards are connected to each other so that every time one channel is triggered by a radiation event all other

channels take a reading at that same time to try to catch a coincident event within a 50 ns window. All recordings taken in this reading are given the same event number and time stamp. However, occasionally one of the XIA cards would take a measurement without activating the other XIA card resulting in an event recorded in only one of the two modules. At the next event the two XIA cards would typically get back in sync with each other however they would record two different event numbers. This abnormality was identified by the time stamp which would be different for the off event and then sync back up for the next correctly recorded event. The longer the system runs the worse this problem becomes. After 30 seconds the events numbers between modules will be off by an average of 12, after 1 minute they are off by an average of 26, after an hour they are off by nearly 2000 events. The time stamp cannot be used as a substitute for the event number to compensate for this because the clock used to generate the time stamp cycles through and resets itself fairly quickly. This means that within several hundred events there is a low but finite possibility of a non-unique time stamp for two different events. When the time stamps do not match between modules 1 and 2 while remaining consistent within an event for a given module it means that one module recorded an event that the other missed, however occasionally the time stamp would be a mismatch within an event and within a given module. The source of this error could not be exactly determined, however it is speculated that this might be an error in triggering the proper 50 ns coincidence window. As longer data runs are conducted to try to improve counting statistics for the results each of these data glitches exacerbate each other.

Although each of these barriers to data analysis is not momentous alone, together they produce a significant hurdle to overcome. A computer code was developed that includes solutions to each of these problems and provides fast and accurate analysis.

Data Analysis Code, Step by Step

Due to the length of the raw data files a computer code algorithm was developed to aid in the data analysis. MatLab was the program chosen in which to develop the code due to MatLab's proficiency at handling large matrices. The full code developed can be found at the end of this document in appendix C. The first task the code needs to do is identify the data file. This is input by the user at the beginning of the code before each data analysis run. At no point does the code open the entire data file at once since this would exhaust the program's memory causing an error. Instead the code reads in the data file only a few lines at a time, first reading in the header scanning for the module start time. This start time is stored for later comparison to the start time of module 2. Once past the header, all four columns of the raw data are read in 10,000 rows at a time and stored in a large matrix in a variable format within MatLab requiring far less storage space than a text document containing the same information. This size of block was chosen because it is small enough to be manageable by the memory resources available in MatLab but large enough to feed in all of the raw data in a timely manner. Each time the code reads in a 10,000 row block of data it is added on to the bottom of the previous block creating one large matrix until it reaches the second header. The code then performs on module 2 the same operations it performed on module 1, scanning the module start time and reading data one large chunk at a time. The result is a variable containing one large matrix with all of the pertinent information from that measurement

run. Because of the size of the matrix this variable is saved in single precision rather than the default double precision. Single precision requires less storage space but has less precision in the individual values. It is a good trade off to forgo the higher precision in exchange for the increase in computing power this provides since the limiting factor on precision is actually the energy resolution of the NaI detector. Once the data are saved into a matrix variable, the document containing the raw data is closed along with other variables created along the way. This is an important step since failure to do so will mean that the program needs to carry large data files along during its other analysis and risks crashing the code out of a lack of available memory. Before moving on, the code compares the module start times that were saved while scanning the header information. If the times match then the code proceeds, if they do not match then the user is presented with an error message.

From here the data are ready for more detailed analysis. The first thing to determine is how many events were successfully recorded free of any equipment glitches. The code compares the number of events in the first module with the number in the second module and takes the fewer of the two as an upper bound. These event numbers will be off because of the error where one XIA card records a measurement without triggering the other. Next, the code systematically combs through the data set reviewing both modules simultaneously checking to see if the time stamp matches for all channels for each event number. If the time stamps do not match within an event then the code checks all measurements in module 2 within 24 rows above and below the expected row to try to find a time stamp that matches that from module 1. Using a range of plus or minus 24 rows was chosen because events are recorded 4 at a time and after analyzing

millions of events they were found to be off by as much as 2 events at a time producing an 8 row abnormality. Just to be certain, this value was tripled to prevent the code from crashing in the unlikely scenario of a 6 event glitch. Using a range of around 2000 in an attempt to be extra cautious causes inaccurate results since it starts to run into the problem of the XIA time stamp clock resetting itself and finding non unique time signatures. Once the corresponding events in module 1 and 2 have been identified by using the time stamp as an identifier the code records the magnitude of the event error. When the code moves on to the next event this event error plus the event number is used as the starting point for identifying matching events between modules rather than the event number alone. This event error increases or decreases each time a new error is identified. By carrying along this evolving event error the code ensures that the event search range of plus or minus 24 will always be sufficient despite the event numbers at the end of the document being off between modules by several thousand.

Once a measurement has been identified with acceptable timing information it is loaded into a new matrix and its format modified. The events between modules 1 and 2 are collated and the channel numbers are altered from a module 1 or 2 channel 0 through 3 format to a simplified one through six. The energy calibration equations are applied at this step and recorded in single precision. The majority of the measurements read zero energy due to the manner in which the XIA cards are wired together to take a reading in all channels each time an event is detected. Only measurements with energy above zero are kept which trims the matrix size immensely yet retaining all relevant data which significantly speeds up processing time. From here the gamma spectra from the

individual channels can be analyzed which is desirable since they will each have their own energy dependant resolutions that need to be identified.

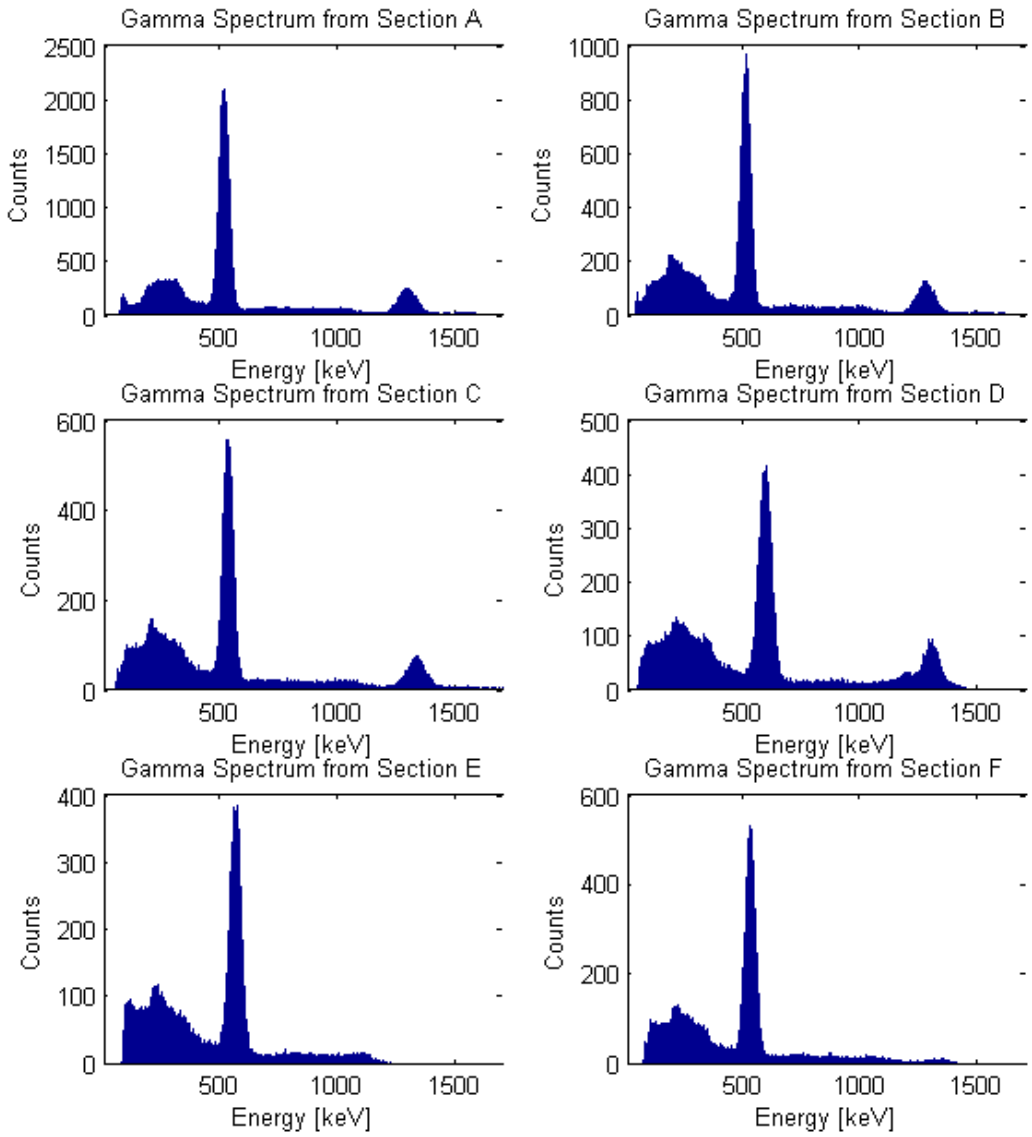

Figure 24. Gamma spectra from NaI ring detector segments displayed individually. These spectra were studied to establish boundaries for energy discrimination for each channel on the 2γ3γ system.

During the experimental setup the resolution of each channel was measured at certain key energies using Igor Pro, however the equations generated for energy

dependant resolution curves did not have strong enough coefficients of determination to be reliable. The resolutions at 511 keV were found to be approximately 7-8% in Igor Pro, however by using the above graphs it is possible to zoom in on the regions of interest to determine acceptable boundary energies manually. The sharp spike at 511 keV on each graph represents the full energy peak of positron annihilation photons. The full width at tenth maximum (FWTM) of this photopeak was used as the upper boundary and the trigger at 40 keV was used as the lower boundary for 2 photon positron annihilation. This liberal energy range is used to catch as many annihilation events as possible, even those that Compton scatter. This range is still reliable because of the added layer of the geometry filter. Another layer of filter is the requirement that only one of the two photons can be a Compton scatter and the other must lie within the full energy peak.

The three photon annihilation curve cannot be visually identified in these graphs due to their low probability. Energy ranges must instead be obtained from theory and the information available. The upper boundary for photon triplet annihilation was determined individually for each channel and is determined by taking several factors into account. The closer the boundary can be pushed to 511 keV, which is the maximum theoretical three photon annihilation energy, the more three photon annihilation events the system will capture. However, there are several factors pulling that boundary down. Although 511 keV is the maximum energy allowable in three photon positron annihilation the probability of any one photon having greater than 500 keV is below 5%. The energy on which the three photon energy filter should primarily be focused is well below the 511 keV limit closer to the most probable energies between 300 and 400 keV. Finally, the greatest risk of error in the three photon energy filter is misidentifying two

photon annihilation events as three photon events. Choosing a value 2σ below the 511 keV photopeak provides a 99.75% certainty that the energy detected is outside of the full energy peak for two photon annihilation events. A value 2σ below the photopeak was determined for each channel individually based on that channel's resolution. Resolutions at this energy ranged from 7-8%. This value was then visually checked on the gamma spectra for each channel in figure 23 and adjusted down if necessary to remain outside the 511 keV photopeak. This provided the upper energy boundary for each channel and the trigger at 40 keV was used as the lower boundary.

In addition to a channel specific energy filter there is also an energy of annihilation filter that ensures that the total energy of all three photons does not exceed 1022 keV, the rest mass energy of the annihilating electron-positron pair. With each photon carrying away a range of possible energies and the resolution of the NaI detector varying significantly with energy it is possible that the sum of the energies detected by these three photons exceeds 1022 keV. To take this into account a scenario is assumed in which the energy of annihilation is parsed equally between three photons, each carrying away 341 keV. The resolution of the detector at this energy is approximately 12% for all sections and it is this resolution that is used to create an upper boundary for the energy of annihilation. The lower boundary assumes the same scenario and allows for one of photons to Compton scatter at as low as 40 keV reflecting that same criterion used in the two photon annihilation detection discriminator. With the appropriate resolutions applied, a lower bound is set for the energy of annihilation filter. This energy of annihilation filter combined with the channel specific energy filter and the three hit geometry filter make up the three photon positron annihilation discriminator.

In most events in the data only one of the NaI ring detector sections detected any energy. These are 1 hit events and no coincidence count is made. Some events have 2 or 3 hits and these measurements then enter either the two or three photon positron annihilation discriminators to determine whether or not a coincidence count can be made. In cases where there are more than three measurements within an event much of the information about the geometry of the event is unknown. With the activity of the sources used in this experiment 5 and 6 hits were extremely rare or not present and their omission from the final counts is unlikely to have significant impact on the results. In 4 hit events some geometry information is inferable when combined with strict energy filters. If hits occur in opposing sections of the ring detector and all energies lie within the full width at half maximum (FWHM) of the 511 keV photopeak then this event is recorded as two simultaneous two photon annihilation events.

Once the code combs through the entire data set with these discriminators all of the two photon annihilation events are summed and compared with the sum of three photon annihilation events. The ratio of these values is the $2\gamma/3\gamma$ annihilation ratio. This ratio does not yet account for background radiation and false coincidences.

Background, Chance Coincidence, and Propagation of Uncertainty

Measurements were taken on a variety of sources using the $2\gamma3\gamma$ system and the data were analyzed using the computer algorithm described in the previous section. One of the sources analyzed was a monocrystalline copper ingot with Na-22 dopant. The activity of this source was found by 2nd Lt Robert Slaughter to be 0.29 μCi on 22 December 2009 using a high purity germanium (HPGe) detector and was calculated to be 0.18 μCi on 4 November 2011 at the time of measurement for this project. The positrons

created from the radioactive β+ decay of Na-22 are born into and annihilate with electrons in the unadulterated copper. This source was measured to obtain a baseline for the two to three photon annihilation ratio of Na-22 under controlled conditions. The computer algorithm separates out two and three photon annihilation events making it possible to graph the gamma spectrum from these types of events individually.

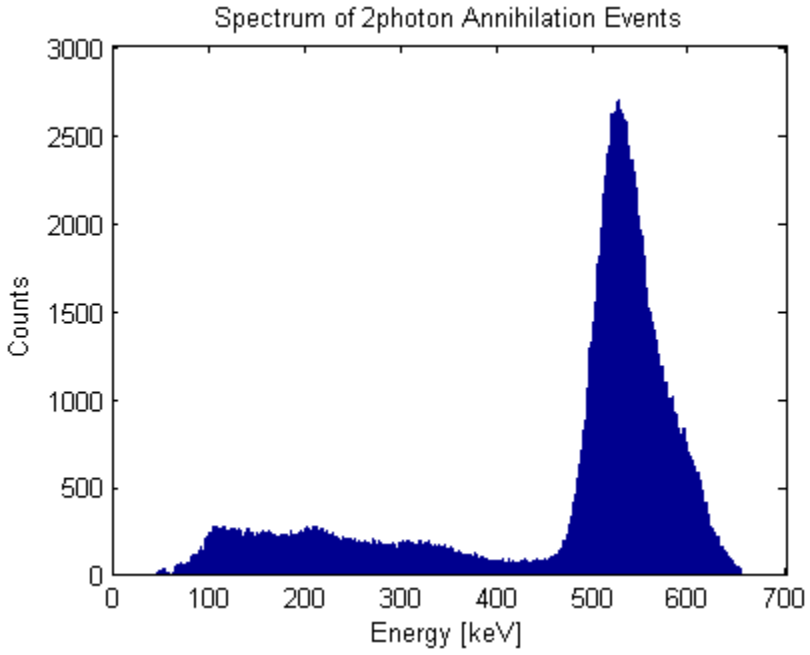

Figure 25. Two photon annihilation events from a Na-22 copper source stripped from the total gamma spectrum by the energy and geometry discriminators developed in the analysis code. Data was collected for 15 minutes

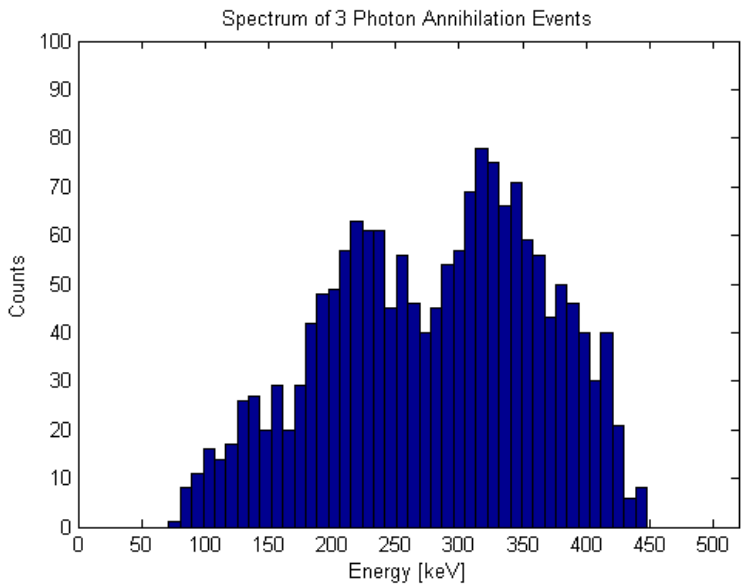

Figure 26. Three photon positron annihilation events stripped from total Na-22 gamma spectrum by data analysis code. A backscatter peak appears just above 200 keV.

Both of these spectra were generated from the copper encased Na-22 source in the same data run with a 15 minute measurement duration. In both the two photon coincidence spectrum and the three photon coincidence spectrum there is a small bump just above 200 keV which likely represents a small number of false coincidences generated by an increased probability of backscatter photons at that energy. A correction for this effect is generated later from a spectrum of Sr-85 which experiences the same backscatter effect.

The distribution of counts on both spectra lend credence to the supposition that the energy and geometry filters are correctly able to identify and discriminate two and three photon annihilation events since they are consistent with the theoretical distribution. The two photon annihilation spectrum clearly shows a full energy peak at 511 keV with the associated Compton continuum at lower energy. The theoretical three photon

distribution in energy, as derived by Ore and Powell, can be graphically represented as a normalized probability.

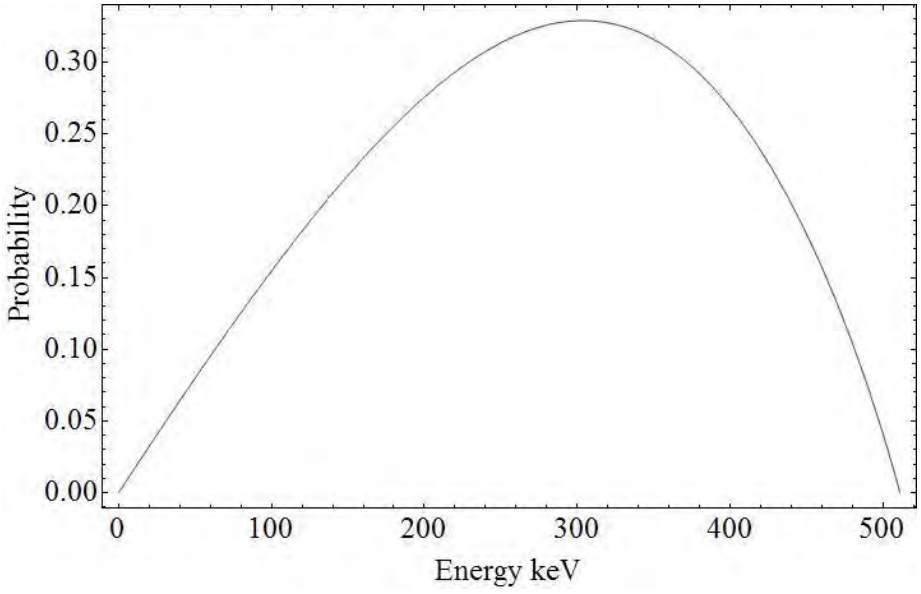

Figure 27. Normalized probability distribution of photon energy for three photon annihilation[10]

This theoretical distribution compares well with the experimentally observed distribution seen in figure 26. It can be seen from a comparison of these two figures that many of the higher energy three photon annihilation events are not identified in the experimental results. This is likely because higher energy photons from three photon annihilation events are emitted at an angle relative to the other annihilation photons that would be discriminated out by the geometry filter.

The experimentally measured $2\gamma/3\gamma$ ratio is compared to the 372 to 1 theoretical value[23]. The total measurement of this source was taken over several runs varying in duration from 30 seconds up to 1 hour for a total duration of 7 hours.

Table 5. Raw Coincidence Counts from Na-22 Copper Standard Source

Na-22 Encased in Copper				
Duration	2g / 3g	per hour	Ratio	Uncertainty
7 hours	6079276	868468	342.46	2.57
	17752	2536		

The reason that the ratio of 342.46 ± 2.57 is different than the theoretical 372 is that the detector has a different efficiency for measuring two photon annihilation events than it does for measuring three photon annihilation events. A ratio between the theoretical and experimental values of the copper sample is used as a correction factor by which all other samples measured on the 2γ3γ system are multiplied. This accounts for the difference in measurement efficiency of two and three photon annihilation events. Another contributing factor to the difference between the observed ratio and the theoretical ratio that should be mentioned is that, as noted earlier, there are likely backscatter photons that are contaminating the three photon annihilation coincidence counts which would drive the ratio down. A more thorough investigation of this effect needs to be conducted if future work is to be performed with this system.

All the measurements taken on the 2γ3γ system are compared to each other on a per hour basis since it provides a useful comparison for different sources that were measured over different durations, none for less than at least one hour. By assuming that errors in measurement are governed by the Gaussian distribution, uncertainty in the 2γ/3γ ratio is determined by adding in quadrature.

$$\left(\frac{\sigma_R}{R}\right)^2 = \left(\frac{\sigma_{2\gamma}}{N_{2\gamma}}\right)^2 + \left(\frac{\sigma_{3\gamma}}{N_{3\gamma}}\right)^2 \tag{11}$$

In this equation $N_{2\gamma}$ is the number of two photon annihilation events detected, $N_{3\gamma}$ is the number of three photon annihilation events detected, R is the ratio of those values, and $\sigma_{2\gamma}$, $\sigma_{3\gamma}$, and σ_R are their corresponding uncertainties. This measured ratio of 342.46 ± 2.57 seems reasonable when compared to the theoretical 372, however, this value does not account for background radiation or chance coincidences.

To gain an understanding of the background radiation a measurement was taken using the NaI ring detector with no source present. A total gamma spectrum was obtained along with the parsed out spectra of false coincidence in two and three photons.

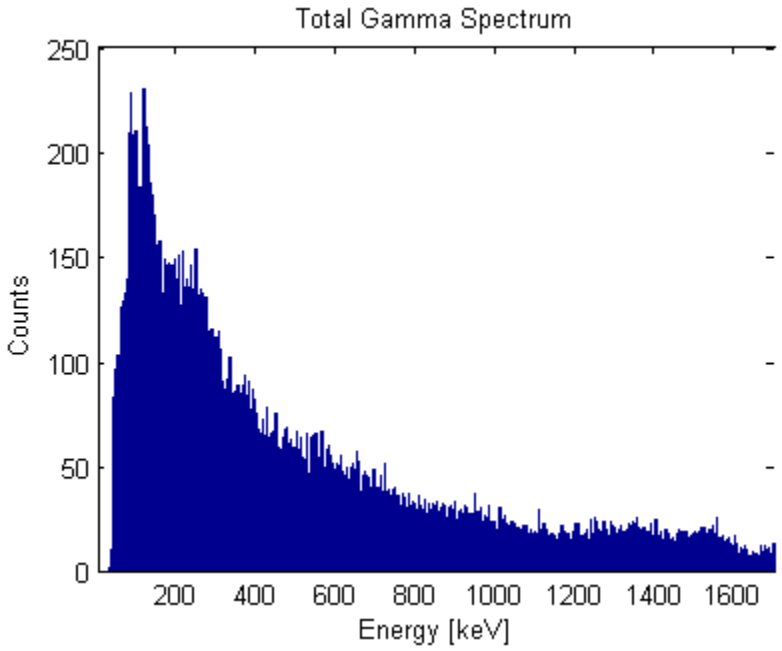

Figure 28. Total background radiation inside lead cave using NaI ring detector. This measurement was made for one hour.

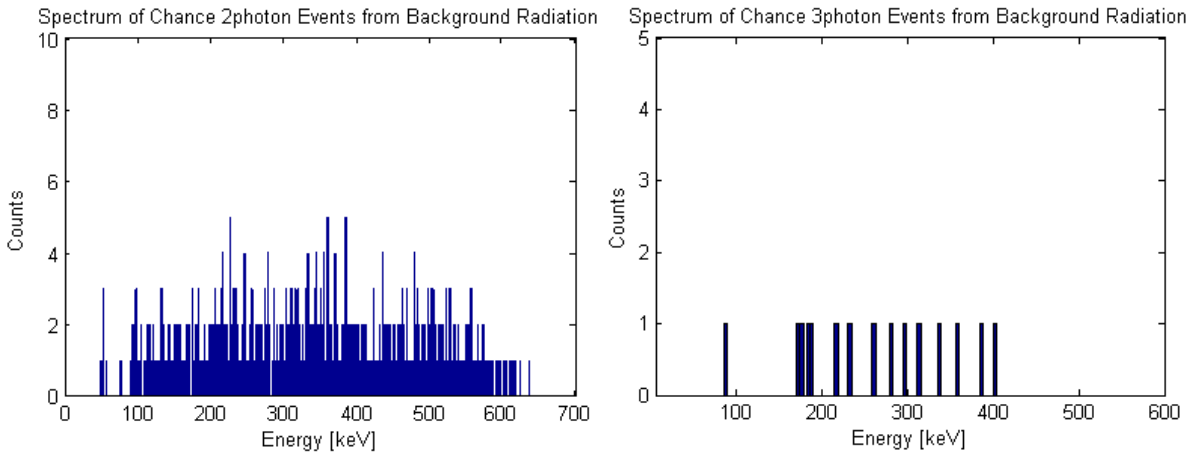

Figure 29. The background radiation inside the lead cave produced a small number of (left) two and (right) three photon chance coincidences.

With no source present this spectrum, generated from a 1 hour collection run, demonstrates both the increased presence of background radiation at lower energies and the increased efficiency of the NaI detector at low energy. This background generated several false two photon and a small number of false three photon coincidences. The false coincidence counts from background radiation are subtracted from the coincidence counts made when a source is present. Uncertainty in the background is determined by assuming that errors in measurement follow the normal distribution. Since measurements are being compared to one another on a per hour basis this needs to be accounted for in the uncertainty by appropriate propagation of error using

$$\sigma_{p/h}^2 = \left({}^1/_d\right)^2 \sigma_{tot}^2 \qquad (12)$$

where σ_{tot} is the uncertainty in the total coincidence count, $\sigma_{p/h}$ is the uncertainty in the coincidence count calibrated to a per hour basis, and d is the duration of the total measurement in hours.

Table 6. Chance Coincidence from Background Radiation in Lead Cave

Background Radiation in Lead Cave			
Duration	2g / 3g	per hour	Uncertainty
4 hours	1564	391	9.89
	20	5	1.12

Propagation of the uncertainty due to subtracting background coincidence counts is performed using the following equation

$$\sigma_{corrected}^2 = \sigma_{count}^2 + \sigma_{bg}^2 \quad (13)$$

where $\sigma_{bg}$is the uncertainty in the background counts, σ_{count} is the uncertainty in the uncorrected measured coincident counts, and $\sigma_{corrected}$ is the resultant uncertainty in the coincident counts after subtracting background counts.

The next factor that needs to be accounted for in the 2γ/3γ ratio obtained from the Na-22 in copper sample is chance coincidences. It is possible to simultaneously detect more than one photon from two different events resulting in a chance coincidence rather than a true coincidence. To measure chance coincidence Sr-85 is used in this experiment. The radioactive decay of Sr-85 is dominated by the release of a 514 keV gamma ray, very close in energy to the 511 keV positron annihilation photons. These photons are emitted isotropically and are not coincident with each other. The NaI ring detector has approximately the same efficiency and resolution at 511 and 514 keV so the coincidence counts detected from Sr-85 serve as a useful estimate for the number of chance coincidences that might come from uncorrelated positron annihilation photons from Na-22.

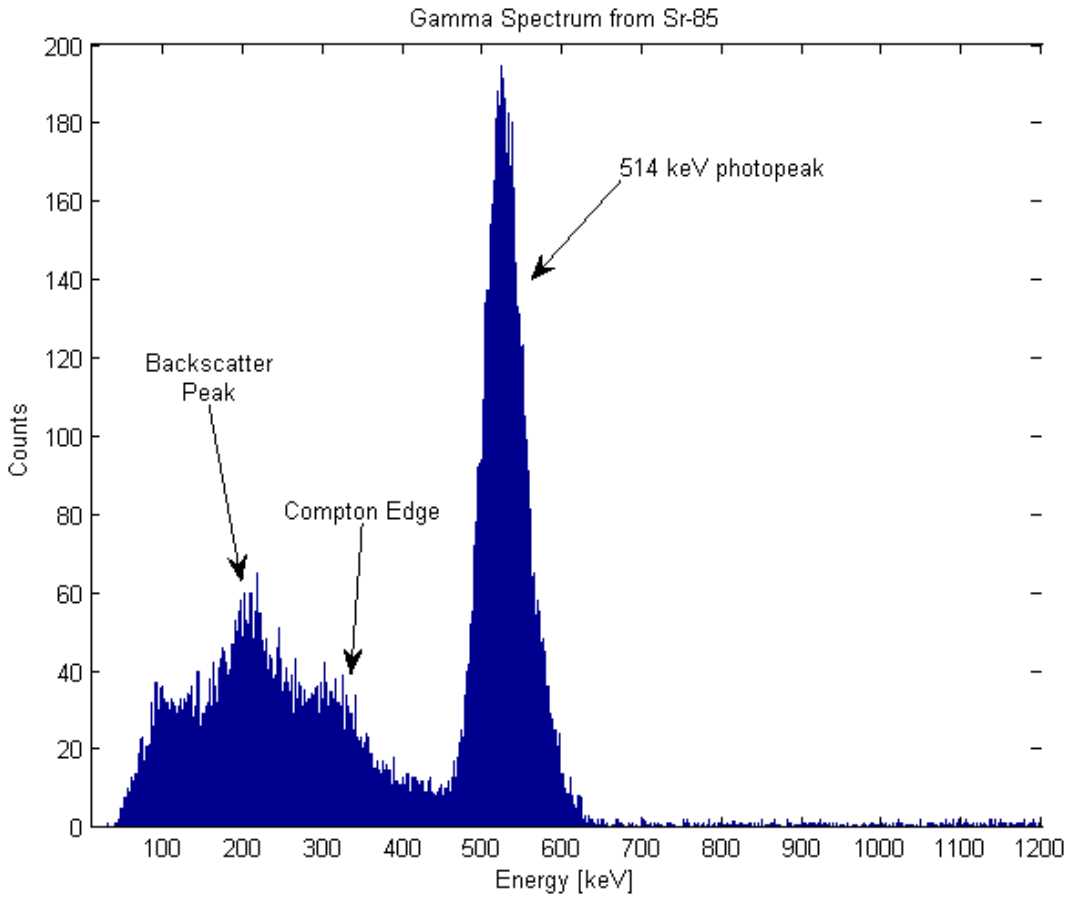

Figure 30. Gamma spectra from Sr-85 collected using the NaI ring detector. With a photopeak at 514 keV, very close to the 511 keV for Na-22, this source was measured to obtain an estimate of false coincidences resulting by chance from photons.

The total gamma spectrum from Sr-85 was compiled from the six section of the NaI ring detector and key features were identified. The presence of a small peak at approximately 200 keV in the Sr-85 spectrum provides further evidence that a similar peak found in the Na-22 spectrum does in fact result from backscatter photons rather than from three photon annihilation events. The presence of this feature in the Sr-85 spectrum allows for the correction of false coincidences resulting from the same effect in the Na-22 spectrum.

Table 7. Gamma Ray Chance Coincidence Correction from Sr-85

Sr-85						
Duration	2g / 3g	w/o noise	per hour	Uncertainty	Activity	cps
5 hours	5763	3808	761.60	15.31	2.67 μCi	64866
	29	4	0.80	1.10		

The rate of chance coincidences generated by the effect detected in Sr-85 is dependent on the activity of the source, the higher the activity the more frequently chance coincidences will occur. Also, a higher activity source will result in increased pileup in the detector. To account for this, this effect needs to be calibrated from one source to another based on the detected counts per second (cps) of that source before chance coincidence can be subtracted from the raw data. The appearance of the backscatter feature identified in the three photon annihilation plot identified earlier in figure 26 seems to suggest that false coincidences are generated at a higher rate than is accounted for in the correction factor generated using the Sr-85 spectrum. This is likely due to the high level of backscattered radiation that occurs inside the lead cave. This effect could be mitigated by moving the experiment out of the lead cave and away from any surfaces that might cause backscattering. The lead cave however provides shielding from background and cosmic radiation which would cause further signal degradation. Future work could make a comparison between these two scenarios.

With the correction factors available taken into account the $2\gamma/3\gamma$ ratio with the appropriate propagation of uncertainty becomes 342.97 ± 2.59 and can be used as a baseline of comparison to other measured $2\gamma/3\gamma$ measurements. This value is different from the theoretical ratio of 372 because of a difference in efficiency for detecting two

photon annihilations and three photon annihilations. The resolution of the NaI ring detector varies by energy so photons emitted in the three photon annihilation energy range are slightly more likely to be detected. Also, three photon annihilations can emit at a variety of angles, any orientation with any one angle less than or equal to 60º will be missed because of the geometry filter. Furthermore, the ring detector does not cover all possible directions that the annihilation photons can travel and the detector may miss one or more of the annihilation photons from two or three photon annihilation events at different rates. Finally, the 2γ/3γ ratio is likely influenced by the presence of 1.274 MeV positron birth gammas. The NaI ring detector is not optimized to detect these photons so they likely Compton scatter within the detection region which means that there is a possibility that they could be mistaken for an annihilation photon. The effect of chance coincidence from birth gammas cannot be taken into account from the Sr-85 data since no birth gammas are present there. The individual effects of each of these factors are unknown, however the cumulative effect of them is that the 2γ/3γ ratio comes out to 342.97 ± 2.59 rather than the 372 one expects from theory. This value is not far off however and a ratio between this value and the theoretical value provides a correction factor for all other measurements made on the 2γ3γ system.

Capillary Tube Results

A thin capillary tube filled with Na-22 was placed under vacuum to a pressure of less than 10^{-3} torr and a potential difference was applied across the inner and outer capillary tube walls. The activity of the capillary tube source was found to be 126 nCi, determined by comparing the counts per second from the tube to the counts per second from another Na-22 source (T107) with a known activity. The magnitude of the voltage

bias placed on the tube wall was varied from 0V to 2500V and the assembly was placed in the NaI ring detector. Measurements were taken for two hours for each data point and the effect of the change in bias on the two to three photon positron annihilation ratio was analyzed. Two additional hours of data were collected for the 0V and 700V points to improve the counting statistics and reduce the uncertainty. Correction factors for background radiation and chance coincidence were, as described in the previous section, taken into account in the final results. A full accounting of the results can be found in appendix D. The results were graphed as a function of applied voltage to see if the voltage has any appreciable effect on the ratio or on the two or three annihilation photon counts.

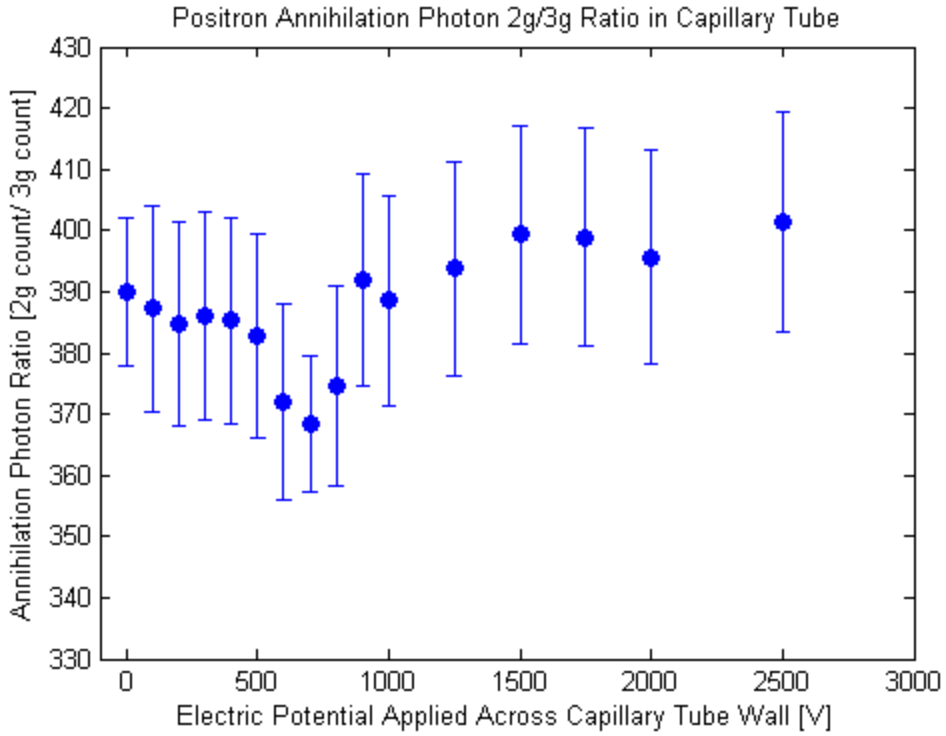

Figure 31. Positron annihilation photon pair/triplet ratio measured from the capillary tube source. Measurements were taken for 4 hours at 0 V and 700 V. At all other voltages measurements were made for 2 hours. The ratios in this plot are calibrated to the known ratio from a Na-22 copper source.

A dip in the ratio appears to form between 600 and 800 V the identification of which was the motivation for the additional data collection at 700V. The $\pm 1\sigma$ error bars suggest that this dip might be an artifact of the uncertainty. The statistical significance of this dip is determined using a student's t-test where the values from 600 to 800 V are compared to the values from 300 to 500 V and compared the values from 900 to 1250 V. The values from 300 to 500 V are also compared to the values from 900 to 1250 V. If this dip is statistically significant rather than an artifact of the uncertainty then it could correspond to an increase rate of positronium formation at the surface of the capillary tube wall.

A paired t-test where the variance is unknown was performed on the ratio data using an α-value of 0.05 meaning that a confidence of 95% is required to reject the null hypothesis. In this case, the null hypothesis is that the difference between the values across one set of voltages as compared to the values across another set of voltages is stasis. That is to say that there is no difference in the measurements compared. The results of the t-test confirmed that the null hypothesis can be rejected when comparing the dip feature to the values at voltages both above and below it with a confidence of 98% and 96.34% respectively. The null hypothesis, which again is that of stasis, could not be rejected when comparing the values surrounding the dip feature. This means that the dip in the ratio from 600 to 800 V is statistically significant and corresponds to a change in the annihilation ratio of positrons over that voltage range.

A further step that can be taken to determine if the dip in the ratio is a real effect or not is to check if there is a corresponding dip in the two photon annihilation events and an increase in the number of three photon annihilation events.

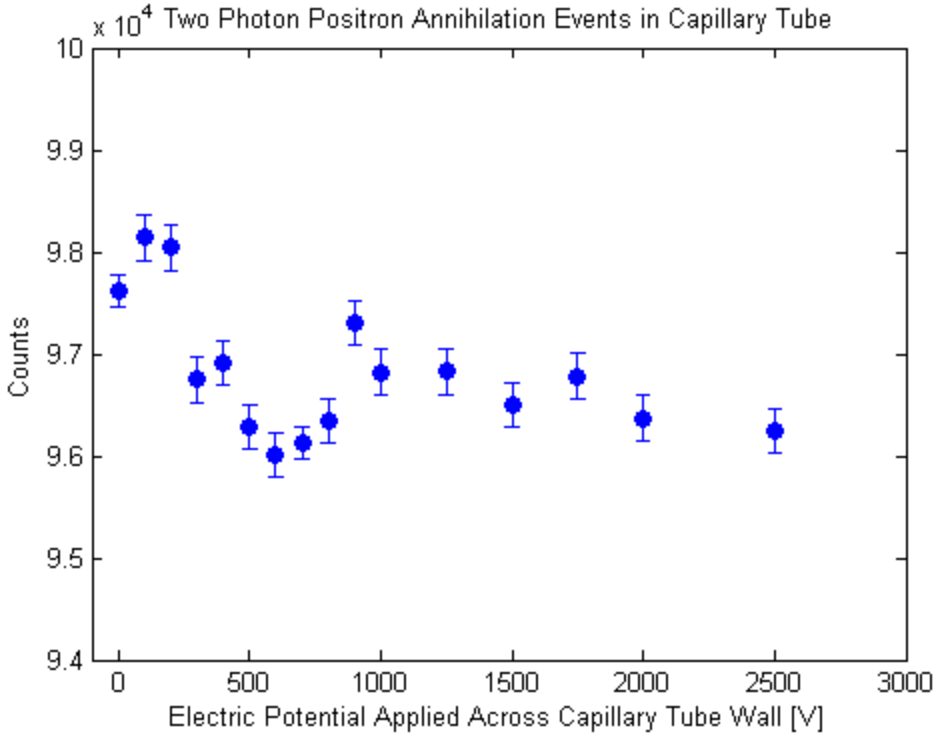

Figure 32. Positron annihilation by emission of two photons from the capillary tube at a range of applied voltages. Measurements were taken for 4 hours at 0 V and 700 V and for 2 hours at all other voltages. Counts are reported on a per hour basis to allow for common comparison.

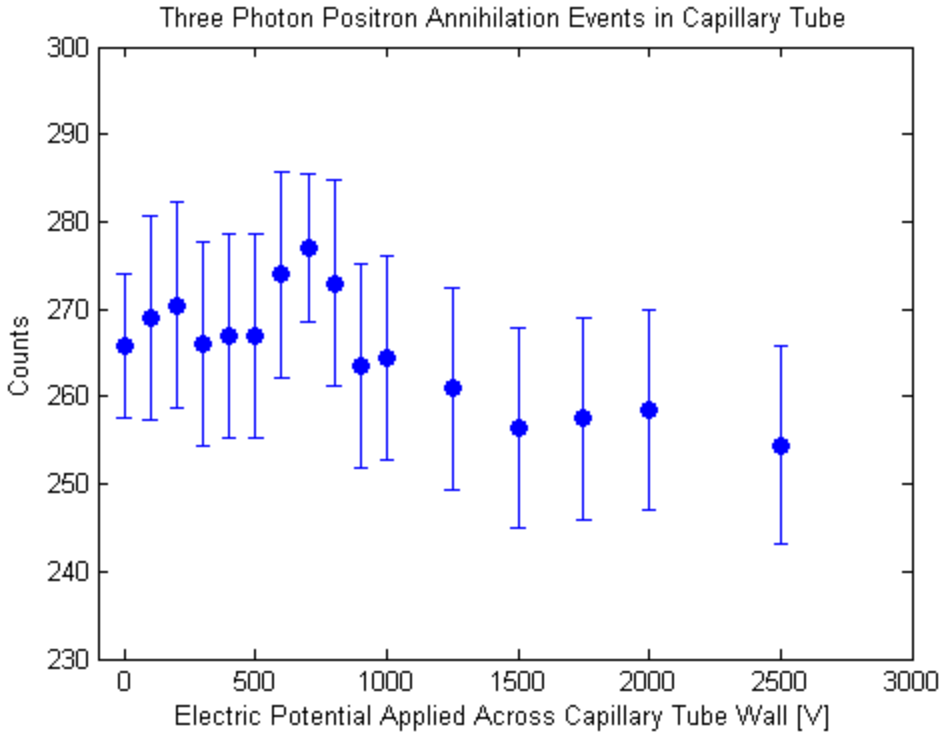

Figure 33. Positron annihilation by emission of three photons from the capillary tube at a range of applied voltages. Measurements were taken for 4 hours at 0 V and 700 V and for 2 hours at all other voltages. Counts are reported on a per hour basis to allow for common comparison.

A dip in the two photon annihilations appears to occur at a voltage range that corresponds with the dip in the ratio over the same voltage. This difference is clearly significant even considering the error bars. Again the assumed hypothesis is a null hypothesis, that there is no difference between the set of values observed. A t-test confirmed that this null hypothesis can be rejected with a 95% confidence using the same voltage grouping used for the ratio comparison. In the three photon annihilations a peak appears to form over the same voltage range which could indicate the formation of positronium, however the peak does not rise above the $\pm 1\sigma$ error bars. A null hypothesis of stasis is assumed and a t-test was performed on the three photon annihilation events which did not reject this null hypothesis. The rise in the rise in the three photon

annihilation rate is statistically significant with only an 89.5% confidence. A full accounting of all t-tests performed on this data can be found in appendix E. With all three graphs showing a consistent pattern, the 2γ3γ system over the voltage range from 600 to 800 V appears to have demonstrated a change in the two and three photon annihilation ratio consistent with an increased rate of positronium formation.

The rise seen in the two photon annihilations seen at 100 V is consistent with results found by 2nd Lt Ariella Walker whose work focused on these lower voltages. Her work found this effect to peak at 75 V and to taper off at higher voltages up to 300 V. The work presented in this paper observes voltages much higher and demonstrates a sudden jump in this effect at voltages higher than 800 V. This likely corresponds with positronium either being ejected from the surface of the capillary tube or positrons arriving at the surface with more energy than is optimal for positronium formation. One would expect this to occur at a much lower voltage if the surface of the capillary tube were clean and the gold layer smooth[7].

Lt Walker calculated that at 600 V applied across the capillary tube wall the applied field at the capillary surface corresponded to 50 kV/cm. The para-positronium intensity is expected to be depressed by about 5% at this field strength[39]. The results found in this project show a reduction of approximately 2% in the two photon emission and an increase of approximately 3% in three photon emission. Since many positrons are likely being lost at the surface, ejected by the high electric field strength, these observed experimental values are comparable and consistent with the expected change.

Conversely, other experiments[13] have suggested that positronium pickoff annihilation is much more dramatically influenced at this field strength which would

indicate a discrepancy between results. It is possible that the fields observed using the $2\gamma 3\gamma$ system in this experiment are capable of altering pickoff annihilation of both ortho- and para-positronium.

It is also interesting to note that the effect seen at the voltages surrounding 700 V reaches a dip in the ratio down to 368.35 ± 11.21 which is very close to the 372 theoretical ratio in copper while the ratio in the capillary tube is much higher at other voltages. This suggests that the capillary tube which, although gold coated, is made mostly from silica with an applied electric field of 700 V is as conducive to positronium formation as copper metal.

Positron Lifetime Spectroscopy

Interpreting the Data

To obtain positron lifetime measurements the scintillation material chosen was barium fluoride (BaF_2) due to its fast response time. The tradeoff of this fast response is that BaF_2 has poor energy resolution and poor efficiency at high energy. This effect is limiting to a point that key features, including full energy peaks, can be difficult to identify. The setup of this experiment of having the photomultiplier tube (PMT) connected directly to the oscilloscope was also chosen to optimize timing information. The lack of any pulse shaping electronics exacerbated the poor energy resolution of the BaF_2 scintillation crystal. Raw data were collected using the MatLab lifetime digital data collection code described in chapter III which is designed to communicate with the oscilloscope and can be found in its entirety in appendix F. This code creates a collection of large matrices called sets and each column of a set contains the digital data points of

one waveform as detected by the oscilloscope. The number of sets in a data collection run and the number of waveforms in a set are all adjustable in the code along with several other parameters to optimize energy resolution and sampling rate. The limiting factor in the timing resolution of each waveform is the sampling rate of the oscilloscope which must be divided equally between each channel in use on the oscilloscope.

Positron lifetime spectroscopy from Na-22 relies on the detection of a positron birth gamma at 1.274 MeV which is emitted 3.7 ps after the positron. Lifetime measurements also depend on the detection of the 511 keV annihilation photons which result when the positron mutually annihilates with an electron. The difference in time between the birth gamma and the annihilation photon, plus the 3.7 ps delay, is the lifetime of the positron. When positrons annihilate they can emit photons at energies other than 511 keV such as is the case in three photon annihilation. However, these cases are ignored in lifetime measurements since they occur at a lower probability. The first step to obtaining lifetime measurements from this data is to identify waveforms that correspond to positron birth and which correspond to positron annihilation. With pulse shaping electronics such as a preamplifier or linear amplifier these effects can be identified as features in a gamma spectrum, however without them this identification becomes challenging.

The first attempt made was to create a histogram of the largest value of each waveform which corresponds with the waveform peak voltage. The idea of this approach is that higher energy radiation will deposit more energy in the scintillation crystal and in turn produce a higher peak voltage in the resultant waveform. By graphing out these peak voltages is was hoped that something similar to a gamma spectrum could be created

and key features identified. Radioisotopes Na-22, Cs-137, Sr-85, Fe-55, and Co-60 were all analyzed using both a small BaF_2 crystal and a large BaF_2 crystal. This was performed until 100,000 waveforms were collected for each radioisotope on each detector. The duration of these runs varied by the activity of the source and the efficiency of BaF_2 at the peak energy emitted by the particular radioisotope being measured and could last for several hours each. Starting with the simplest case, Cs-137 has only one full energy peak and at 662 keV this peak is conveniently located between the two energies of interest in Na-22. If the full energy peak from Cs-137 could be identified in the peak voltage spectrum then it could provide a useful point of reference in a Na-22 spectrum.

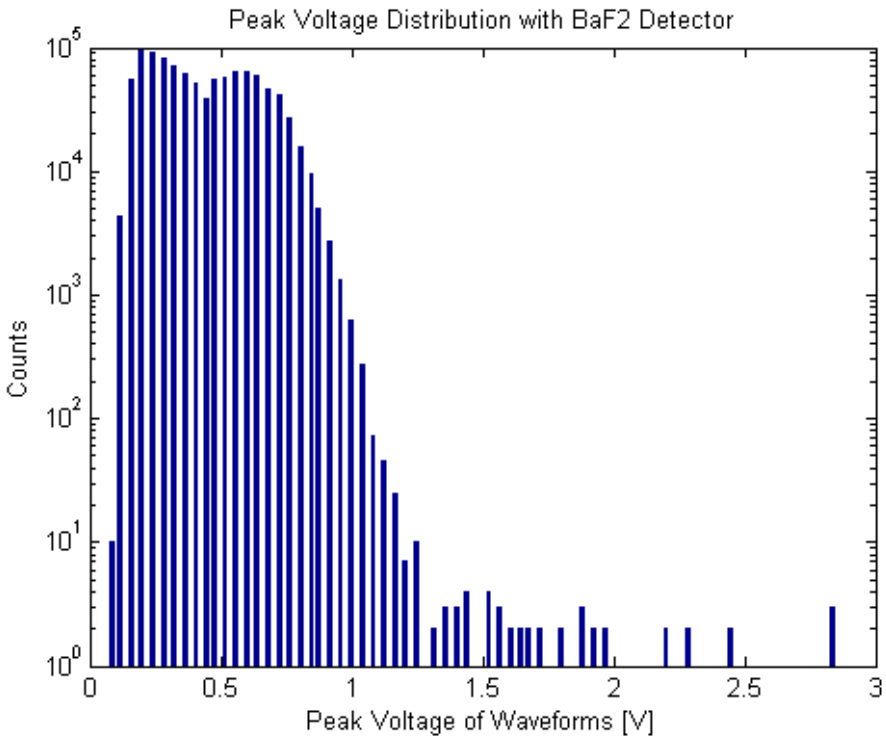

Figure 34. Peak voltage distribution of waveforms collected from Cs-137 using a BaF_2 detector. Significant features are not readily identifiable.

Unfortunately, BaF_2 is more sensitive at low energy and therefore highly susceptible to noise. This, combined with the poor energy resolution of BaF_2, meant that no key features could be definitively identified from the peak voltage histogram nor could they be identified from any of the other radioisotopes measured.

Although the peak voltage distribution concept was still valid, a fresh perspective on the response of the BaF_2 scintillation crystals was needed. The detectors were then connected to pulse shaping electronics and the GammaVision software. This experimental setup is described in further detail in chapter III. The purpose of this setup was to optimize the energy resolution of the BaF_2 detector despite sacrificing timing information. The detector was left to run overnight, long enough until key features in the Na-22 spectrum could be identified.

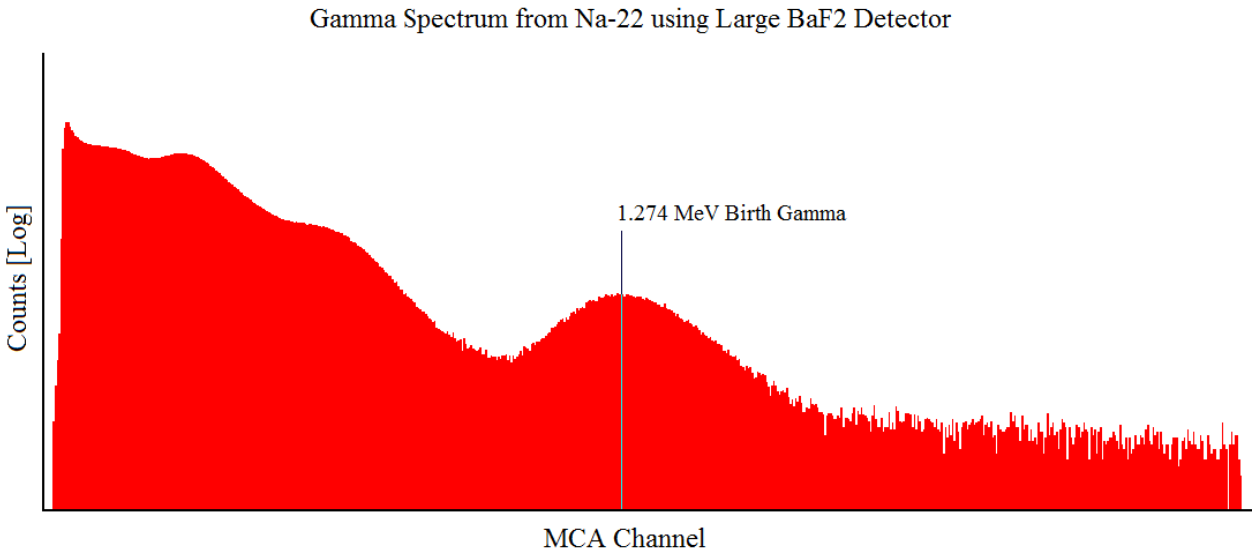

Figure 35. Spectrum of Na-22 with BaF_2 detector highlighting birth gamma

Viewing the spectrum with the vertical axis set to logarithmic scale revealed a peak believed to be the result of positron birth gammas. Lower energy features can be seen, but are better identified on a linear scale.

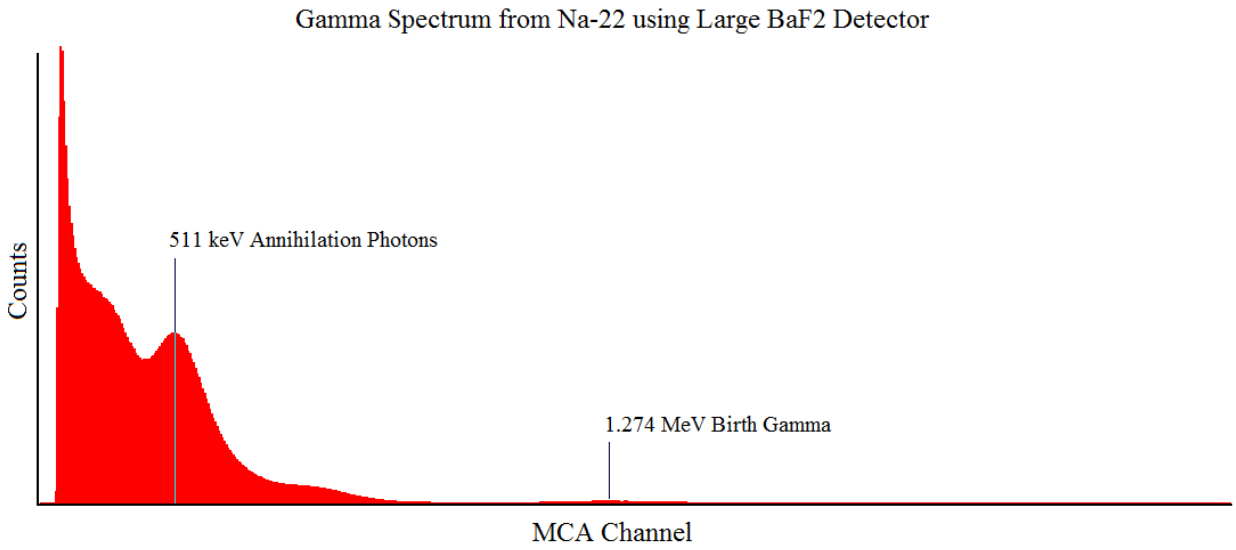

Figure 36. Na-22 spectrum with BaF_2 detector highlighting positron annihilation

The features identified in the gamma spectrum of Na-22 were confirmed by comparing a similar spectrum from Cs-137 which exhibited a 662 keV peak at an appropriate bin between the two peaks identified from Na-22. This process was repeated using the small BaF_2 crystal; the 511 keV photopeak was identified and again compared to Cs-137, however the photopeak from the birth gammas could not be clearly identified.

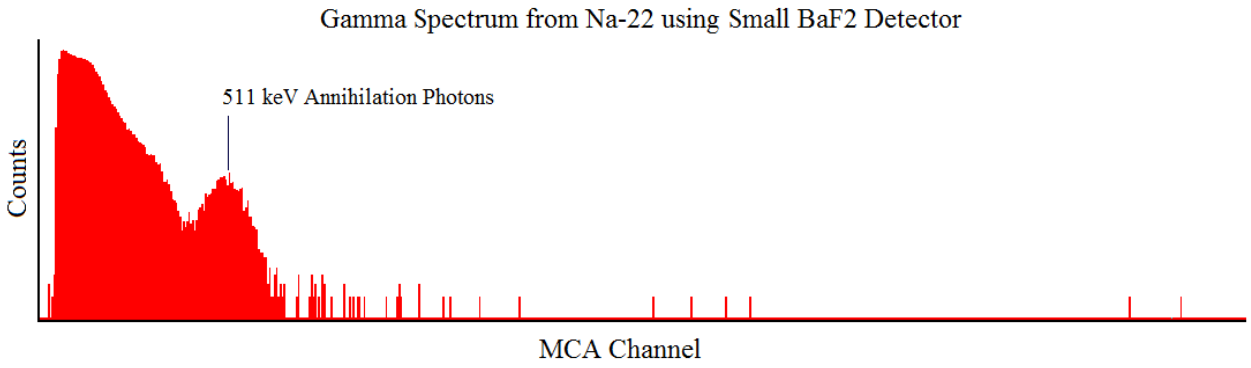

Figure 37. Gamma spectrum from Na-22 with small BaF_2 detector

The poor counting statistics in the region expected to correspond with positron birth gammas in the smaller BaF_2 crystal is likely due to high energy gamma rays passing right through it without depositing all of their energy. Because of this, during positron lifetime measurements, the small BaF_2 detector is set up to detect annihilation photons while the large BaF_2 detector is set up to detect positron birth gammas.

These spectra provide a general idea of the BaF_2 scintillator response to radiation from Na-22 and serve as a guideline as to what features can be identified from graphs generated from the data collected using the first positron lifetime spectroscopy experimental setup. To accurately analyze these data the MatLab code needs to recreate those functions performed by the pulse shaping electronics. The first device added in the second experimental setup is the preamplifier which, while keeping the output pulse rise time short, makes the decay time large to allow for full collection of the charge from the PMT to occur before decay of the pulse sets in. Without a preamplifier the signal to noise ratio can become very small. The first step to simulate this function within MatLab using only the raw waveform data was to observe the waveforms themselves.

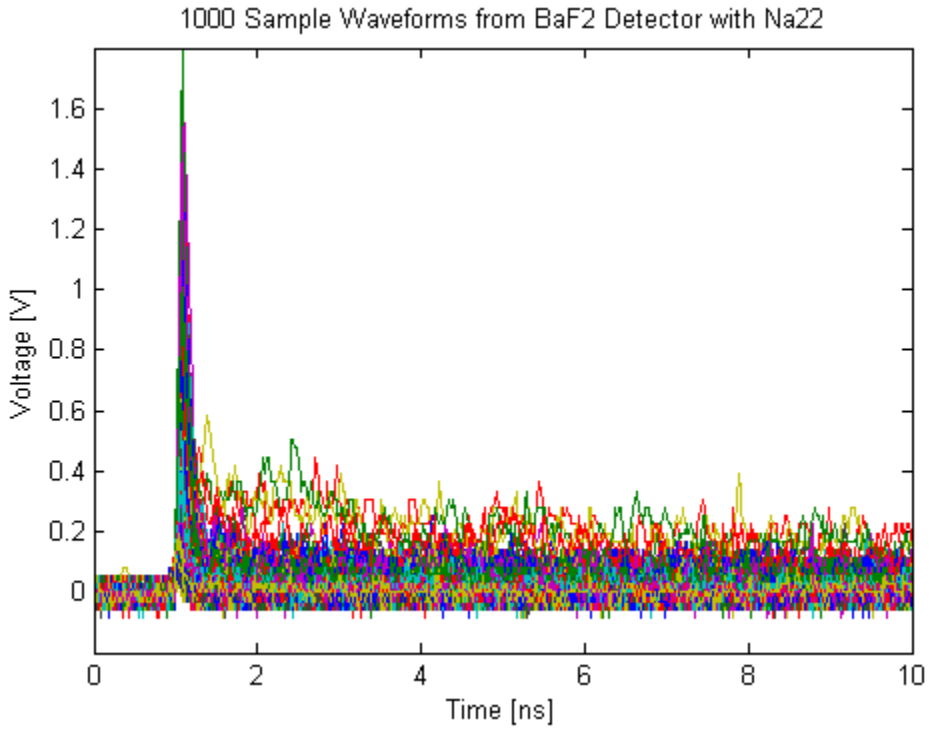

Figure 38. Set of 1000 waveforms from large BaF_2 detector revealing general behavior and fast decay.

Observing a full set of waveforms at once reveals the general behavior of all types of waveforms. Before the trigger at 1 ns they all behave similarly, however after the trigger they decay by a range of decay times and some continue to fluctuate wildly long after the initial triggering event. By viewing waveforms one at a time it can be seen that many of the waveforms display a quick rise time and have a slightly longer decay time.

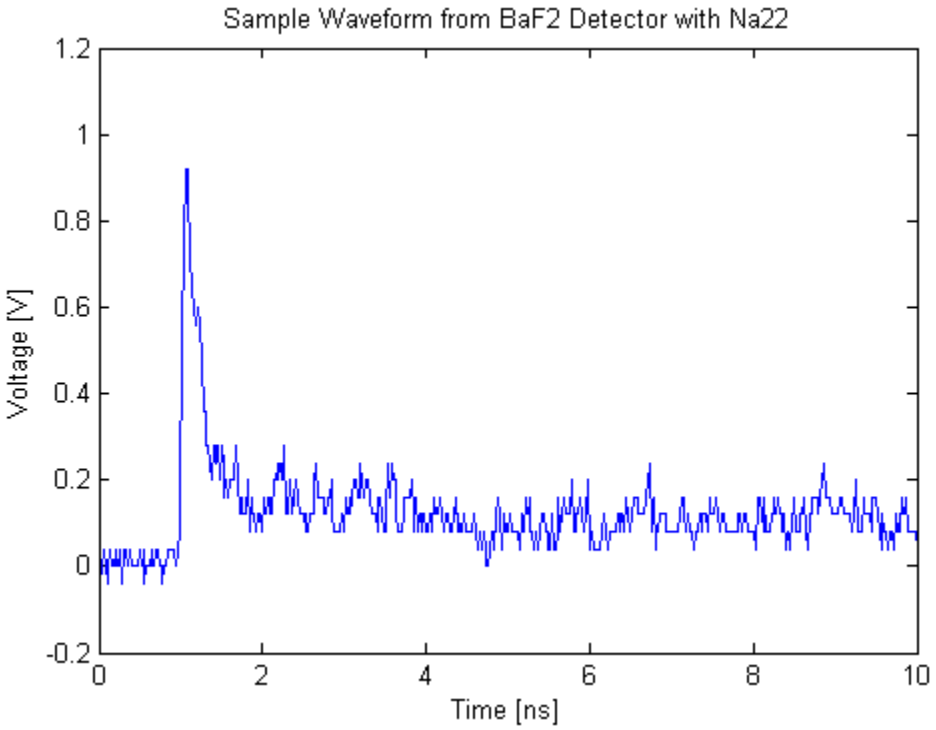

Figure 39. Waveform of scintillation event from BaF_2 detector. This is identified as a scintillation event because the decay of the pulse corresponds to the decay of scintillation photons in BaF_2 crystal.

These waveforms are displaying characteristics consistent with what is expected from a scintillation event in the BaF_2 crystal caused by energy deposition from incident radiation. Some waveforms however do not display this characteristic decay time and have only one or two points above the noise. In these waveforms the decay time is as fast as the rise time.

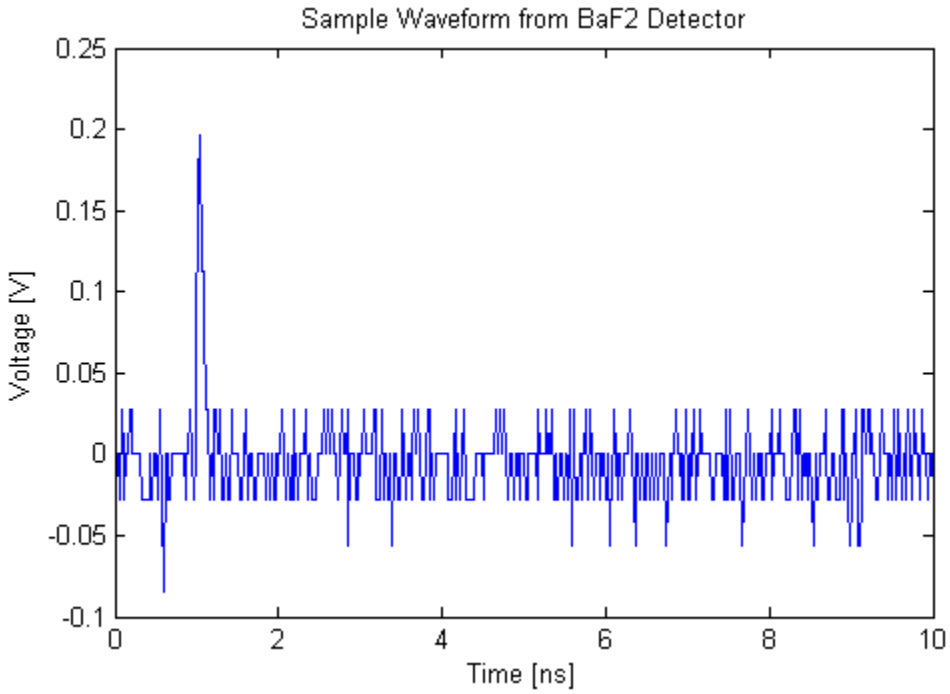

Figure 40. Waveform of suspected noise event lacking the characteristic decay of a scintillation event.

These spike type events are common when any of the radioisotopes mentioned earlier are observed, however they dominate when no source is present. Because of this it is believed that these waveforms represent noise, likely due to thermal noise in the photocathode. Electrons at various dynodes in the PMT are on the edge of being liberated due to the high bias voltage placed on the PMT. If one of these receives a small amount of energy due to thermal interactions it could cause an electron avalanche in the PMT creating a quick sharp signal. Either this or the spike type event could be generated by a single photon event coming out of the scintillating material due to potential radioactive isotopes naturally present in the crystal. A true signal event resultant from energy deposited by an external radiation source should cause many scintillation photons

some of which arrive at the PMT slightly delayed resulting in a more gradual decay in the pulse.

Although a waveform from noise and a waveform from a scintillation event might have the same peak voltage, the pulse from a scintillation signal would have a larger area under the curve. Integration of the waveforms plotted as a histogram can reveal this difference. This operation was initially performed on data collected from Cs-137 for a simplest case scenario. Noise from the electronics, as seen in the above waveforms before the trigger at 1 ns, is of low amplitude, centered on zero and randomly distributed above and below zero. Because of this the electronic noise should cancel itself out when the waveform is integrated over the full 100 ns window. For this reason integrating the waveforms should distinguish signal pulses from noise pulses without electronics noise being a significant contributor.

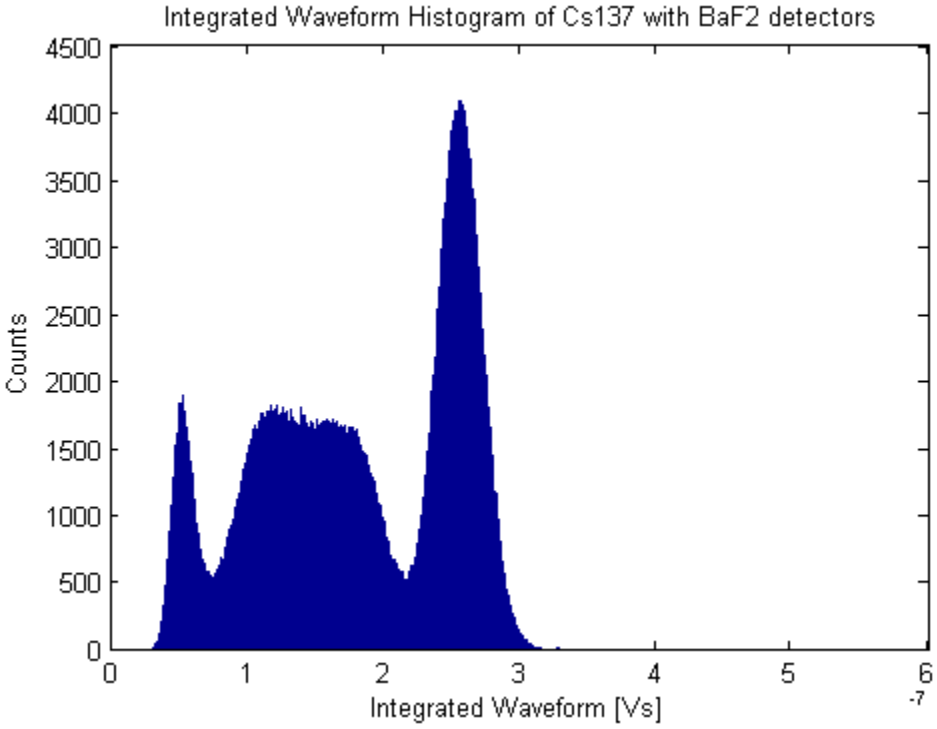

Figure 41. Histogram of waveforms from Cs-137 collected using BaF_2 detectors integrated over 100ns. The leftmost peak is suspected to be noise while the other two features correspond to the full energy peak and the affiliated Compton continuum.

Three features are clearly visible in the integrated waveform histogram and it is theorized that the thermal noise pulses should have the lowest value, however some form of confirmation of this assumption is needed before filtering out these events can be justified.

It is possible that some thermal noise events could have high enough of a peak to give it a large integrated value despite the quick decay time, so the integrated waveform is not enough of a discriminator on its own. A way to distinguish slowly decaying waveforms from quickly decaying waveforms, regardless of the peak voltage, would be a measure of the ratio between the mean value and the maximum value of a waveform.

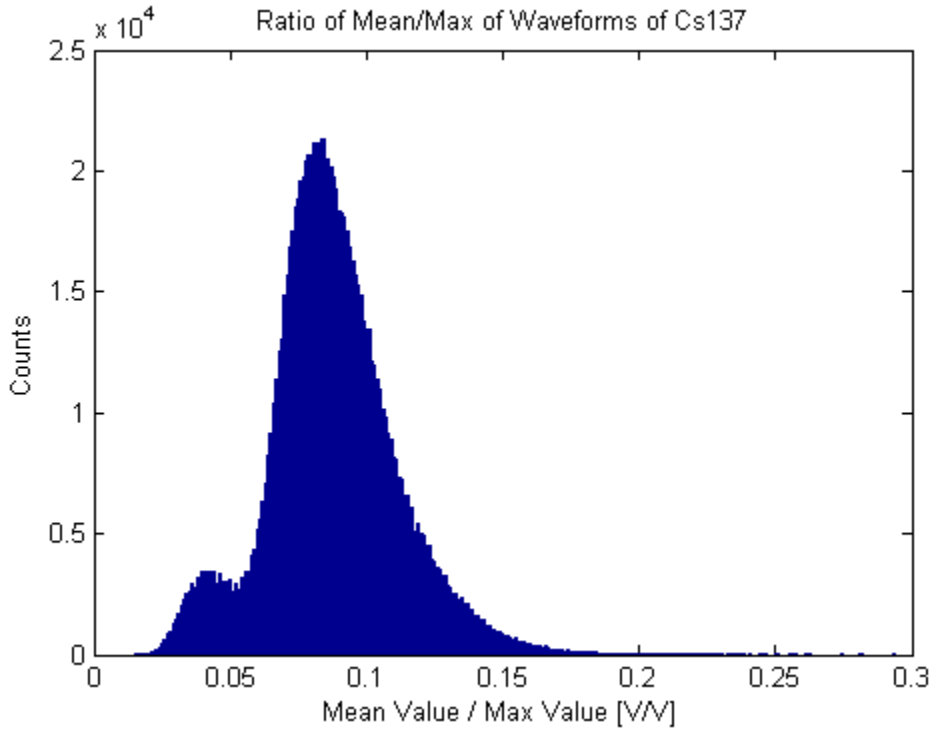

Figure 42. Ratio of waveform mean to maximum voltage from Cs-137 collected using BaF_2 detector. The left feature results from noise events while the larger distribution on the right is from radiation detection events.

A waveform from noise with a high peak voltage and consequently a high maximum value should have a proportionally higher mean. Therefore the ratio between the two should remain roughly the same with variation in this ratio due only to errors in measurement governed by the Gaussian distribution. The same should be true of pulses from scintillation events regardless of the amount of energy deposited in the detection region except that the distribution should be centered on a higher ratio. Two normal distributions are apparent in the ratio histogram; the smaller one has a lower value and is theorized to be noise. The data were analyzed again, this time with the left most peak of the three features in the integrated waveform histogram filtered out to observe how this affected the ratio histogram.

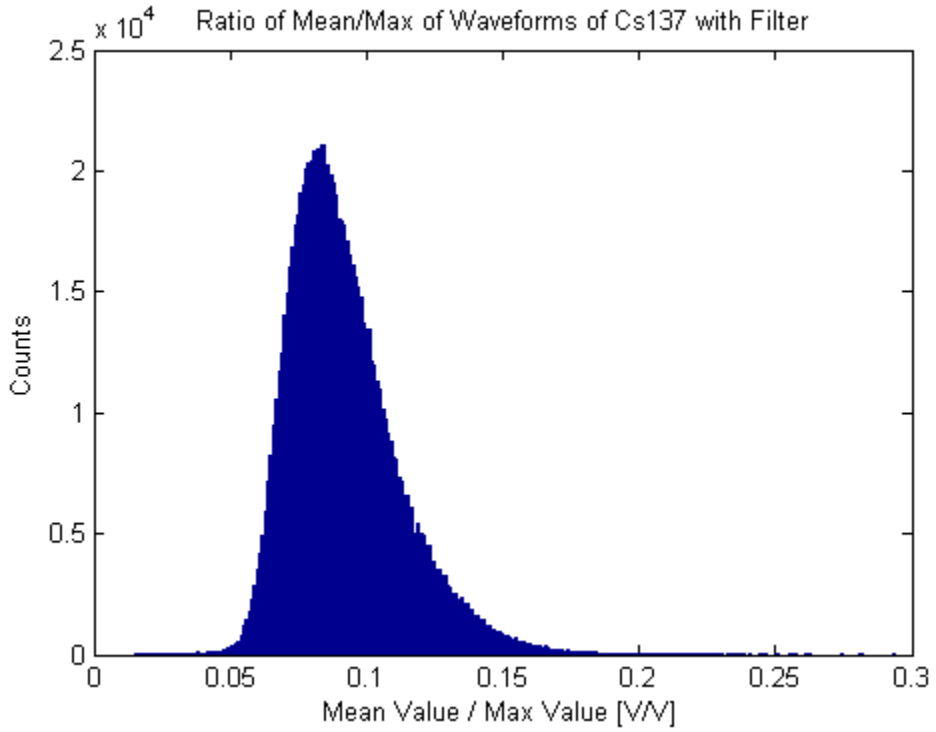

Figure 43. Ratio of waveform mean to maximum voltage with noise removed. The bimodal distribution is no longer present suggesting a proper removal of noise.

The lower value peak in the previous ratio histogram is not present in the ratio histogram with the filter applied to the integrated waveform histogram. This filter was removed and replaced by a similar filter that required a minimum ratio to observe how this affected the integrated waveform. When the data were reanalyzed a similar effect was observed with the peak corresponding to noise removed in the integrated waveform plot. This confirmed that these two features correspond to each other and since they were both theorized to be noise this cross correlation supports the theory that they are in fact from noise.

With a means of discriminating out noise waveforms it is possible to identify key features from the integrated waveform histogram similar to identifying features from the gamma spectra obtained from the GammaVision software.

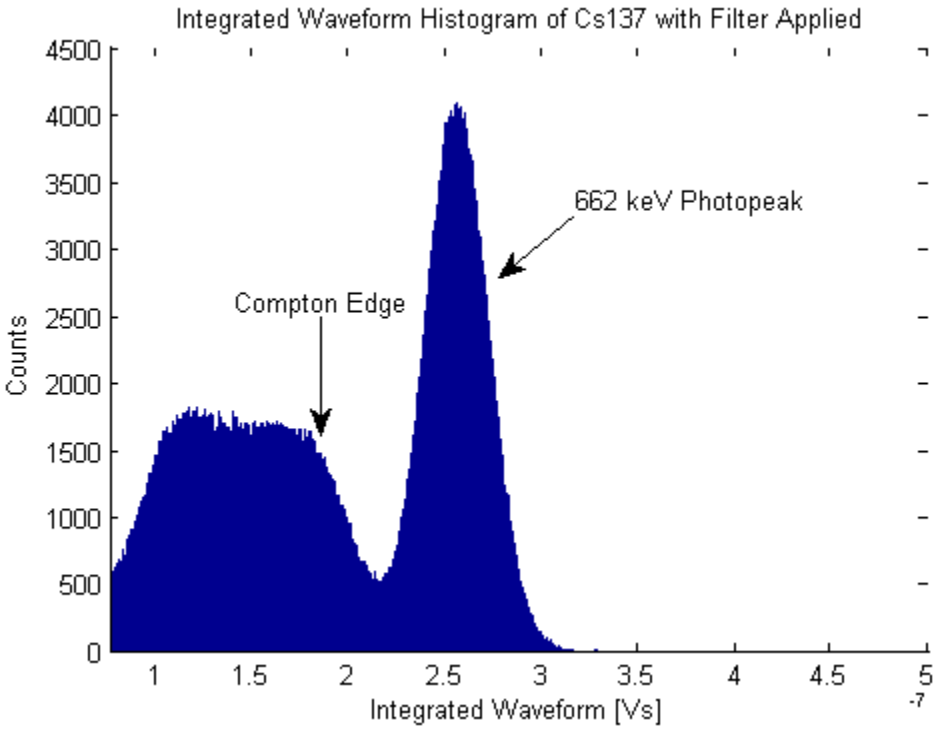

Figure 44. Waveforms from Na-22 integrated over 100ns with noise removed. This spectrum is similar to the gamma spectra generated using pulse shaping electronics.

The advantage of identifying features in this manner rather than with the experimental setup using GammaVision is that it can be done directly from the PMT and therefore without sacrificing timing information. The resolution of this spectrum is 15.3% at 662 keV which is sharper than is typically achieved with BaF_2 detectors even with pulse shaping electronics. With these filters on the ratio of waveform mean over maximum and the integrated waveform in place the peak voltage distribution could be revisited.

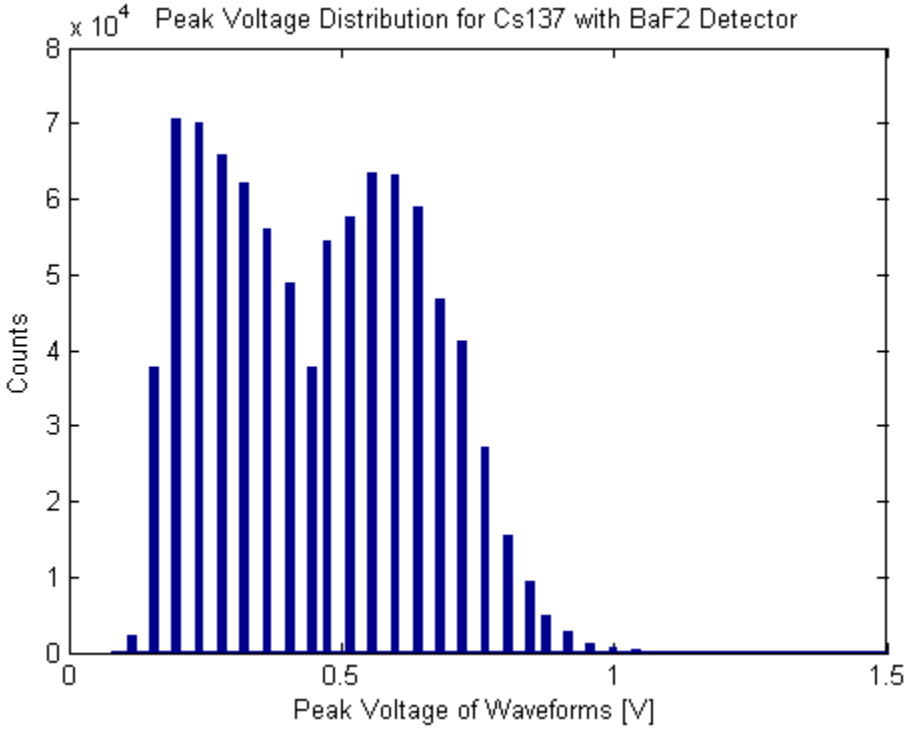

Figure 45. Peak voltage distribution from Cs-137 bimodal distribution. With the noise removed peak voltages corresponding to full energy deposition and Compton scatters can be identified.

With filters in place on the ratio and the integrated waveform two distinct features could be identified in the new peak voltage distribution from Cs-137. A cross correlation check was performed between the peak voltage distribution and the integrated waveform histogram similar to the cross correlation performed between the ratio and the integrated waveform. The feature identified on the integrated waveform as the Compton continuum was found to correspond to the left peak on the peak voltage distribution and the peak on the right was found to correspond with the full energy peak. In this manner upper and lower bounds can be set on the peak voltage of a waveform that corresponds with a particular energy of incident radiation. Three discriminators, one each for the ratio of mean over maximum, the integrated waveform, and the peak voltage, all working

together ensure that a radiation event of interest can be reliably and consistently identified. The primary limitation to this ability is the 100 ps per point time resolution of the oscilloscope when two channels are in use.

This process was performed on Cs-137 as a proof of concept. The entire process was repeated for Na-22 so that radiation from the birth and annihilation of positrons could be identified. Initially the unfiltered peak voltage distribution was observed to optimize the voltage range settings on the oscilloscope.

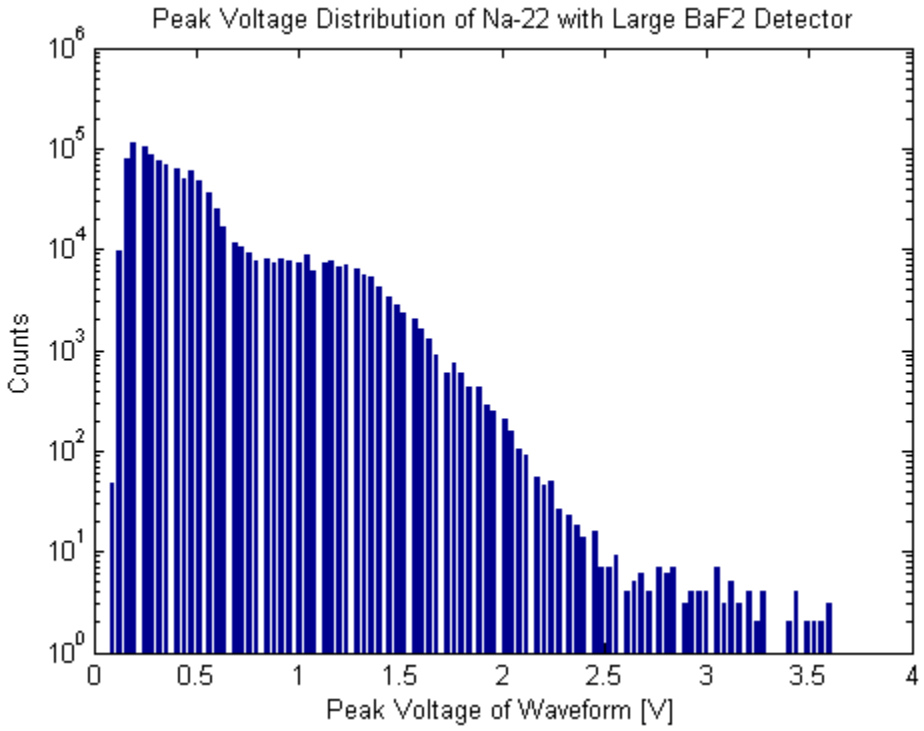

Figure 46. Peak voltage distribution from Na-22 collected using a BaF_2 detector. As before with the Cs-137 no significant features in the spectrum are easily identifiable.

As expected the positron birth gammas and annihilation photons are indistinguishable on this plot and further analysis of the waveforms is needed. Plotting

the integrated waveforms as well as plotting the ratio of the mean over the maximum value of each waveform is more telling than the raw peak voltage distribution.

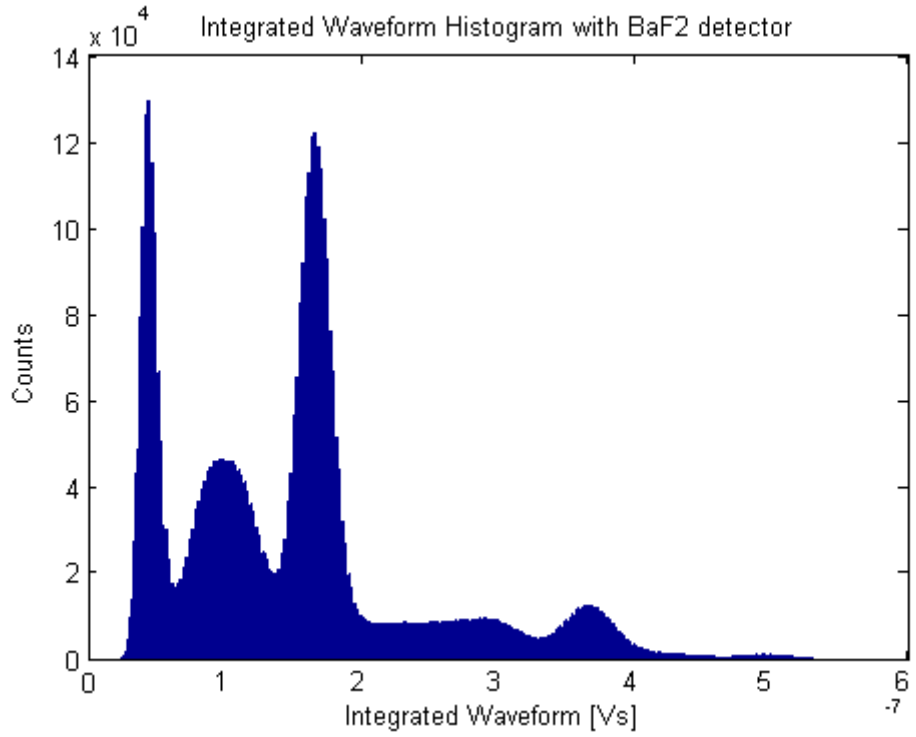

Figure 47. Waveforms from Na-22 integrated over 100ns collected using a BaF_2 detector. The leftmost peak is suspected to be noise as was the case with Cs-137. The other features correspond to the positron birth and annihilations and their affiliated Compton continua.

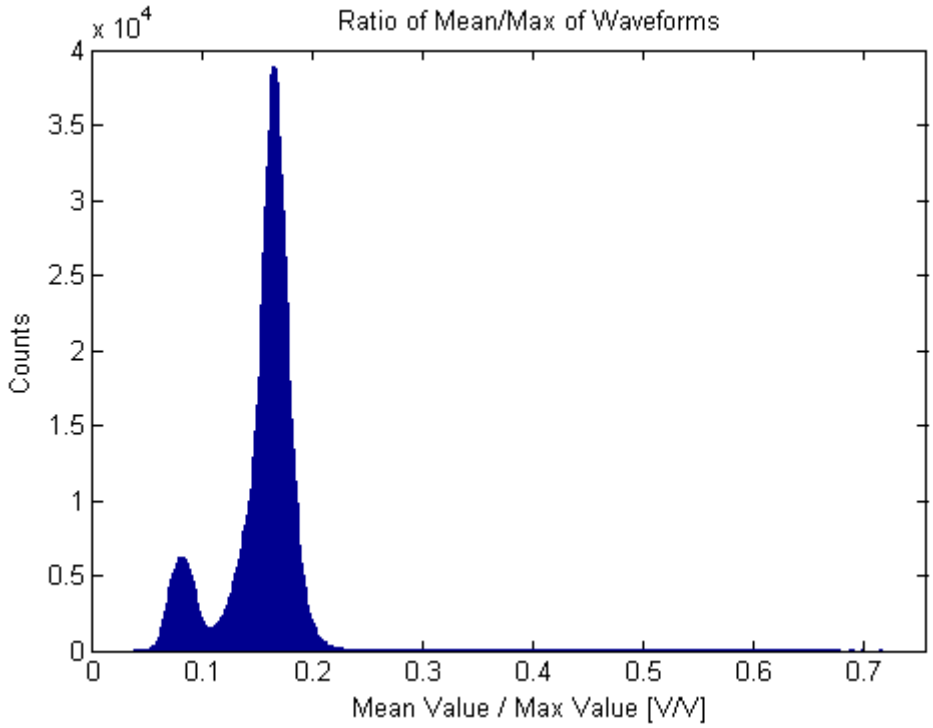

Figure 48. Ratio of waveform mean to maximum voltage from Na-22 showing distinct bimodal distribution. The feature on the left corresponds to noise and is filtered out by the data analysis code. The feature on the right corresponds to the radiation depositing energy in the detection region and causing a scintillation event.

The left most peak in the integrated waveform histogram was found to correspond with the small peak on the left in the ratio histogram and the large peak on the right was found to correspond with all other features in the integrated waveform plot. This was done using a cross correlation technique demonstrated earlier on Cs-137. Using the method demonstrated on Cs-137 employing discriminators based on the ratio and on the integrated waveform allowed for the identification of key features of the Na-22 spectrum.

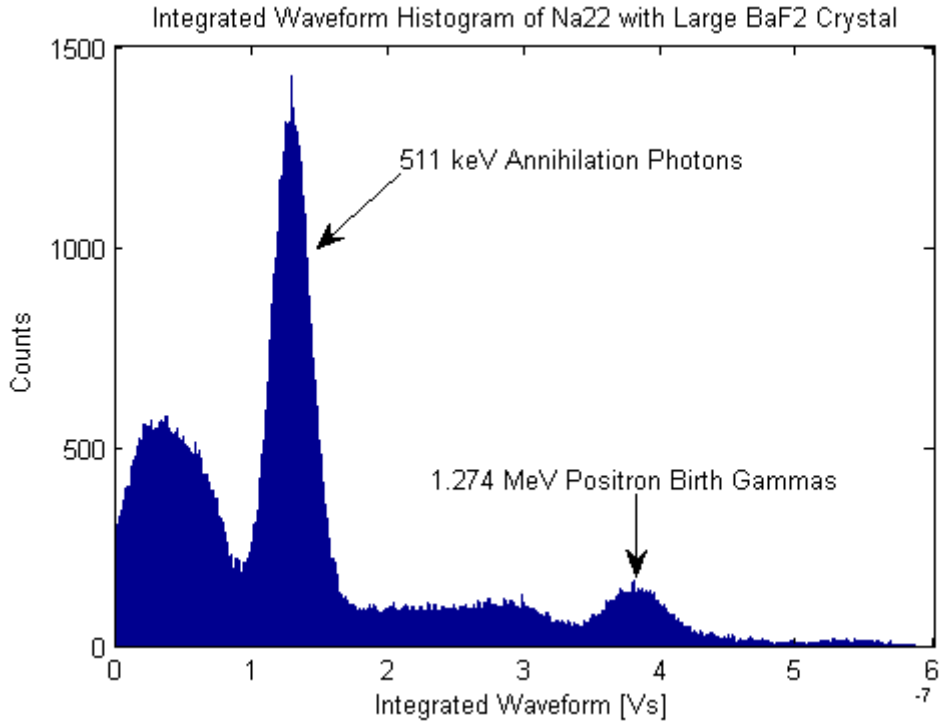

Figure 49. Waveforms from Na-22 integrated over 100ns collected using the large BaF_2 detector with noise removed. This spectrum is used to identify positron birth photons.

With this information a discriminator was created for the large BaF_2 crystal that passed only those waveforms resultant from positron birth gammas.

The small BaF_2 crystal is intended to detect positron annihilation photons so that a comparison of the timing of the pulses from the two waveforms can be compared to obtain a positron lifetime measurement. To isolate 511 keV annihilation photons from waveforms collected using the small BaF_2 crystal this entire process was repeated on the smaller detector. Eventually an integrated waveform histogram was obtained from Na-22 using the small BaF_2 detector and waveforms from positron annihilations could be identified.

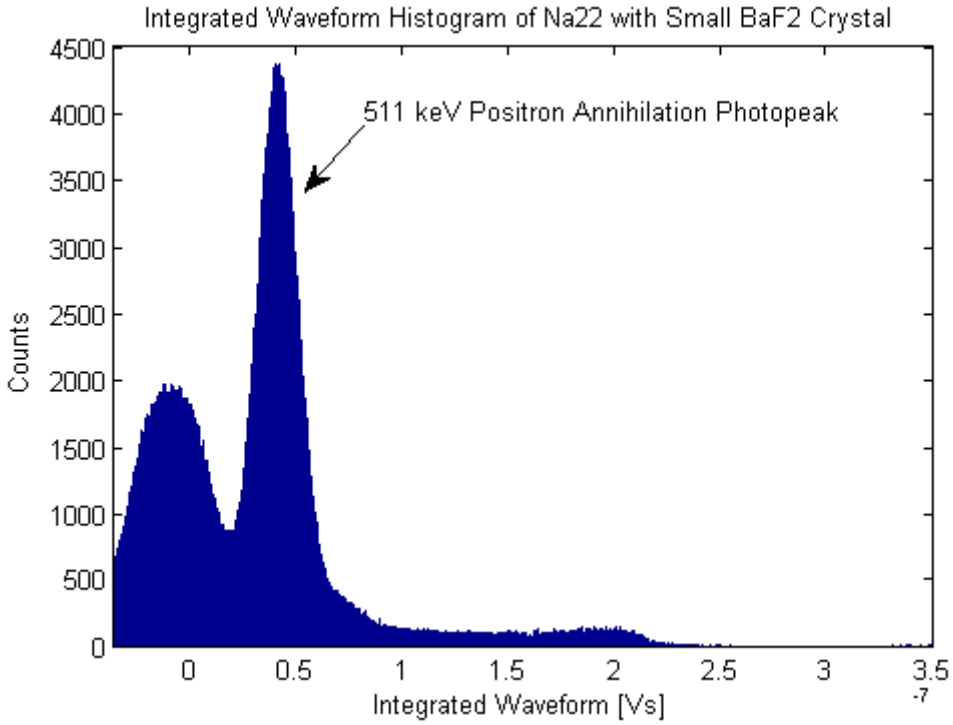

Figure 50. Waveforms from Na-22 integrated 100ns using small BaF_2 detector with noise removed. Birth photons are detected with poor efficiency because of the small size of the detection crystal.

As expected, the small BaF_2 detector exhibited low counts at the energy associated with positron birth gammas. Discriminators based on the ratio of mean over maximum waveform voltage and based on the integrated waveform allowed that a plot of the peak voltage distribution could be created.

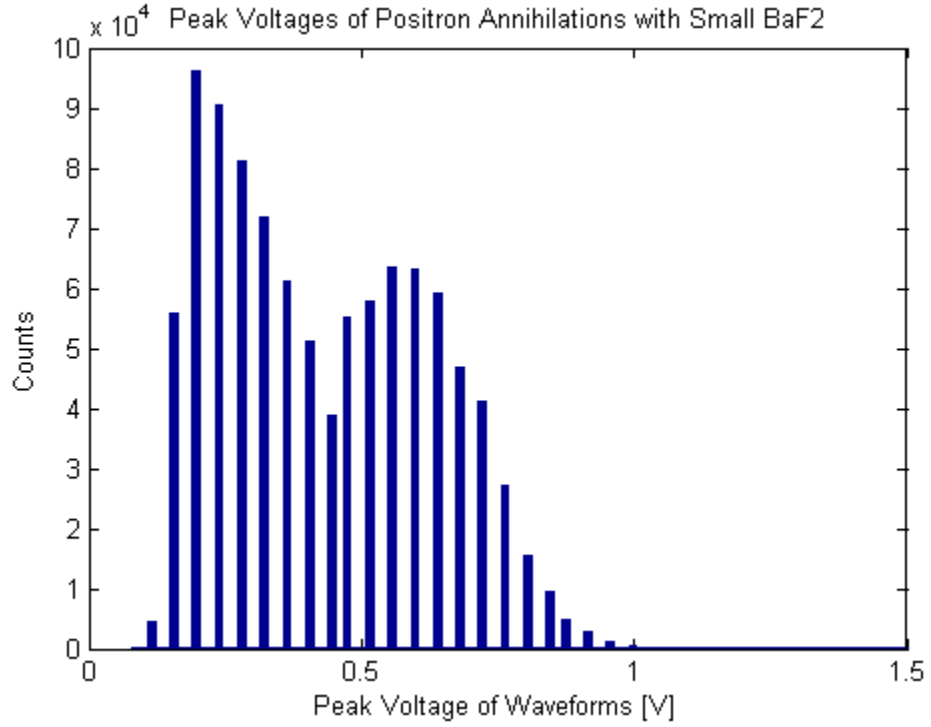

Figure 51. Peak voltage distribution from Na-22 from positron annihilation.

Since the large detector is optimized to detect positron birth gammas, the small detector is intended to only detect annihilation photons which act as the stop signal for positron lifetime measurements. Because of this separate optimization of the two detectors the waveforms collected using the small BaF_2 detector from all events other than positron annihilation are filtered out. The two features seen in the peak voltage distribution both correspond to positron annihilation, one to the Compton continuum and the other to the full energy peak. This correlation was confirmed by comparing the peak voltage distribution to the integrated waveform histogram using the cross correlation technique described earlier. An analysis of the peak voltage distribution is important since it allows for accurate upper and lower bounds for the peak voltage of a waveform for a radiation event of interest.

The integrated waveform discriminator on the small detector allowed for an accurate peak voltage range to be determined from the peak voltage distribution histogram. This peak voltage discriminator paired with the ratio discriminator proved capable of discriminating signal from noise. Discriminating annihilation signals from positron birth signals is handled by the upper bound of the peak voltage discriminator and is not a high concern in the small BaF_2 detector due to its poor efficiency at high energy. During lifetime measurements pulses from annihilation photons can occur anywhere in the 100 ns time window. The integration of a waveform could potentially be truncated for long lived positrons so an upper bound is used on the integrated waveform discriminator instead of a lower bound. The ratio discriminator could potentially be affected by this as well, although not as severely so due to a strong distinction in the bimodal distribution in the ratio plot for the small detector. The ratio discriminator is useful for identifying signal from noise while the integrated waveform is primarily useful for distinguishing annihilation photons from birth gammas which is less of a concern in the small BaF_2 detector due to its low efficiency at the energy of birth gammas. The exact values used in these discriminators for both detectors can be found in appendix H.

The signals from both the large and small BaF_2 detectors can be reliably interpreted on a system without any pulse shaping electronics to preserve the timing information despite the poor energy resolution of BaF_2. This is done by setting up discriminators on the signals formulated by analyzing the waveforms based on a peak voltage distribution, an integration of the waveform over a time window, and a ratio between the mean and the maximum voltage.

Lifetime Measurements

With the large BaF_2 scintillator optimized to detect birth gammas and the small BaF2 scintillator optimized to detect annihilation photons, lifetime measurements can be made by measuring the difference in the timing of the two signals and correcting for the 3.7 ps delay of the birth gamma. The lifetime data collection code described earlier in chapter III is set up to treat the large BaF_2 detector as the primary detector. The trigger is set to 792 mV, the minimum peak voltage found to correspond to positron birth gammas. When the trigger is activated a waveform is captured on both channels and the digital data points stored for analysis after the data collection run is complete. This trigger is very high compared to the typical waveform peak voltages generated from the BaF_2 detectors. This is done because if the waveform does not meet this minimum peak voltage then it does not represent a positron birth gamma. If no birth gamma is detected then there is no need to capture any waveforms since a lifetime measurement cannot be made without a birth gamma. Because of this high trigger the system operates slowly, limited by the poor efficiency of BaF_2 at high energy.

If a waveform from the large BaF_2 crystal passes through all the filters and is found to qualify as a birth gamma then the waveform from the small crystal is analyzed using the peak voltage discriminator and the ratio discriminatoris found to qualify as an annihilation gamma then a lifetime measurement can potentially be made if the waveforms pass a new set of requirements as a pair. The first requirement is that the two waveforms must be from the same waveform frame from within the same matrix set in their respective channels meaning that they were acquired simultaneously. This is necessary so that a difference in the timing of the pulses can be accurately assessed. The

next requirement is that the annihilation pulse must not occur earlier than the birth pulse. If it were it would mean that the two pulses were from two different positrons and are not useful for positron lifetime measurement.

A further requirement is that the waveforms must not exhibit any pileup effect from 1 ns to 0.2 ns prior to the trigger level on the pulse of interest. Pileup due to a previous pulse could cause a false positive by pushing the pulse up into a higher peak voltage and would also influence the value of the integrated waveform or the ratio between the mean and the maximum voltages. This pileup filter was created after careful analysis of the electronic noise clearly visible in the waveforms just prior to the trigger.

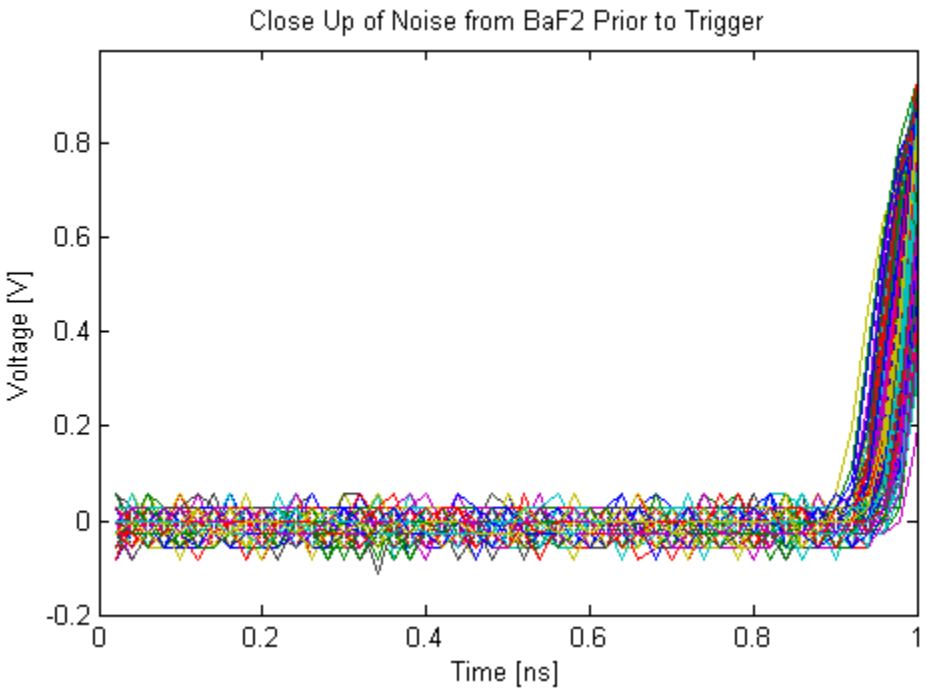

Figure 52. Electronics noise on BaF_2 detector. This noise consistently remains below a predictable level before the trigger. Noise rising above this reliable limit could indicate pulse pileup.

This noise is due to imperfections in the electronics and behaves erratically within predictable bounds. The maximum value of this noise does not typically exceed 24 mV on the large BaF_2 detector and 36 mV on the small detector. Waveforms that deviate from these predictable limits on the electronic noise are filtered out. Any data points in the waveform higher than these values in the region prior to the pulse could be the remnants of a previous pulse which could produce pileup.

Once both waveforms have satisfied all of the stringent requirements to qualify as a positron lifetime event, the timing of the pulses themselves must be determined before a lifetime measurement can be made. A constant fraction pick-off timing method was used. This method was chosen because the timing of this point is independent of pulse amplitude. This eliminates the effect of amplitude walk and experiences less jitter than other methods (Paulus 1985). The minimum peak voltage of interest in this experiment is 100 mV which is the lower bound for annihilation photons in the small BaF_2 crystal. The electronic noise in the small crystal does not exceed 36 mV. A constant fraction of 37% was chosen as the percentage for constant fraction timing. It is desirable to have a percentage as close as possible to the optimal percentages from 10 to 20% and anything lower than 37% could potentially confuse noise for signal in the small crystal.

The limiting factor for the timing resolution in this experiment is the sampling rate of the oscilloscope. The initial setup used an oscilloscope that was capable of 5 billion samples per second (GS/sec). This sampling rate has to be divided evenly between each channel in use which meant that with two active channels the available timing resolution was 400 picoseconds per point (ps/pt). The expected average lifetime of a positron is theorized to be between 1 and 10 ns. Since the expected value of the

lifetime measurements is potentially less than an order of magnitude away from the resolution of the oscilloscope, as limited by the sampling rate, it was determined that this was an unacceptable level of uncertainty and a new oscilloscope with a higher sampling rate was needed. A new oscilloscope was obtained and updated drivers were downloaded. The lifetime data collection code was modified to apply to the new oscilloscope and the connection driver for the oscilloscope was loaded onto the data collection computer. The new oscilloscope had a higher sampling rate providing a timing resolution of 100 ps/pt. Unfortunately, all of the upper and lower bounds for all of the discriminators in the lifetime code including peak voltage, integrated waveform, and mean over maximum voltage ratio had to be recalibrated to the new oscilloscope. Switching oscilloscopes meant that the entire procedure for lifetime measurements starting with the first unfiltered peak voltage distribution had to be repeated and it had to be done for both the small and large BaF_2 crystals. Once completed, this allowed for lifetime measurements to be made at a much lower uncertainty of ±0.71 ns per lifetime measurement.

Results

The desired minimum number of measurements needed to analyze a spectrum of positron lifetimes is 10^6 valid lifetime measurements. Collecting waveforms using this experimental setup runs quickly and efficiently, however only a small fraction of the waveforms collected are useful for positron lifetime measurements due to the strict criteria that must be met by the signal from both detectors to satisfy the discriminators. Approximately 0.16% of all coincident waveforms collected are useable as lifetime measurements. One million coincident waveform pairs can be collected in a matter of

seconds or minutes with a lower trigger, however with the high trigger used in this experiment this same number of coincident waveform pairs is collected in approximately 10.3 hours. Waveforms can be collected quickly, but lifetime events are detected slowly due to the inefficiency of BaF_2 at the high energy of the positron birth gamma and other inefficiencies inherent in the system such as geometric inefficiency and low activity in the source. To collect the desired 10^6 lifetime measurements one data collection run would need to acquire 625 million coincident waveforms and would last for approximately 268 days. Obviously that amount of time was not available during this project.

Table 8. Positron Lifetime Measurement Events

Source	Isotope	Bias	Waveform Pairs	Lifetime Events
Planchette	Na-22	0 V	1.0E+07	17408
Capillary	Na-22	0 V	1.0E+07	16070
Capillary	Na-22	600 V	1.0E+07	15450

Three data runs were conducted to collect 10 million waveform pairs which lasted from 4 to 5 days each. The first run was done using a Na-22 planchette source. The other two were conducted on the Na-22 filled capillary tube under a vacuum of 10^{-3} Torr. In one of these two runs a potential difference of 600 V was applied across the inner and outer walls of the capillary tube. In the other run on the capillary tube no bias voltage was applied.

Table 9. Positron Lifetimes

Source	Pressure [Torr]	Bias [V]	Average Lifetime [ns]	Uncertainty [ns]
Planchette	768	0	1.86	± 0.07
Capillary	1.00E-03	0	1.99	± 0.07
Capillary	1.00E-03	600	2.35	± 0.07

The enhanced lifetime in the experiment with 600 V applied could correspond to an increased rate of ortho-positronium formation, however the observed increase is much longer than what is anticipated for ortho-positronium in polymer films. The average lifetimes from a limited sample size is an admittedly limited metric and any real difference between the results of this experiment and previous experimenters is likely largely influenced by the outer gold surface[24].

A spectrum of the positron lifetimes could potentially show features representative of long lived ortho-positronium discernable from shorter lived positrons and para-positronium. Unfortunately, such features are not easily identified in this experiment because not enough lifetime events were definitively identified. Individually however, each positron lifetime recorded in this experiment can be reported with high confidence due to the strict criteria set by the many filters employed in this experiment.

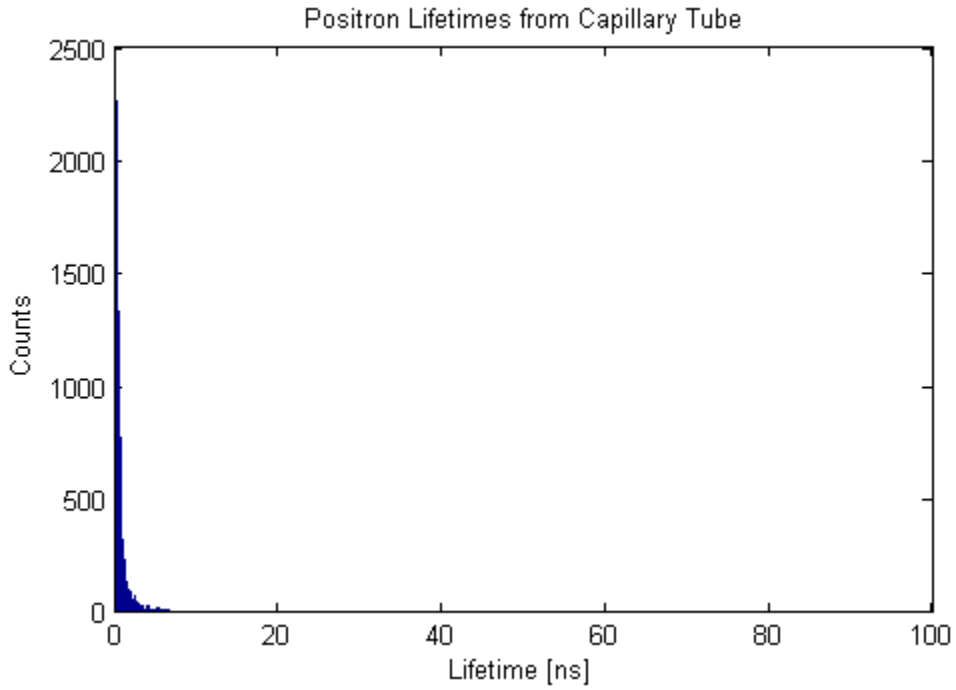

Figure 53. Positron lifetime spectrum 600V electric potential on capillary tube. Lifetimes are observed all the way out to 96 ns however short lifetimes clearly dominate. This spectrum suffers from low counting statistics.

Although the positron lifetime spectrum includes lifetimes up to 96 ns the spectrum is dominated by lifetimes less than 10 ns.

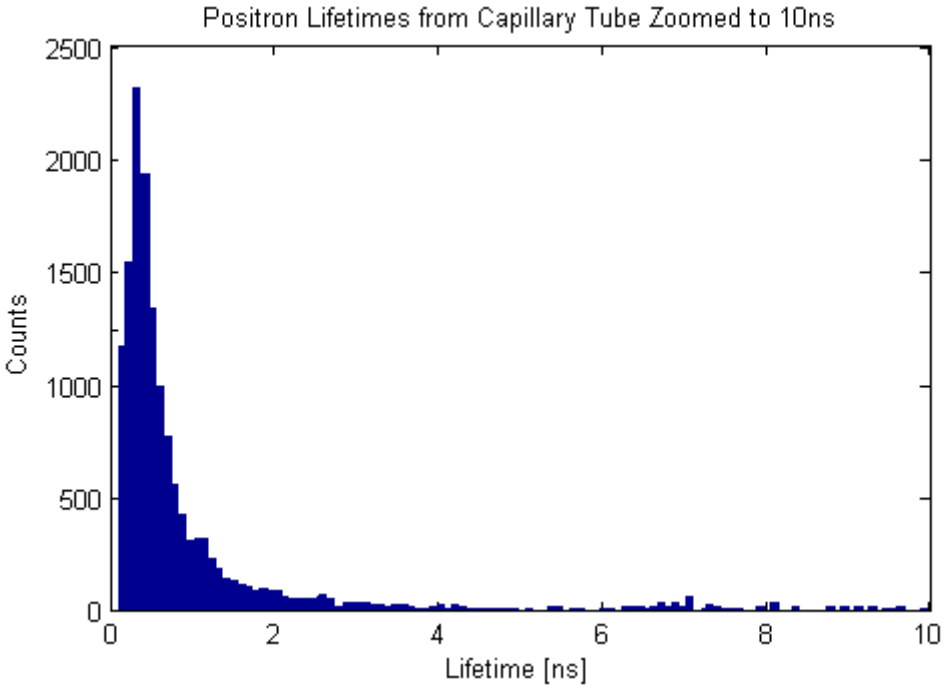

Figure 54. Spectrum of positron lifetimes less than 10ns from the capillary tube with 600 V applied. These short lifetimes dominate the spectrum.

The lifetime spectra from each data run were very similar in appearance to each other and the primary feature that could be definitively identified was a sharp peak between 0 and 1 ns. The average lifetimes varied between each data run by an amount greater than the uncertainty. The third data run had the highest average which was accompanied by an increased median lifetime of 0.3 ns compared to 0.2 ns in the other two runs. This increase in median is not definitive since the uncertainty for an individual lifetime measurement is 0.05 ns.

Features in the lifetime spectra can become more apparent on a semi-log plot. A comparison of the results from the capillary tube with and without an applied bias of 600V reveals some differences.

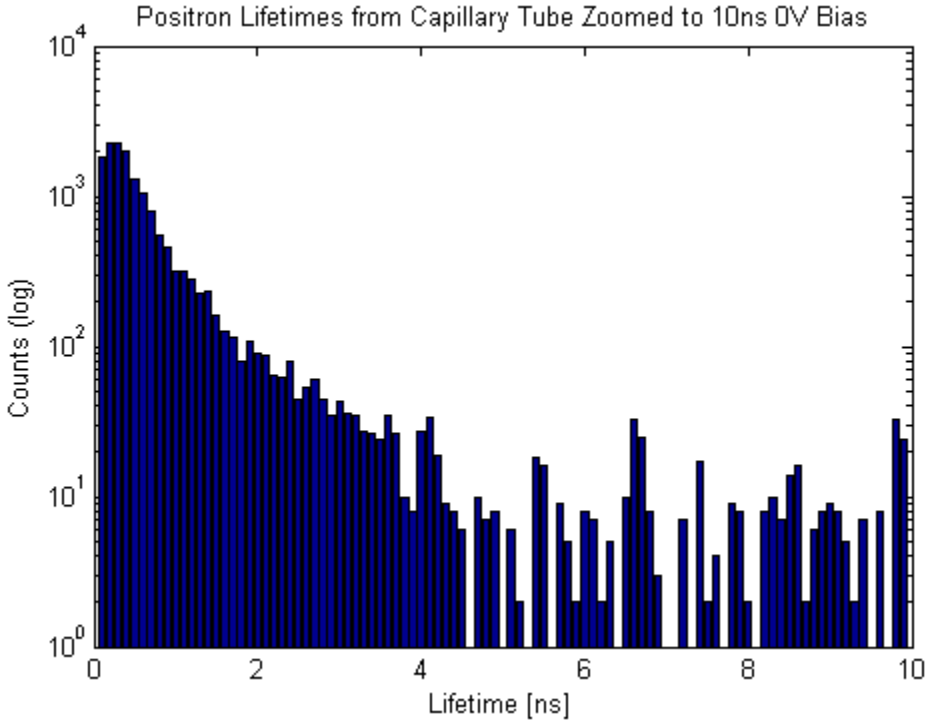

Figure 55. Lifetimes less than 10 ns from capillary tube without bias applied

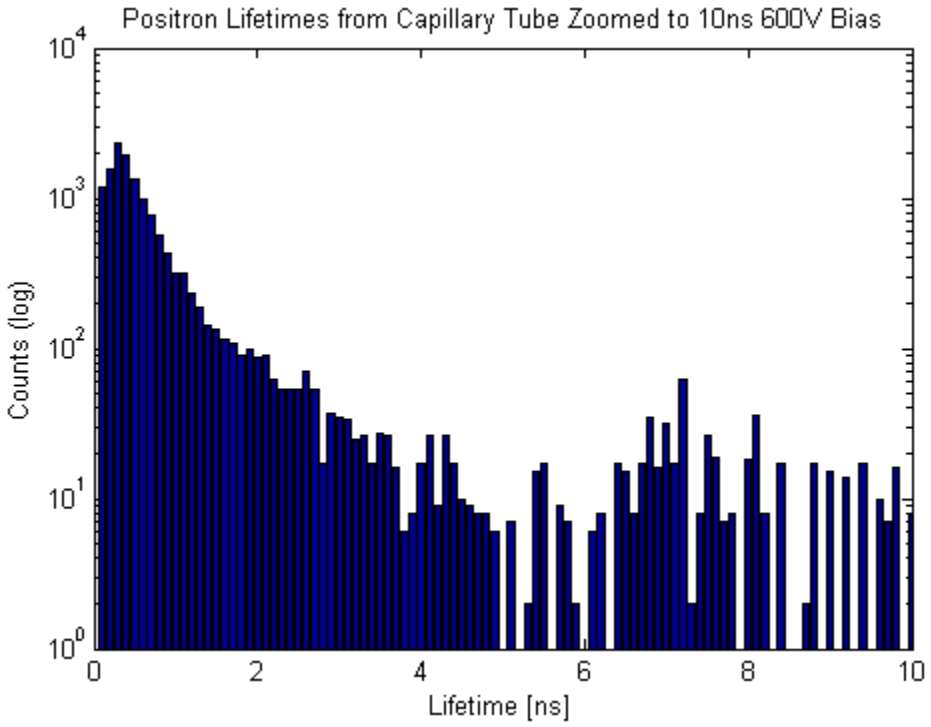

Figure 56. Lifetimes less than 10 ns from capillary tube with 600V applied with cluster feature at 7 ns.

The plot from the capillary tube with an applied bias appears to show some positron lifetimes clustered around 7ns. This could correspond to an increased rate of positronium formation if this cluster is the result of ortho-positronium annihilation. The binning in these plots corresponds to the timing resolution of the oscilloscope, but by making the binning coarser one can sacrifice timing resolution to compensate for low counting statistics in identifying features.

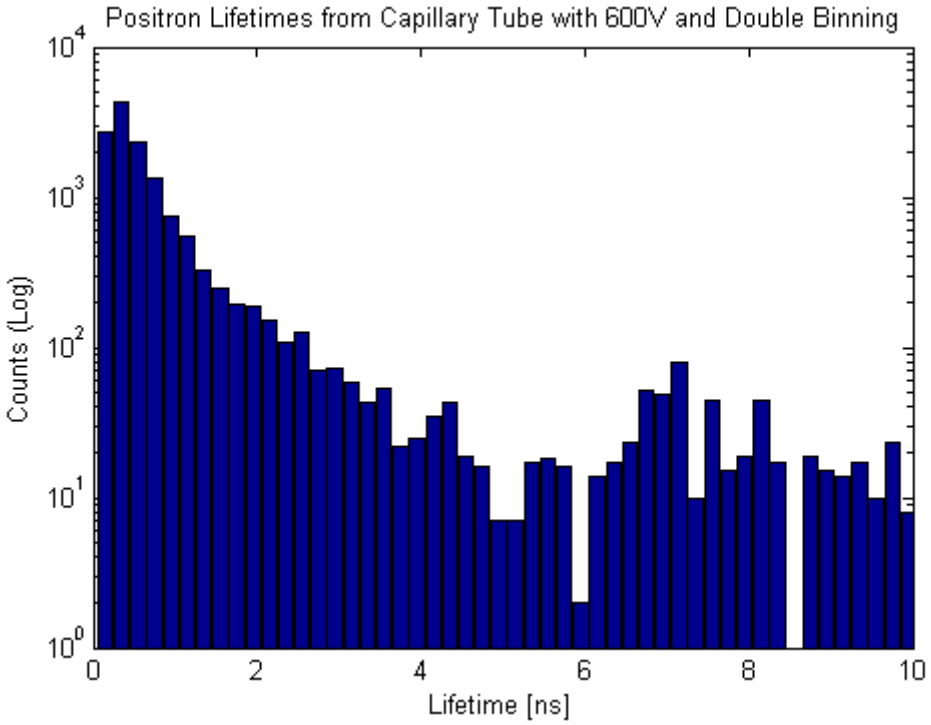

Figure 57. Positron lifetimes from capillary tube with 600V applied and 0.2 ns binning to highlight boundaries of cluster feature identified near 7 ns.

With the binning increased to 0.2 ns the plot of lifetimes when 600 V are applied to the capillary tube still shows the feature centered on 7 ns. The change in binning makes the edges of the feature more easily identifiable and the feature is seen to occur between 6 and 8.5 ns. A student's t-test was performed on the counts over this range comparing the 0 V and 600 V lifetime spectra. A confidence limit of 95% was used and the null hypothesis was that the the data are a random sample from a normal distribution with a mean of the difference centered on zero and an unknown variance. This null hypothesis was tested against the alternative that the mean of the difference was not zero. Although the total number of waveforms collected in for 0 V applied and 600 V applied was the same, a different total number of positron lifetime events were identified. To

compare the two data sets the counts from the 0 V experiment were calibrated by the ratio of total counts in the 600 V experiment to counts in the 0 V experiment. The results of the t-test confirmed that null hypothesis can be rejected with a confidence of 96.45%. This means that the feature seen on the lifetime plot from 6 to 8.5 ns is statistically significant and likely represents ortho-positronium lifetimes.

Analysis of the shorter positron lifetimes below 4 ns is more challenging. An attempt was made to fit the slope to a decaying exponential, however the closest function that could be generated was not a strong fit. The decay seen in the lifetime spectra plots is likely the result of two different positron lifetimes layered on top of each other yet testing this theory would require a higher number of counts to be statistically significant. One would expect that if applying 600 V to the capillary tube does result in an increased rate of positronium formation then the slope on the 600 V plot should decay more quickly. This comparison can be made by plotting the counts from the decay region from the experiment with no voltage applied against the counts from the 600 V experiment over the same range. As before the counts from one experiment are calibrated to the other to compensate for the difference in the total number of positron lifetimes.

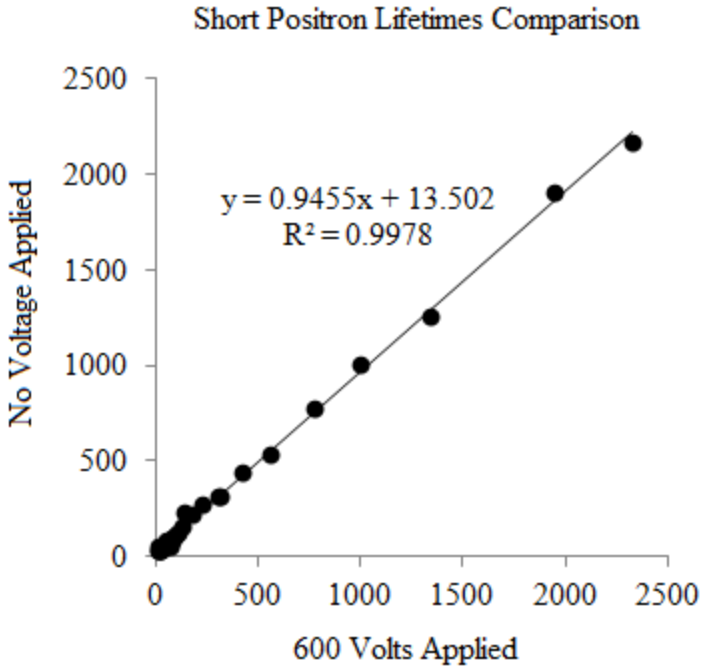

Figure 58. Short lifetime comparison of 0V to 600V applied to capillary tube. The values from the decay region of the positron lifetime spectra from these two experiments are plotted against each other to identify which decays for rapidly. A slope less than 1 suggests that the spectrum with 600 V applied decays more rapidly.

A linear function was fit to the comparison a demonstrated a slope very near to but less than one. This suggests that the rate of decay in the two experiments is very similar, but that these short lifetimes decay slightly more quickly when 600 V is applied. This suggests that some positron lifetimes are extended out of this short lifetime range and out into longer lifetimes when 600 V are applied. This prolongation of positron lifetime is most likely the result of an increase in the rate of ortho-positronium formation. The usefulness of this comparison of short lifetimes is limited due to the low number of counts.

From the massive number of waveforms collected for lifetime analysis the number of actual useable lifetime measurements is fewer than desired to identify features

in the positron lifetime spectra. The increase in the average positron lifetime in the capillary tube with a bias voltage of 600 V applied, although an admittedly limited metric, is suggestive of an increased rate of positronium formation. More convincingly, the statistical significance of the feature identified at 7 ns likely corresponds to an increased rate of positronium formation. This lifetime corresponds to an ortho-positronium atom in a cubical volume of about 9 nm^3 as shown by previous experimenters[40]. This dimension is on the same order of magnitude as the nanoparticle linkers used by Lt Slaughter in connecting the gold nanoparticles onto the surface of the capillary tube. This possible connection merits further investigation and determining the exact size of these linkers should be measured in future work. It is possible that the feature observed at 7 ns corresponds to the lifetimes of ortho-positronium atoms residing in the region of the nanoparticle linkers.

V. Conclusion

This research seeks to characterize the annihilation of positrons and investigates the formation of positronium. The first method pursued in this experiment was to measure the ratio of quanta of light emitted in positron annihilation using the NaI ring detector. The rough position sensitivity of this detector, provided by its segmentation into six detection regions, along with the reasonable energy resolution of NaI provides a means of discriminating two photon annihilation events from three photon annihilation events. An increase in the rate of three photon events as compared to two photon events is taken to coincide with an increased rate of positronium formation. The next method used in this experiment to detect the presence of positronium was to measure the lifetime of positrons using BaF_2 scintillators paired with fast photomultiplier tubes. By taking the difference in timing of annihilation photons from birth gammas and including a correction for the birth gamma delay, the lifetime of a positron can be directly measured. Longer lifetimes are taken to coincide with an increased rate of positronium formation. Both methods are used on a source system comprised of a Na-22 doped gold coated capillary tube in a vacuum chamber. This system is designed to create an environment optimal for the formation of positronium. Both measurement systems have, to a limited degree, found evidence of positronium formation.

2γ3γ System

The experiment on the 2γ3γ system appears to show a dip in the two to three photon positron annihilation ratio at approximately 700V with a corresponding dip in the two photon annihilation counts and peak in the three photon annihilation counts at the

same voltage. These ratios are calibrated to a copper source with a known ratio and include a correction for background radiation and chance coincidence from gamma rays emitted from the source. The annihilation photon ratios identified in the capillary tube are generally higher than the 372 ratio for copper. This could be because the capillary tube is a long thin source rather than a point source which could influence the difference in the efficiency of the detector for two or three photon annihilation events. This effect is likely small and the most probable reason for the high ratios in the capillary tube is that the tube is primarily made of silica and the surface of the tube is not clean or smooth. These factors are not favorable for positronium formation and likely are the cause in a high rate of two photon annihilation events. The dip in the ratio of two to three annihilation photon events when 600 to 800 V are applied across the capillary tube wall, an effect that was found to be statistically significant by a student's t-test, suggests an increase in the rate of positronium formation. The change in the annihilation ratio centered on 700 V corresponds with a similar result observed by 2nd Lt Ariella Walker when 75 V were applied across the capillary tube wall and 600 V were applied from the exterior wall of the capillary tube to the interior wall of the vacuum chamber for a total of 675 V potential difference from the center of the tube to the chamber wall. It is possible that these two experiments are observing the same effect on the positrons.

Lifetime Spectroscopy

In the two runs performed on the capillary tube the run with an applied electric field had a longer average lifetime than the data run without an applied electric field. Since ortho-positronium typically exhibits a lifetime an order of magnitude greater than

unbound positrons even a small increase in the rate of positronium formation should have a significant impact on the average positron lifetime. The increase in average positron lifetime in the third data run potentially suggests an increased rate of positronium formation. A comparison of the rate of decay of the positron lifetime spectra for lifetimes less than 4 ns revealed that positrons are pushed to the longer lifetimes at a higher rate when 600 V is applied to the capillary tube. Both the change in average lifetime and the short lifetime comparison are insensitive metrics and do not provide definitive evidence of an increased rate of positronium formation. However, a feature in the positron lifetime spectrum with 600 V applied to the capillary tube was identified centered on 7 ns. This feature was found to be statistically significant and is indicative of extended positron lifetimes, likely due to an increased rate of positronium formation. One would expect this to occur at much lower applied voltages if the capillary tube were clean, smooth and defect free. This change in lifetimes at this high applied voltage corresponds with the change in the two to three photon annihilation ratio observed using the $2\gamma3\gamma$ system.

Recommendations

More data needs to be collected over longer durations to improve the counting statistics in both systems. The data collection codes developed in this project work efficiently and accurately. Improving the efficiency of data collection could most readily be accomplished by increasing the concentration of radioactive Na-22 in the capillary tube. This would increase the count rate and speed up detection. This would particularly help the lifetime spectroscopy system since the limiting factor to data collection on that system is the detection of positron birth gammas by BaF_2 which is inefficient at that

energy. For any lifetime measurements that are taken in future research, an oscilloscope with a high sampling rate should be used. Much of the time spent conducting lifetime measurements in this experiment were conducted using an older oscilloscope with poor timing resolution. It was only towards the end of the experiment that a switch to a newer scope was made. Making the switch earlier would have saved a significant amount of time and allowed for more data collection. The XIA cards used in the 2γ3γ system are out of date. The code developed in this project for the 2γ3γ system pushes these cards to their maximum capability, however the plethora of glitches in the output data files generated by the XIA cards is worrisome. They should be replaced by a data digitization system that has at least six channels so that all sections of the NaI ring detector are collected on the same unit. The computer codes developed in this experiment were largely a feat in data processing due to the large size of the data files and the high rate at which data needed to be collected. These codes and the systems they analyze and interact with have been proven to efficiently and accurately collect and analyze data for positron annihilation spectroscopy.

Appendix A. NaI Ring Detector Energy Calibration Equations

NaI Ring Detector Energy Calibration Equations				
Format: $y = \alpha x^2 + \beta x + \gamma$ where y = Energy [keV] and x = bin number				
Channel	α	β	γ	R^2
A	-0.003	16.871	79.275	1
B	-0.0074	36.587	-46.365	0.9998
C	-0.0135	55.077	-1439	0.9996
D	-0.0129	50.358	-137.51	0.9894
E	-0.0266	86.044	-3954.4	0.9947
F	-0.0194	74.437	-3638.6	0.9998

Appendix B. NaI Ring Detector Energy Dependent Resolution Equations

Energy Dependent Resolution			
Format: $y = \alpha x^{\beta}$ where y = Resolution and x = Energy			
Channel	α	β	R^2
A	495.64	-0.642	0.9809
D	310.61	-0.581	0.9608
C	788	-0.718	0.9645
B	2194.3	-0.873	0.968
E	4324.7	-0.986	0.9596
F	2608.6	-0.899	0.969

Appendix C. 2γ3γ Data Analysis Code

```
close all
clear all
clc

tic
clear segarray;
delete('data_compiled.mat','data_ready.mat','figure1.fig','figure2.fig');

file_id = fopen('17 vac 2_5kV 15m0001.dat');
block_size = 3;
headertext_mod1 = textscan(file_id,'%s',block_size,'delimiter','\n');
block_size = 1;
headertext_mod1_2 = textscan(file_id,'%s%n',block_size,'delimiter','\t');
Run_start_mod1 = headertext_mod1_2(2);
Run_start_mod1 = cell2mat(Run_start_mod1);
block_size = 3;
headertext_mod1_3 = textscan(file_id,'%s',block_size,'delimiter','\n');

block_size = 10000;
count1 = 0;
data_compiled = [];
while ~feof(file_id)
    segarraymod1 = textscan(file_id,'%n%n%n%n%n%n',block_size, ...
        'delimiter','\t');
    [mod_1_data_new]=process_data_xia(segarraymod1);
    if length(mod_1_data_new) == 10000
        data_compiled(count1*10000+1:count1*10000+10000,:) = ...
            mod_1_data_new(:,:);
    end
    if length(mod_1_data_new) < 10000
        data_compiled = [data_compiled; mod_1_data_new(:,:)];    %#ok<AGROW>
    end
    [mod_1_elem,~] = size(mod_1_data_new);
    count1 = count1+1;
    if mod_1_elem < block_size
        break
    end
end
block_size = 2;
headertext_mod2 = textscan(file_id,'%s',block_size,'delimiter','\n');
block_size = 1;
headertext_mod2_2 = textscan(file_id,'%s%n',block_size,'delimiter','\t');
Run_start_mod2 = headertext_mod2_2(2);
Run_start_mod2 = cell2mat(Run_start_mod2);
block_size = 3;
headertext_mod2_3 = textscan(file_id,'%s',block_size,'delimiter','\n');
block_size = 10000;
mod1_end = length(data_compiled);
count2 = 0;
while ~feof(file_id)
    segarraymod2 = textscan(file_id,'%n%n%n%n%n%n',block_size, ...
        'delimiter','\t');
    [mod_2_data_new]=process_data_xia(segarraymod2);
    if length(mod_2_data_new) == 10000
        data_compiled(count2*10000+1+mod1_end:count2*10000+10000+ ...
            mod1_end,:) = mod_2_data_new(:,:);
    end
    if length(mod_2_data_new) < 10000
        data_compiled = [data_compiled; mod_2_data_new(:,:)];    %#ok<AGROW>
```

```
    end
    [mod_2_elem,~] = size(mod_2_data_new);
    count2 = count2+1;
    if mod_2_elem < block_size
        break
    end
end
save data_compiled.mat;
fclose(file_id);
if Run_start_mod1 ~= Run_start_mod2
    error('Run Start Times are not the same for both modules')
end

clear all
close all

data = load('data_compiled', 'data_compiled');
data = single(data.data_compiled);

[row,~] = size(data);
event2=data(row,1);

[row2_start,c_gar] = find(data(10:end,1)==1,1,'first');
event1=data((row2_start+8),1);

if event1<event2
    event=event1;
else
    event=event2;
end

bar1 = waitbar(0,'please wait...');
steps = event;
event_err = 0;
data_ready = single(zeros(event*6,4));
ready_index = 1;

A_spect = single(zeros(event,1));
B_spect = single(zeros(event,1));
C_spect = single(zeros(event,1));
D_spect = single(zeros(event,1));
E_spect = single(zeros(event,1));
F_spect = single(zeros(event,1));

for i=1:event

    k=0;
    if (data(4*i-3,4)==data(4*i-2,4)) && (data(4*i-3,4)==data(4*i-1,4))...
            && (data(4*i-3,4)==data(4*i,4)) && ...
            (data(4*i-3,4)==data(4*event+((i-1)*4)+1+event_err,4)) && ...
            (data(4*i-3,4)==data(4*event+((i-1)*4)+2+event_err,4)) && ...
            (data(4*i-3,4)==data(4*event+((i-1)*4)+3+event_err,4)) && ...
            (data(4*i-3,4)==data(4*event+((i-1)*4)+4+event_err,4))
        k=i;
    else
        for j=i-24+event_err:i+24+event_err
            if ((j>0) && (j<=event2))
                if data(4*i-2,4)==data(4*event+((j-1)*4)+1,4)
                    if (data(4*i-2,4)==data(4*i-1,4)) && ...
                       (data(4*i-2,4)==data(4*event+((j-1)*4)+1,4))...
                       &&(data(4*i-2,4)==data(4*event+((j-1)*4)+2,4))...
```

```
                    && (data(4*i-2,4)==data(4*event+((j-1)*4)+3,4))...
                    && (data(4*i-2,4)==data(4*event+((j-1)*4)+4,4))
                     k=j;
                     event_err = j-i;
                end
            end
        end
    end
end

if k>0
    %Identify detection regions of NaI ring detector sections A-F
    A=data(4*i-2,:);
    A(:,2) = 1;
    B=data(4*event+((k-1)*4)+1,:);
    B(:,2) = 2;
    C=data(4*event+((k-1)*4)+2,:);
    C(:,2) = 3;
    D=data(4*i-1,:);
    D(:,2) = 4;
    E=data(4*event+((k-1)*4)+3,:);
    E(:,2) = 5;
    F=data(4*event+((k-1)*4)+4,:);
    F(:,2) = 6;
    if A(:,3) > 0
        A(:,3) = single(0.0000014616*A(:,3)^2 + 0.051751*A(:,3) + ...
            7.7078);
        data_ready(ready_index,1:4) = A;
        A_spect(ready_index,1) = A(:,3);
        ready_index = ready_index + 1;
    end
    if B(:,3) > 0
        B(:,3) = single(0.00000039814*B(:,3)^2 + 0.02265*B(:,3) + ...
            17.574);
        data_ready(ready_index,1:4) = B;
        B_spect(ready_index,1) = B(:,3);
        ready_index = ready_index + 1;
    end
    if C(:,3) > 0
        C(:,3) = single(0.00000027532*C(:,3)^2 + 0.01332*C(:,3) + ...
            47.974);
        data_ready(ready_index,1:4) = C;
        C_spect(ready_index,1) = C(:,3);
        ready_index = ready_index + 1;
    end
    if D(:,3) > 0
        D(:,3) = single(0.000000368582*D(:,3)^2 + 0.012621*D(:,3) + ...
            40.545);
        data_ready(ready_index,1:4) = D;
        D_spect(ready_index,1) = D(:,3);
        ready_index = ready_index + 1;
    end
    if E(:,3) > 0
        E(:,3) = single(0.00000022*E(:,3)^2 + 0.0052414*E(:,3) + ...
            82.861);
        data_ready(ready_index,1:4) = E;
        E_spect(ready_index,1) = E(:,3);
        ready_index = ready_index + 1;
    end
    if F(:,3) > 0
        F(:,3) = single(0.00000017725*F(:,3)^2 + 0.0096241*F(:,3) + ...
```

```
                68.536);
            data_ready(ready_index,1:4) = F;
            F_spect(ready_index,1) = F(:,3);
            ready_index = ready_index + 1;
        end
    end
    waitbar(i/steps)
end
close(bar1)

figure(1)
hist(data_ready(:,3),10000)
title('Total Gamma Spectrum')
xlabel('Energy [keV]')
ylabel('Counts')
xlim([10 1700])
save figure1.fig;

figure(2)
subplot(3,2,1)
hist(A_spect,10000)
title('Gamma Spectrum from Section A')
xlabel('Energy [keV]')
ylabel('Counts')
xlim([10 1700])

subplot(3,2,2)
hist(B_spect,10000)
title('Gamma Spectrum from Section B')
xlabel('Energy [keV]')
ylabel('Counts')
xlim([10 1700])

subplot(3,2,3)
hist(C_spect,10000)
title('Gamma Spectrum from Section C')
xlabel('Energy [keV]')
ylabel('Counts')
xlim([10 1700])

subplot(3,2,4)
hist(D_spect,10000)
title('Gamma Spectrum from Section D')
xlabel('Energy [keV]')
ylabel('Counts')
xlim([10 1700])

subplot(3,2,5)
hist(E_spect,10000)
title('Gamma Spectrum from Section E')
xlabel('Energy [keV]')
ylabel('Counts')
xlim([10 1700])

subplot(3,2,6)
hist(F_spect,10000)
title('Gamma Spectrum from Section F')
xlabel('Energy [keV]')
ylabel('Counts')
xlim([10 1700])
save figure2.fig;
```

```
%pause

save data_ready.mat;
close all
clear all

data = load('data_ready', 'data_ready');
data = single(data.data_ready);

[row,column] = size(data);
count2 = 0;
count3 = 0;
data_2g_spect = [];
data_3g_spect = [];

bar2 = waitbar(0,'Step 2 of 2: Checking Coincidence');
steps = row;
timestamp_old = -1;
for i = 1:row
    hit = 0;
    timestamp = data(i,4);
    if timestamp ~= timestamp_old
        hit = 1;
        A = 0;
        B = 0;
        C = 0;
        D = 0;
        E = 0;
        F = 0;
        if data(i,2) == 1
            A = data(i,3);
        elseif data(i,2) == 2
            B = data(i,3);
        elseif data(i,2) == 3
            C = data(i,3);
        elseif data(i,2) == 4
            D = data(i,3);
        elseif data(i,2) == 5
            E = data(i,3);
        elseif data(i,2) == 6
            F = data(i,3);
        end

        for j = (i+1):(i+5)
            if (j <= row) && (data(j,4) == timestamp)
                hit = hit + 1;
                if data(j,2) == 2
                    B = data(j,3);
                elseif data(j,2) == 3
                    C = data(j,3);
                elseif data(j,2) == 4
                    D = data(j,3);
                elseif data(j,2) == 5
                    E = data(j,3);
                elseif data(j,2) == 6
                    F = data(j,3);
                end
            end
        end
        if hit==2
```

```
%           check if hits are on opposite PMT's for 2gamma count
            if (A>=40)&&(D>=40)&&(A<=564)&&(D<=652)&&(A+D>=470)
                count2=count2+1;
                data_2g_spect = [data_2g_spect;A;D];            %#ok<AGROW>
            elseif (B>=40)&&(E>=40)&&(B<=553)&&(E<=617)&&(B+E>=455)
                count2=count2+1;
                data_2g_spect = [data_2g_spect;B;E];            %#ok<AGROW>
            elseif (C>=40)&&(F>=40)&&(C<=582)&&(F<=575)&&(C+F>=465)
                count2=count2+1;
                data_2g_spect = [data_2g_spect;C;F];            %#ok<AGROW>
            end
        end

        if hit==3
            sum = 0;
            new_120_3g = [];
            if (A>=40)&&(C>=40)&&(E>=40)&&(A<420)&&(C<430)&&(E<445)
                sum= A + C + E;
                new_120_3g = [A;C;E];
            elseif (B>=40)&&(D>=40)&&(F>=40)&&(B<415)&&(D<450)&&(F<425)
                sum= B + D + F;
                new_120_3g = [B;D;F];
            end
            if (sum>=638)&&(sum<=1145)
               %upper bound is 1022/3=340.6-->340.6*1.12(res at 340)*3=1145
               %and one Compton Scatter event
               %lower bound, is two 340 at 12%
               count3=count3+1;
               data_3g_spect = [data_3g_spect;A;B;C;D;E;F];     %#ok<AGROW>
            end
        end

        if hit==4  %use FWHM for all 4
            if (A>=470)&&(D>=472)&&(B>=474)&&(E>=475) &&...
               (A<=552)&&(D<=549)&&(B<=548)&&(E<=546)
                   count2 = count2 + 2;
                   data_2g_spect = [data_2g_spect;A;D;B;E];     %#ok<AGROW>
            elseif (A>=470)&&(D>=472)&&(C>=473)&&(F>=472) &&...
                   (A<=552)&&(D<=549)&&(C<=549)&&(F<=549)
                   count2 = count2 + 2;
                   data_2g_spect = [data_2g_spect;A;D;C;F];     %#ok<AGROW>
            elseif (B>=474)&&(E>=472)&&(C>=473)&&(F>=472) &&...
                   (B<=548)&&(E<=546)&&(C<=549)&&(F<=549)
                   count2 = count2 + 2;
                   data_2g_spect = [data_2g_spect;B;E;C;F];     %#ok<AGROW>
            end
        end
    end
    timestamp_old = timestamp;
    waitbar(i/steps)
end
close(bar2)

figure(3)
hist(data_2g_spect,1000)
title('Spectrum of 2photon Annihilation Events')
xlabel('Energy [keV]')
ylabel('Counts')

figure(4)
hist(data_3g_spect,100)
```

```
title('Spectrum of 3photon Annihilation Events')
xlabel('Energy [keV]')
ylabel('Counts')
xlim([5 550])

TimeElapsed = toc                                                    %#ok<NOPTS>
count2                                                               %#ok<NOPTS>
count3                                                               %#ok<NOPTS>

function [event_number] = process_data_xia(segarray)
event_number = cell2mat(segarray(:,1:4));
end
```

Appendix D. 2γ3γ Results on Capillary Tube

Capillary Tube 2g3g Results with Correction Factors Applied and Calibrated to 1 Hour			
Voltage	Results 2g / 3g	Ratio	Uncertainty
0	97609.14	389.84	12.11
	265.71		
100	98137.64	387.22	16.91
	268.96		
200	98044.14	384.70	16.75
	270.46		
300	96745.14	386.03	16.96
	265.96		
400	96915.64	385.26	16.89
	266.96		
500	96282.64	382.74	16.78
	266.96		
600	96010.64	371.91	16.09
	273.96		
700	96133.39	368.35	11.21
	276.96		
800	96341.14	374.56	16.24
	272.96		
900	97302.14	391.94	17.30
	263.46		
1000	96820.64	388.52	17.12
	264.46		
1250	96828.14	393.76	17.47
	260.96		
1500	96498.64	399.31	17.87
	256.46		
1750	96784.14	398.93	17.82
	257.46		
2000	96368.64	395.69	17.64
	258.46		
2500	96246.14	401.39	18.03
	254.46		

Appendix E. Student's t-test Results of 2γ3γ Data

Student's t-test Results			
Ratio 2g/3g			
600-800V	vs.	300-500V	96.34%
600-800V	vs.	900-1250V	98.00%
300-500V	vs.	900-1250V	90.20%
2 Photon Data			
600-800V	vs.	300-500V	87.73%
600-800V	vs.	900-1250V	95.21%
300-500V	vs.	900-1250V	74.06%
3 Photon Data			
600-800V	vs.	300-500V	88.88%
600-800V	vs.	900-1250V	89.49%
300-500V	vs.	900-1250V	85.77%

Appendix F. Positron Lifetime Data Collection Code

```
clc
clear all
close all

%connection to device
visa_brand = 'tek';
visa_address = 'TCPIP::169.254.235.51::INSTR'; %oscilloscope ip address
buffer = 4000 * 1024;
fclose('all');
dpo = visa(visa_brand, visa_address, 'InputBuffer', buffer, ...
    'OutputBuffer', buffer);
fopen(dpo); %commands can now be sent to device

%reset scope factory defaults and any inadvertant settings
fprintf('Scope reset to factory defaults.\n');
fprintf('Configuring scope....');
frames = 1000; %Number of waveforms to capture in FastFrame mode
record = 1000; %Number of points in a waveform, based on timing resolution
Ch1VPos = 4.0; %divisions on vertical axis -5.0 to 5.0
Ch1HPos = 10; %divisions on horizontal axis 0 to 100
Ch2VPos = 4.0; %divisions on vertical axis -5.0 to 5.0
Ch2HPos = 10; %divisions on horizontal axis 0 to 100
Ch1Scale = 0.300; % [V]
Ch2Scale = 0.300; % [V]
Ch1Offset = 0.0; % [V]
Ch2Offset = 0.0; % [V]
TimeWindow = 10.0E-9; %increment of time axis [s]
TimeStep = TimeWindow/record; % [seconds per point]
timearray = (1:1:record)*(TimeWindow/record)*1E9;

fwrite(dpo,'ACQ:STATE 0');
fwrite(dpo,'HEAD 0');
fwrite(dpo,'ACQUIRE:MODE SAMPLE');
fwrite(dpo,'ACQUIRE:SAMPLINGMODE RT');
fwrite(dpo,'HOR:MODE MANUAL');
fprintf(dpo,'HOR:MODE RECORD %i', record);
fwrite(dpo,'HOR:FAST:STATE 1');
fprintf(dpo,'HOR:FAST:COUNT %i', frames);
fprintf(dpo,'DATA:START 0');
fprintf(dpo,'DATA:STOP %i', record);
fwrite(dpo, 'DATA:ENCDG SRIBINARY');

fprintf(dpo,'WFMInpre:BN_FMT RI');
fprintf(dpo,'WFMInpre:BYT_OR LSB');
fprintf(dpo,'WFMInpre:BYT_NR 1');

fprintf(dpo,'WFMOutpre:BYT_NR 1');
fprintf(dpo,'WFMOutpre:BN_FMT RI');
fprintf(dpo,'WFMOutpre:BYT_OR LSB');

fwrite(dpo,'Ch1:Termination 50')
fwrite(dpo,'Ch2:Termination 50')
fwrite(dpo,'Select:Ch1 On');
fwrite(dpo,'Select:Ch2 On');
fwrite(dpo,'DATA:SOURCE Ch1, Ch2');
fprintf(dpo,'Horizontal:Position %i', Ch1HPos);
fprintf(dpo,'ch1:Scale %i', Ch1Scale);
fprintf(dpo,'ch2:Scale %i', Ch2Scale);
fprintf(dpo,'CH1:Position %i', Ch1VPos);
```

```
fprintf(dpo,'CH2:Position %i', Ch2VPos);
fprintf(dpo,'Ch1:Offset %i', Ch1Offset);
fprintf(dpo,'Ch2:Offset %i', Ch2Offset);
fprintf(dpo,'Horizontal:Scale %i', TimeWindow);
fprintf(dpo,'Horizontal:AcqLength %i', record);

query(dpo,'WFMOutpre:YMult?');
Ch1YMult = str2double(query(dpo,'WFMOutpre:YMult?'));%vertical scale factor
Ch1Yoff = Ch1VPos*Ch1Scale;  %offset from zero
Ch2YMult = str2double(query(dpo,'WFMOutpre:YMult?'));
Ch2Yoff = Ch2VPos*Ch2Scale;

%trigger settins
fwrite(dpo,'Trigger:A:Type Edge');
fwrite(dpo,'Trigger:A:Edge:Slope Fall');
fwrite(dpo,'Trigger:A:Level -0.792'); %trigger voltage [V]
fprintf(dpo,'Trigger:A:Mode Normal'); %do not use auto
fprintf('Done!\n');

%data acquistion
sets = 1000;  %number of data sets to record, primary driver of duration
tic
Ch1 = zeros(record,frames);
Ch2 = zeros(record,frames);
for i=1:sets
    fprintf(dpo,'Acquire:StopAfter Sequence');
    fwrite(dpo,'ACQ:STATE 1');
    fprintf('Acquiring data set #%i........', i);
    dpo.Timeout = 1000;
    query(dpo,'*opc?');
    dpo.Timeout = 10;
    fprintf('Done!\n');

    fprintf('  Asking for waveforms....');
    fwrite(dpo, 'curve?'); %request waveforms
    %waveform preamble and binary data stored in memory
    fprintf('Done!\n');

    fprintf('  Reading waveforms....');
    fread(dpo,1);
    bytes = str2double(char((fread(dpo,1))));
    fread(dpo, bytes); %throw away remaining header
    header = (1+1+bytes);
    raw1 = fread(dpo, record*frames,'int8'); %store waveform data
    fread(dpo, header);
    raw2 = fread(dpo, record*frames, 'int8'); %store waveform data
    fprintf('Done!\n');
    fread(dpo,1); %termination character

    start = 1;
    stop = record;
    for j=1:frames
        Ch1(1:record, j) = raw1(start:stop);
        Ch2(1:record, j) = raw2(start:stop);
        start = stop+1;
        stop = start+record-1;
    end

    Ch1 = -(Ch1YMult*Ch1-Ch1Yoff);
    % Apply scale and offset to match voltage
    Ch2 = -(Ch2YMult*Ch2-Ch2Yoff);
```

```
    % Apply scale and offset to match voltage
    savename = ['Ch1_' num2str(i) '.mat'];
    save(savename,'Ch1') %saving waveforms
    savename = ['Ch2_' num2str(i) '.mat'];
    save(savename,'Ch2') %saving waveforms
end
fprintf('**********  %i waveforms recorded!  **********\n', sets*frames*2);
TimeElapsed = toc
```

Appendix G. Positron Lifetime Data Analysis Code

```
%this code is meant to be used as a tool to better analyze and calibrate
%data collected for positron lifetime measurements using an oscilloscope
close all
clear all
clc

tic;
% note that these values must match the values used during data collection
sets = 10000; %number of data sets collected on either channel
frames = 1000; %the number of screen shots recorded in each set
record = 1000;  %a limiting factor determined by resolution of O-scope
timewindow = 100e-9; %the timeframe over which a pulse is displayed

peakval_ch1 = zeros(sets*frames,1); %preallocate variables
peakval_ch2 = zeros(sets*frames,1);
mean_ch1    = zeros(sets*frames,1);
peakrat_ch1 = zeros(sets*frames,1);
peakrat_ch2 = zeros(sets*frames,1);
area_ch1    = zeros(sets*frames,1);

bar = waitbar(0,'Please wait...');
steps = sets;

for i = 1:sets
    load(['Ch1_' num2str(i)])
    load(['Ch2_' num2str(i)])
    for j = 1:frames
        waveform1 = Ch1(1:record,j);
        ratio1 = (mean(waveform1))/max(waveform1);
        int1 = sum(waveform1)*timewindow;
        if (max(waveform1) <= 2.69) && (sum(waveform1)*timewindow >= 0) ...
                && (sum(waveform1)*timewindow <= 2.9e-6)
            peakval_ch1(frames*(i-1)+j,1) = max(waveform1);
            peakrat_ch1(frames*(i-1)+j,1) = (mean(waveform1))/ ...
                max(waveform1);
            area_ch1(frames*(i-1)+j,1) = sum(waveform1)*timewindow;
            mean_ch1(frames*(i-1)+j,1) = mean(waveform1);
% the next 2 lines allow the user to view waveforms one at a time
%             plot(waveform1)
%             pause
        else
            peakval_ch1(frames*(i-1)+j,1) = NaN;
            peakrat_ch1(frames*(i-1)+j,1) = NaN;
            area_ch1(frames*(i-1)+j,1)    = NaN;
            mean_ch1(frames*(i-1)+j,1)    = NaN;
        end
        waveform2 = Ch2(1:record,j);
        if (min(waveform2) >= -0.20) %&& (mean(waveform1) >= 0)
            peakval_ch2(frames*(i-1)+j,1) = max(waveform2);
            %peakrat_ch1(frames*(i-1)+j,1) = max(waveform1);
%             plot(waveform2)
%             pause
        else
            peakval_ch2(frames*(i-1)+j,1) = NaN;
        end
    end
    waitbar(i/steps)
end
```

```
close(bar)

figure(1)
hist(peakval_ch1,250)
ph = get(gca,'children');
vn = get(ph,'Vertices');
vn(:,2) = vn(:,2) + 1;
set(ph,'Vertices',vn);
set(gca,'yscale','log')
xlabel('Peak Voltage of Waveforms [V]')
ylabel('Counts')
title('Peak Voltage Distribution with BaF2 Detector')

figure(2)
hist(mean_ch1,10000)
title('Mean')

figure(3)
hist(area_ch1,10000)
xlabel('Integrated Waveform [Vs]')
ylabel('Counts')
title('Integrated Waveform Histogram')

figure(4)
hist(peakrat_ch1,500)
xlabel('Mean Value / Max Value [V/V]')
ylabel('Counts')
title('Ratio of Mean/Max of Waveforms')

figure(5)
hist(peakval_ch2,200)
ph = get(gca,'children');
vn = get(ph,'Vertices');
vn(:,2) = vn(:,2) + 1;
set(ph,'Vertices',vn);
set(gca,'yscale','log')
xlabel('Peak Voltage of Waveforms [V]')
ylabel('Counts')
title('Peak Voltage Distribution from Small BaF2 Crystal')

TimeElapsed = toc
```

Appendix H. Positron Lifetime Spectroscopy Code

```
close all
clear all
clc

tic;
% note that these values must match the values used during data collection
sets = 10000; %number of data sets collected on either channel
frames = 1000; %the number of screen shots recorded in each set
record = 1000;  %a limiting factor determined by resolution of O-scope
timewindow = 100e-9; %the timeframe over which a pulse is displayed
sample_rate = 100e-12; %sample rate measured in sec/point
pickoff_fraction = 0.37;%constant fraction pickoff percentage,10-20% ideal
lifetime_array = [];
count = 0;
bar = waitbar(0,'Please wait...');
steps = sets;
for i = 1:sets
    load(['Ch1_' num2str(i)])
    load(['Ch2_' num2str(i)])
    for j = 1:frames
        waveform1 = Ch1(1:record,j);
        if (max(waveform1) >= 0.8) && ...
           (max(waveform1) < 2.7) && ...
           (sum(waveform1)*timewindow >= 5.5e-6) && ...
           (sum(waveform1)*timewindow <= 1.3e-5) && ...
           (max(waveform1(1:40)) <= 0.024)
            waveform2 = Ch2(1:record,j);
            if (max(waveform2) >= 0.100) && ...
               (max(waveform2) <= 0.500) && ...
               (sum(waveform2)*timewindow >= 8e-8) && ...
               (sum(waveform2)*timewindow <= 2.9e-6) && ...
               (max(waveform2(1:40)) <= 0.036)
                [max_time1,~] =find(waveform1 == max(waveform1),1,'first');
                [max_time2,~] =find(waveform2 == max(waveform2),1,'first');
                [timing_ch1,~] = find(waveform1 >= pickoff_fraction* ...
                    max(waveform1(max_time1-15:max_time1)), 1, 'first');
                [timing_ch2,~] = find(waveform2 >= pickoff_fraction* ...
                    max(waveform2(max_time2-15:max_time2)), 1, 'first');
                if (timing_ch1 < timing_ch2) && (max_time1 < max_time2)
                    lifetime = (timing_ch2-timing_ch1)*sample_rate+3.7e-12;
                    lifetime_array = [lifetime_array;lifetime]; %#ok<AGROW>
                    count = count + 1;
                end
            end
        end
    end
    waitbar(i/steps)
end
close(bar)

figure(1)
hist(lifetime_array/1e-9,record)%abscissa in ns, binning matches resolution
xlabel('Lifetime [ns]')
ylabel('Counts')
title(['Positron Lifetime from ' num2str(count) ' Measurements'])

TimeElapsed = toc                               %#ok<NOPTS>
AvgLifetime = (sum(lifetime_array)/count)       %#ok<NOPTS> %output in seconds
Uncertainty = (((sample_rate/2)^2)*2)^(1/2)     %#ok<NOPTS> %output in seconds
```

Bibliography

1. M. Charlton and J.W. Humberston. *Positron Physics*. Cambridge University Press, New York, 2005.

2. Y. C. Jean, P.E. Mallon, and D. M. Schrader. *Principles and Applications of Positron and Positronium Chemistry*. World Scientific, New Jersey, 2003.

3. Glenn F. Knoll. *Radiation Detection and Measurement 4th edition*. John Wiley and Sons, Inc., New Jersey, 2010.

4. P. A. M. Dirac *Proc. Camb. Phil. Soc.* 26, 361. 1930.

5. C. D. Anderson *Phys. Rev.* 43, 491. 1933.

6. Harrison H. Barrett, William Swindell. *Radiological Imaging: The Theory of Image Formation, Detection, and Processing.* Academic Press, Inc. San Diego, 1981.

7. Burggraf, Larry. Professor, AFIT Department of Engineering Physics, WPAFB, OH. Personal correspondence

8. Kowash, Benjamin, Maj, USAF. Assistant Professor, AFIT Department of Engineering Physics, WPAFB OH. Personal correspondence

9. Williams, Christopher, Lt Col, USAF. Assistant Professor, AFIT Department of Engineering Physics, WPAFB OH. Personal correspondence

10. Slaughter, Robert. *Positron Annihilation of Radiation Spectroscopy (PsARS) Applied to Positronium Formation Studies*: AFIT. 2010

11. Walker, Ariella. *Positron Annihilation Ratio Spectroscopy Study of Electric Fields Applied to Positronium at Material Interfaces:* AFIT. 2011

12. M. M. Nieto, M. H. Holzscheiter, and T. J. Phillips. 2003 *J Opt. B* 5 S547-S552.

13. Y. Ito. 2003 *Radiation Physics and Chemistry*. 68 403-7.

14. A. P. Mills Jr., D. B. Cassidy, and R. G. Greaves 2004. *Material Science Forum*. 445-446424-9.

15. C. S. Williams et all. 2010. *IEEE*. 75 860-9.

16. M. H. Weber and K. G. Lynn. 2000. *Radiation Physics and Chemistry*. 58 749-753.

17. A. Ore and J. L. Powell 1949. *Physical Review*. 75 1696-9.

18. S. DeBenedetti and R. T. Siegel 1954. *Physical Review*. 94 955-9.

19. A. Sun, C. Edwards, A. Kane, and S. Pandipati. 1993 *IEEE* November 44-6.

20. Teasdale. *Solid Rocket Microrockets*. UC Berkeley. 2000. http://wwwbsac.eecs.berkeley.edu/projects/microrockets/masters_report.pdf

21. R. M. Nieinen and J. Oliva 1980 *Phys. Rev. B* 22 2226-47.

22. S. Mukherjee et all. 2008. *Applied Surface Science*. 255 223-6

23. M. Bertolaccini, C. Bussolati, and L. Zappa. 1965. *Physical Review A*. 139 696-9.

24. R. J. Stevens and P.C. Lichtenberger 1972. Physc. Rev. Lett., 29, 166-9. 103

25. "Pixie-500," *XIA*. 10 Jan 2011. <http://xia.com/DGF_Pixie-500.html>.

26. Bailey, Townsend, Valk, Maisey (2005). *Positron Emission Tomography: Basic Sciences*. Secaucus, NJ: Springer-Verlag. ISBN 1-85233-798-2

27. "Positron Lifetime Spectroscopy" *PositronAnnihilation.Net.* 28 Jan 2011. <http://www.positronannihilation.net/index_files/Positron%20Lifetime%20Spectroscopy.pdf>.

28. "DGF4C" *XIA*. 11 Feb 2011. <http://www.xia.com/Datasheets/DGF_F_flyer.pdf>.

29. S. Szpala et all. 1996. *Physical Review B*. 54 4722-4731.

30. C. H. Hodges and M. J. Scott. 1973. *Physical Review B*. 7 73-9.

31. T. M. Mayer et all. 1999. *Journal of Applied Physics*. 85 8170-7.

32. J. V. Olsen, P. Kirkegaard, N. J. Pedersen, and M. Eldrup. 2006. "PALSfit: A computer program for analyzing positron lifetime spectra*" Risø National Laboratory.*

33. D. G. Costello, D.E. Groce, D.F. Herring, and J. Wm. McGowan. 1972. *Phys. Rev. B* 5 1433-6

34. R. Krause-Rehberg and H.S. Leipner. *Positron Annihilation in Semiconductors*. Springer, New York, 1999.

35. Laval, Moszyński, Allemand, Cormoreche, Guinet, Odru, Vacher, J. (1983). "Barium fluoride – Inorganic scintillator for subnanosecond timing". *Nuclear Instruments and Methods in Physics Research* 206: 169

36. Hamamatsu Photonics K.K., Electron Tube Division 314-5, Shimokanzo, Iwata City, Shizuoka Prefecture, Japan (81) 539/62-5248

37. "Data Acquisition," *Wavemetrics 30 Dec 2010.* <http://www.wavemetrics.com/products/igorpro/dataaccess/hardwaredata.htm>.

38. H. Saito, Y. Nagashima, T. Kurihara, T. Hyodo. 2001. "A new positron lifetime spectrometer using a fast digital oscilloscope and BaF_2 scintillators". *University of Tokyo Institute of Physics*

39. R. J. Stevens and P.C. Lichtenberger 1972. Physc. Rev. Lett., 29, 166-9

40. Goworek, Tomasz. Journal of Nuclear and Radiochemical Sciences, Vol. 1, No. 1, pp. 11−13, 2000

REPORT DOCUMENTATION PAGE

Form Approved
OMB No. 074-0188

PLEASE DO NOT RETURN YOUR FORM TO THE ABOVE ADDRESS.

1. REPORT DATE *(DD-MM-YYYY)*	2. REPORT TYPE	3. DATES COVERED *(From – To)*
22-03-2012	Master's Thesis	20 August 2010 – 22 March 2012

4. TITLE AND SUBTITLE
Positron Lifetime Modulation by Electric Field Induced Positronium Formation on a Gold Surface

5a. CONTRACT NUMBER

5b. GRANT NUMBER

5c. PROGRAM ELEMENT NUMBER

6. AUTHOR(S)
Higgins, Daniel J., Captain, USAF

5d. PROJECT NUMBER
N/A

5e. TASK NUMBER

5f. WORK UNIT NUMBER

7. PERFORMING ORGANIZATION NAMES(S) AND ADDRESS(S)
Air Force Institute of Technology
Graduate School of Engineering and Management (AFIT/EN)
2950 Hobson Way
WPAFB OH 45433-7765

8. PERFORMING ORGANIZATION REPORT NUMBER
AFIT/NUCL/ENP/12-M03

9. SPONSORING/MONITORING AGENCY NAME(S) AND ADDRESS(ES)
Dr Michael Berman
Air Force Office of Scientific Research
Aerospace, Chemical and Material Sciences Directorate
Wright-Patterson AFB, OH

10. SPONSOR/MONITOR'S ACRONYM(S)

11. SPONSOR/MONITOR'S REPORT NUMBER(S)

12. DISTRIBUTION/AVAILABILITY STATEMENT
APPROVED FOR PUBLIC RELEASE; DISTRIBUTION UNLIMITED

13. SUPPLEMENTARY NOTES

14. ABSTRACT

The purpose of this project is to study the lifetime and annihilation mode of positrons, the antimatter counterpart to electrons, and the formation rate of positronium on a gold surface modified by gold nanoparticles under the influence of radial electric fields measured using two independent systems. The positron annihilation photon pair/triplet spectroscopy system uses a sodium iodide ring detector segmented into six detection regions providing rough position sensitivity to measure the ratio of two to three photon positron annihilation events. An increased rate of three photon annihilation events and a decreased rate of two photon annihilation events are observed when the source is exposed to an externally applied radial electric field. This change is found to be statistically significant suggesting an increased rate of positronium formation. The second system conducts positron lifetime spectroscopy on the same source and measures the effect of radial electric fields on positron lifetime. It uses barium fluoride, a fast inorganic scintillator, to measure the lifetime of a positron directly by comparing the time of arrival of a gamma ray accompanying positron birth in Na-22 with photons resultant from positron annihilation. Prolongated positron lifetimes, found to be statistically significant, are observed in the source when exposed to electric fields. The effects on positron annihilation and lifetime observed using each system are consistent with each other and suggest that the lifetime of positrons on a gold surface can be modulated by the application of strong radial electric fields

15. SUBJECT TERMS
Positron, Positronium, Positron Annihilation Spectroscopy, Positron Lifetime

16. SECURITY CLASSIFICATION OF:			17. LIMITATION OF ABSTRACT	18. NUMBER OF PAGES	19a. NAME OF RESPONSIBLE PERSON
a. REPORT	b. ABSTRACT	c. THIS PAGE			Dr. Larry W. Burggraf
U	U	U		155	19b. TELEPHONE NUMBER *(Include area code)* (937) 255-3636, x 4507 larry.burggraf@afit.edu